DISCRETE ATOMIC SIMULATION OF FRACTURE IN IRON

BY

©

Mayes Mullins

B. Eng. (McMaster)

A Thesis

Submitted to the Faculty of Graduate Studies

in Partial Fulfilment of the Requirements

for the Degree

Doctor of Philosophy

McMaster University

(May) 1980

DISCRETE ATOMIC SIMULATION OF FRACTURE IN IRON

DOCTOR OF PHILOSOPHY   McMASTER UNIVERSITY
(Mechanical Engineering)   Hamilton, Ontario

TITLE: DISCRETE ATOMIC SIMULATION OF FRACTURE IN IRON

AUTHOR: Mayes L. Mullins, B. Eng. (McMaster)

SUPERVISOR: Dr. M. A. Dokainish

NUMBER OF PAGES: x, 218

ABSTRACT

The thesis is concerned with improving the understanding of materials at the atomic level by computer simulation. The work has centered on three areas: a study of the efficiency of various computer algorithms used to carry out these simulations; the development of a new and very versatile boundary condition scheme for such problems; and the application of the results of these two studies to the simulation of (001) plane fracture in α-iron.

Tests were performed comparing various solution methods used for atomic level computer modelling. The results are presented and indicate the most efficient method to be chosen for various problems. This may allow a reduction in computer cost by factors of two or three over that of other, often used, methods.

The new boundary scheme which was developed involves the use of the finite element method. This offers several advantages over previous methods.

The new boundary scheme was applied to the (001) plane crack in α-iron. Two dimensional cracks with crack line directions of [010] and [110] were modelled. Significant differences in lattice trapping limits and crack propagation speeds were observed between these two cases. Information on the magnitude and shape of the non-linear component of the crack tip displacement field is provided for both cases. No dislocations were emitted at low temperatures from these models, but warming the [010] model to 400 K apparently resulted in the emission of a dislocation from the crack tip. Experimental information available in the literature pertaining to these points is discussed and possible future work is described.

ACKNOWLEDGEMENTS

TABLE OF CONTENTS

TABLE OF CONTENTS

LIST OF ILLUSTRATIONS

vii

LIST OF ILLUSTRATIONS

LIST OF ILLUSTRATIONS

LIST OF TABLES

x

1. INTRODUCTION

The study of materials and their associated defects at the
atomic level by computer simulation is a relatively new field of
materials research. Materials are studied at this level in order to
better understand their macroscopic properties, such as mechanical
strength, by observing their behaviour at the microscopic level. Since
it is very difficult to examine real materials at this small scale, this
work is most easily accomplished by studying model materials using
computer simulation. This technique has been used to study the
formation and migration energies of interstitials and vacancies; the
structure of static dislocations; the Peierls barrier for moving
dislocations; the structure of crack tips; the structure and energy of
grain boundaries and surfaces; the damage of solids by nuclear radiation
and high intensity shock waves; and, the statistical mechanics
properties of solids and liquids.

The present work is concerned with the application of computer
simulation techniques in the study of solid defects, particularly crack
tips. Sufficient work in this area could improve our understanding of
brittle-ductile transition phenomena, acoustic emission non-destructive
testing, static and dynamic fatigue, and all other aspects of material
behaviour which are related to atomic level events. The major
limitations on this work are the construction of adequate interatomic
potentials, the selection of a boundary scheme to be used around the

1

discrete area of the model, and the cost of the computer calculations.

This thesis makes some contribution to the solution of the last two of these problems. After a brief description of a typical problem setup, and an examination of previous work in the pertinent areas, a comparison of various solution schemes for use with these models is presented. This allows the most efficient scheme to be chosen to minimize solution cost for a given problem. After this, a new boundary scheme is described which makes use of the finite element method. This seems to offer several advantages over those which have been used in the past. Finally, this boundary scheme is applied to the problem of the (001) plane crack in α-iron. Some interesting behaviour, not previously noted, was observed with this crack model. Some published experimental work is cited which appears to support these observations, but more such work will be necessary before they can be considered to be confirmed.

2 TYPICAL PROBLEM SETUP

This chapter contains a description of a typical atomic level
computer simulation problem. The method of modelling the crystal and
general descriptions of the interatomic force laws and solution schemes
used for these problems are presented. The primary emphasis will be on
simulations which study defect properties in solids. The description in
this chapter is limited to the types of models studied in this thesis.
These correspond to the so-called "molecular dynamics" models. A small
amount of work has been done in the past with another type of model
known as "lattice statics" models. These will be described briefly in
section 3.6 .

Figure 1 illustrates the crystallographic axes of bcc crystals
which will be referred to in this, and in later chapters.
Crystallographic directions are written in square brackets, for example,
[110]. Crystallographic planes are described by the direction of their
normals written in round brackets, for example, (001). Negative
components are indicated by a minus sign above the corresponding number,
for example, ($\bar{1}$01). A complete discussion of this method of describing
crystal directions, known as Miller indices, can be found in [1].[*]

[*] Numbers in square brackets indicate references in Chapter 8.
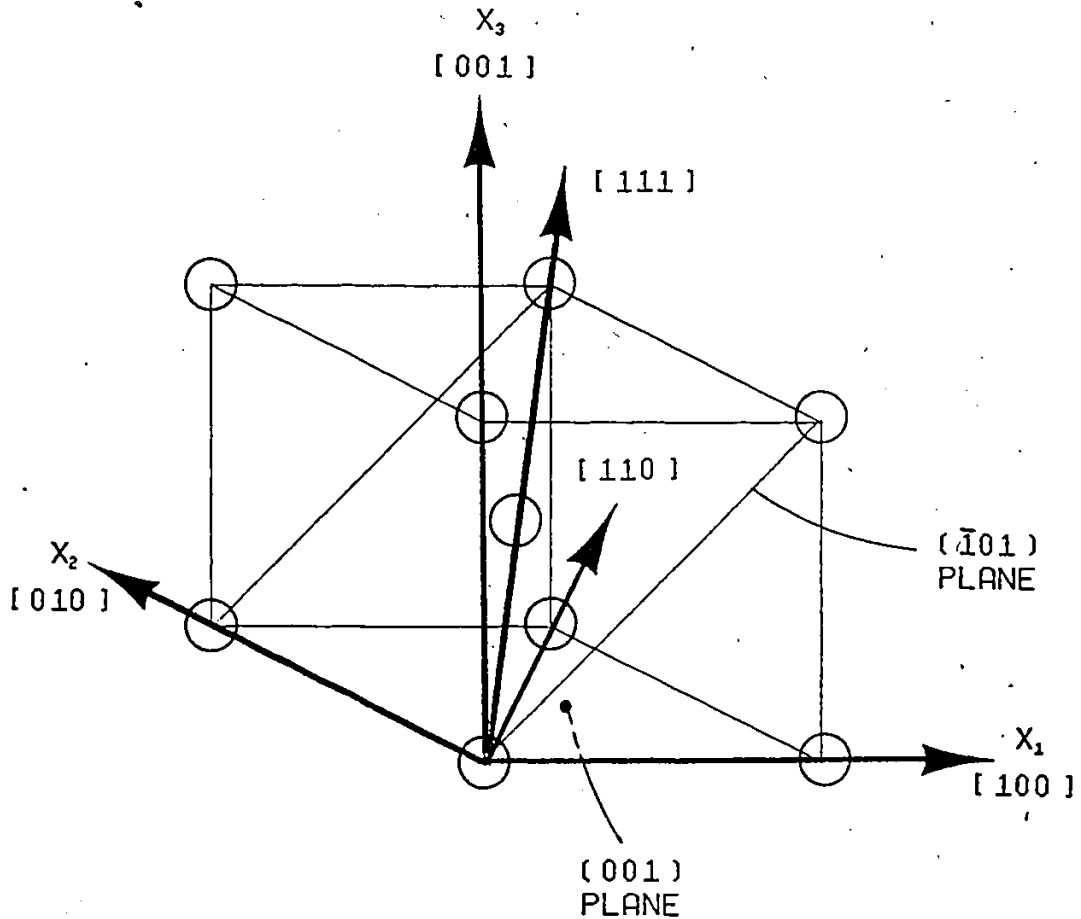
Figure 1. Crystallographic directions and planes of bcc crystals. The x_1 and x_2 axes are positioned as shown for the [010] crack model studied in Chapter 6, and are rotated 45° from these positions for the [110] crack model.

Figure 2 is a schematic illustration of a typical atomic simulation model. A crack tip problem is shown. If the purpose of the simulation is to study a solid mechanics defect, the defect is located at the center of a section of crystal modelled to the atomic level. Studies of liquids or gases or of the statistical mechanics properties of solids do not involve defects but there is, in all such studies, a region of crystal modelled to atomic detail. With very minor and elementary exceptions, this atomic level modelling has so far been done with classical mechanics. No quantum mechanical effects have been taken into account in the equations of motion describing the system although, for some materials, the interatomic force law may be initially derived from fundamental quantum mechanical considerations. Classical mechanics provides sufficient accuracy except for the study of material properties at very low temperatures when the system energy is comparable to its zero-point energy. Classical models would not show superfluidity, for example, which is a quantum effect. The model of the atomic area thus takes the form of a series of mass points representing the atoms connected by interatomic forces.

One of the main difficulties in atomic simulations is the description of these interatomic forces. In real materials, the behaviour of these forces is very complex. The force on an atom depends on the relative positions of all other atoms in the crystal, although the magnitude of this effect decreases with distance. The distance at which this effect declines to a negligible value depends on the material. Materials which are strongly covalently bonded, such as
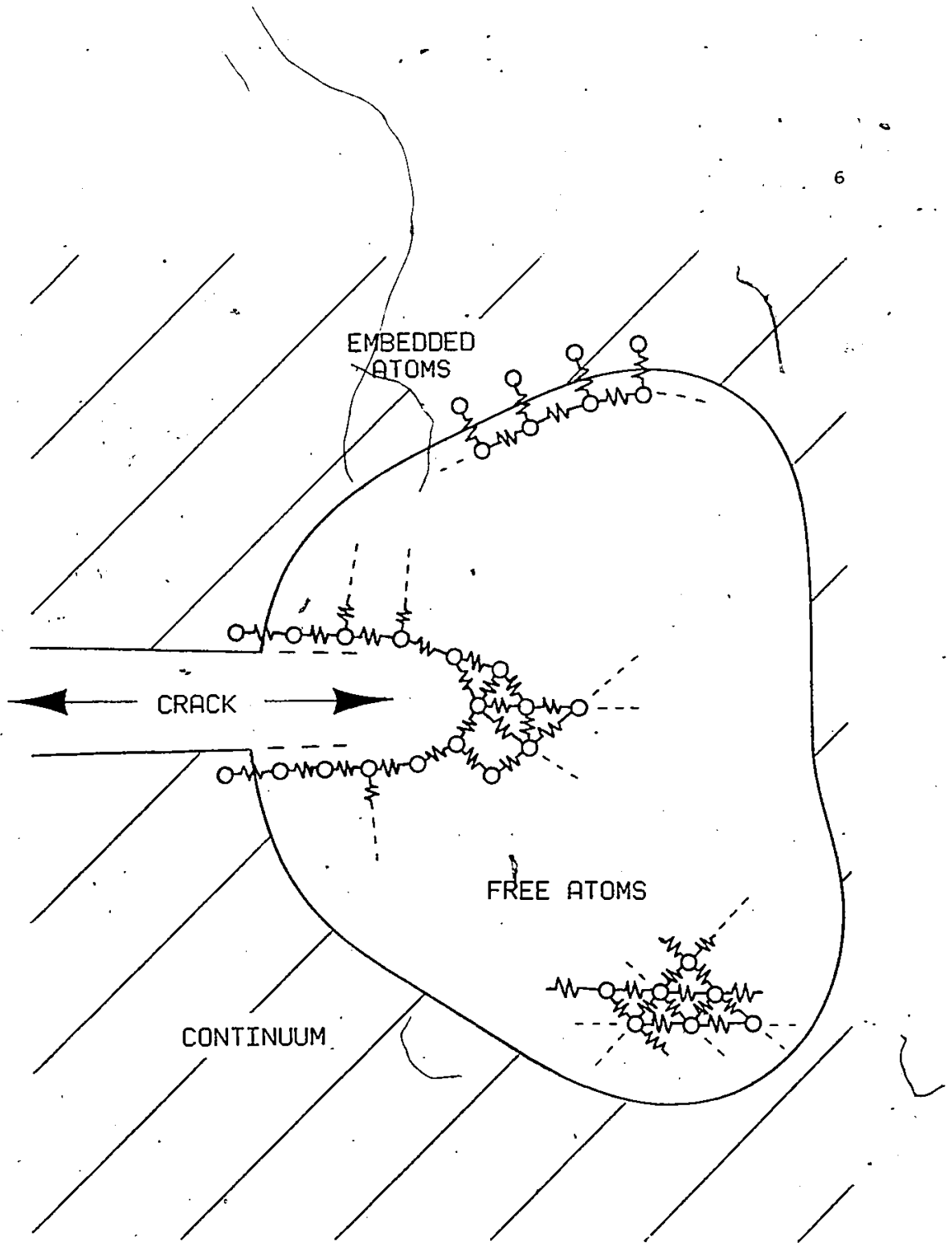
Figure 2.   Schematic illustration of a typical atomic simulation
             problem.

diamond, are probably adequately described by including the effect of nearest neighbour bonds only. Materials such as the alkali metals, on the other hand, seem to show significant bonding out to sixth nearest neighbours. A further complication is that, in general, the bonding cannot be considered to be by pairs only, ie. the total force on an atom cannot be broken down into a set of forces, one to each neighbouring atom. The total force depends in a complex way on the positions of all neighbouring atoms. In order to keep computer costs tractable, some simplification has to be made to describe this behaviour. The specifics of this point will be examined in greater detail in section 3.4 .

Acting in response to the interatomic forces, the atomic mass points in the central region of the model of Fig. 2 are allowed to move freely. In the most general case, this central region may be extensive in three dimensions and the atoms may be free to move in all three coordinate directions. Some atomic simulation models have been described which are only one dimensional and allow only one degree of freedom per atom, but by far the most common are two dimensional models. These provide enough information to be interesting in many cases, while requiring much smaller amounts of computer effort for their solution than would a general three dimensional model.

The condition in the third direction of two dimensional models is usually plane strain. The stress field in the immediate vicinity of a long defect, which is the usual center of interest in a problem of this type, is much higher than that existing at large distances from the defect. The large area of low stressed material tends to support the

material close to the defect in the direction parallel to its axis, and this results in plane strain conditions.

The number of planes of atoms which must be included in a two dimensional model depends on the crystal structure and orientation. For example, a model of a bcc material in which the axis of the model is [010] or [110] (this will be referred to as the x_2-axis in agreement with the models described later in this thesis) would require two active planes, while other directions would require more. Bonds to atoms outside these active planes may be accounted for by computer bookeeping or by the addition of image planes of atoms above and below the active planes. The positions of these image atoms are maintained in a fixed relation to the positions of the corresponding active atoms in order to produce the desired x_2 relationship, which is usually plane strain as described above. The number of image planes is chosen in accordance with the interatomic potential so that all atoms in the active planes have a complete set of bonds. A typical example is the bcc crystal with x_2-axis of crystal type [010] mentioned above. For an interatomic potential which cuts off between second and third nearest neighbours, four image planes would be required in addition to the two active planes.

The size of the area of crystal modelled to atomic detail in a computer simulation study is restricted to the order of several hundred to several thousand atoms by computer cost. Often, this is too small for the atomic level effects to be negligible at the boundaries, and one of the major problems in the application of this technique is the

determination of the boundary conditions to be applied to the atomic
area. The manner of applying the boundary conditions generally involves
considering the outer layer of atoms to be embedded in, and moving with,
a surrounding continuum region. All other atoms in the discrete region
are free to move independently, constrained only by their interatomic
bonds. Forces or displacements are applied to the outer edge of the
continuum (which may be infinitely large and is at least many times the
diameter of the atomic area) in accordance with the problem to be
solved. The degree to which the discrete atomic area and the continuum
interact and the accuracy with which the continuum is modelled determine
the effectiveness of the boundary condition scheme used. A great deal
of effort has been expended in previous work to establish a boundary
scheme which performs well. The problems which may be studied and the
model results are often intimately connected with the particular scheme
adopted. Further details on this point will be provided in the next
chapter.

Atomic simulations may be divided into two types, static and
dynamic. In a static simulation, only the equilibrium arrangement of
atoms in the model is found. This allows the determination of the
energy and equilibrium structure of crystal defects. In a dynamic
analysis, the motion of the atoms with time is followed and it is the
properties of this motion which are of interest. This may be to study
the motion of crystal defects as a result of applied stress or thermal
activation; nuclear radiation or shock wave damage; or various
thermodynamic or lattice dynamic properties. There is some overlap

between these two types of simulations and sometimes the same problem can be solved by either method. For example, the distribution of normal modes of lattice vibrations around a crystal defect may be determined as the eigenvalues of the displacement-force matrix for the crystal for small displacements about its equilibrium position. This equilibrium position can be found by a static simulation for the defect. Alternatively, the lattice may be allowed to experience random vibrations corresponding to thermal motion in a dynamic simulation. Statistical analysis of this motion can also provide the information being sought.

Dynamic simulations obviously involve solving or integrating the equations of motion obtained from Newton's second law applied to each atom in the discrete area, and from a description of the motion allowed in the continuum region, if any. The equilibrium configurations required as solutions of static simulations may be found in a number of ways. The equations of motion of the system may be integrated, as in a dynamic simulation, with the addition of some type of artificial damping. Various methods of applying this damping are possible. In addition, optimization techniques may be used to find equilibrium positions defined as potential energy minima. The efficiency with which the equations of motion may be integrated in a dynamic model, and with which the excess energy of the system may be removed in a static simulation define the amount of computer time needed to solve a problem. This in turn determines the size and complexity of the model which may be studied. The method of solution used is, therfore, an important

parameter in a model. This point will be examined in more detail in

Chapter 4 when a comparison is made between the efficiency of various

solution methods.

This chapter has provided a general description of typical

atomic level computer simulation models. It can be seen that the

primary difficulty associated with these models is the selection of the

interatomic potential, the boundary condition scheme, and the solution

method to be used. These points will be discussed in greater detail in

later chapters with regard both to work which has been done previously

by others, and work done in these areas in the present study.

3 LITERATURE SURVEY

This chapter provides a survey of the literature in areas
pertaining to the work presented in this thesis and indicates the
relationship of this work to these areas. It is intended to provide an
illustration of the current state of the art in two related fields. The
first of these is concerned with general theoretical and experimental
work pertaining to microscopic level fracture mechanics, the second with
the area of computer simulation of materials at the atomic level. This
is first discussed in general and then particular emphasis is given to
the study of cracks in solids by this technique. This in turn relates
to the first area described above.

3.1 Microstructural Fracture Mechanics - Theoretical

Fracture mechanics is concerned with the rupture of materials
under various conditions of loading and environment. An introduction to
general fracture mechanics can be found in [2], and a much more detailed
discussion in [3].

The most important parameter for characterizing the loading
condition on a crack is the stress intensity factor, k, which has units
of $[pressure][length]^{1/2}$, or, $[force][length]^{-3/2}$. It can be shown
that, for a long, sharp crack in a linear elastic solid, such as that
shown in Fig. 3(a), the stress at a point near the tip of the crack is

X_3

r

θ

CRACK

X_1
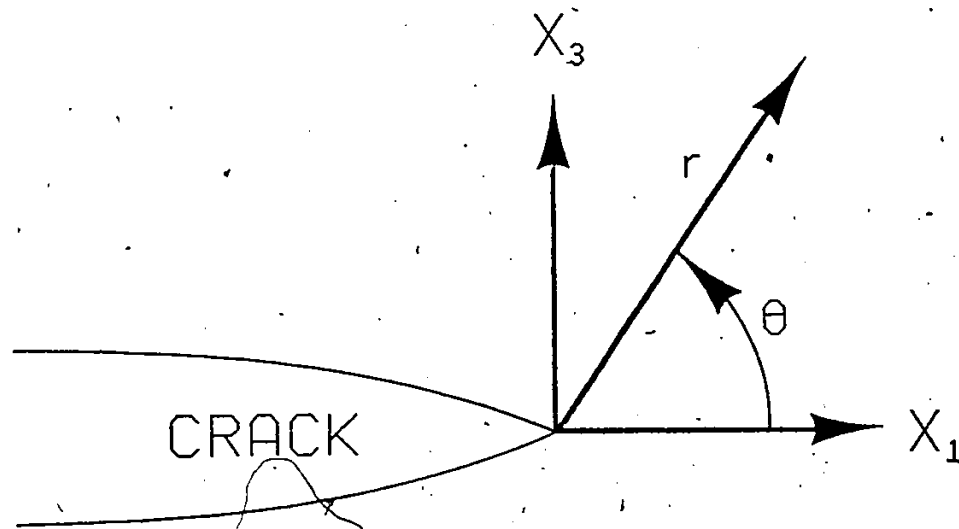
Figure 3(a). Coordinates at a crack tip.
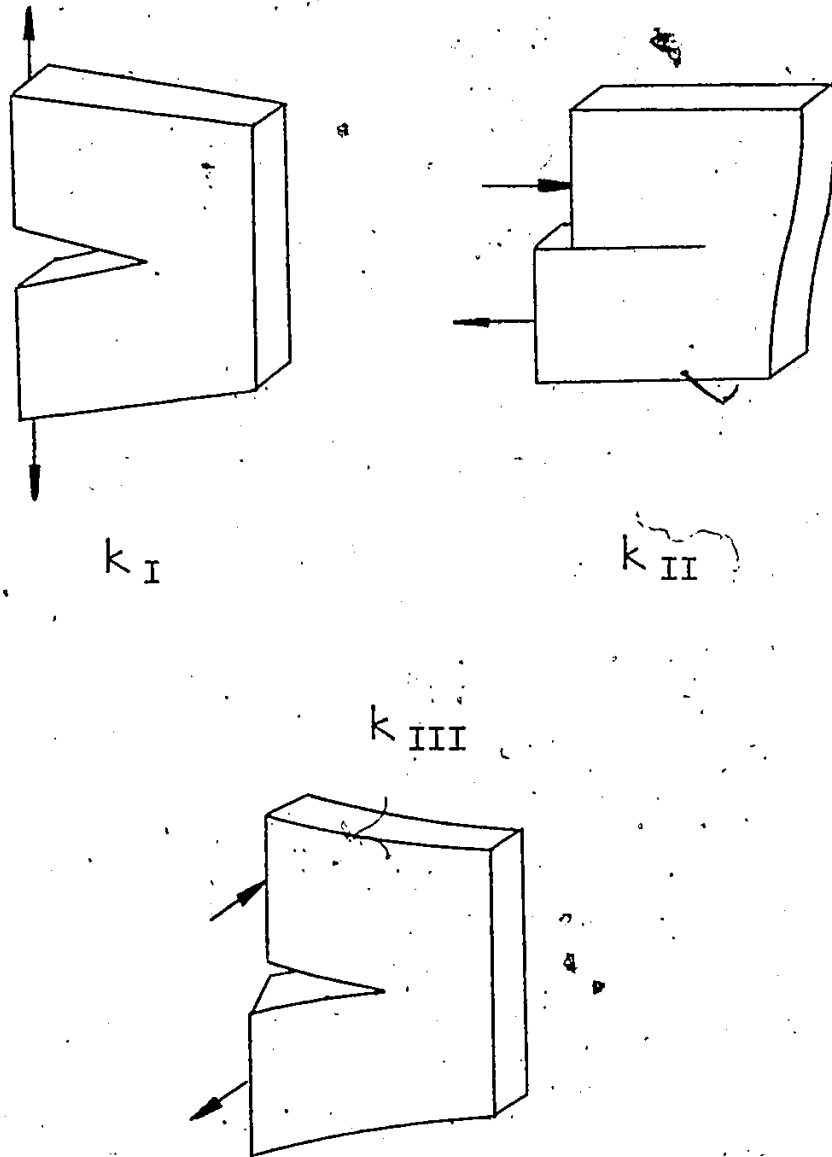
$$k_I \qquad k_{II}$$

$$k_{III}$$

Figure 3(b).   Effect of k_I, k_{II} and k_{III} type loads.

given by

$$\sigma_{ij} = k_I \frac{f_{ijI}(\theta)}{r^{1/2}} + k_{II} \frac{f_{ijII}(\theta)}{r^{1/2}}$$

$$+ k_{III} \frac{f_{ijIII}(\theta)}{r^{1/2}} \tag{1}$$

+ terms of order r^0 and higher

and the displacements are given by

$$u_i = k_I r^{1/2} g_{iI}(\theta) + k_{II} r^{1/2} g_{iII}(\theta)$$

$$+ k_{III} r^{1/2} g_{iIII}(\theta) \tag{2}$$

+ terms of order r and higher

where r and θ are defined in Fig. 3(a). The functions f and g are

independent of the loading condition far from the crack. The parameter

k_I characterizes that part of load which is attempting to pull the crack

faces apart; k_{II}, that part attempting to shear the crack faces parallel

to themselves; and k_{III}, that part attempting to shear the crack faces

out of their plane, as shown in Fig. 3(b).

Equation (1) predicts the stress at the crack tip to be

infinite. This is obviously physically incorrect and material and

geometrical non-linearities arise to limit the stress to a finite value

everywhere. It has been found, however, that the value of k

characterizes the fracture properties of materials with good accuracy

over a large range of loading conditions. If the non-linear behaviour

is concentrated in a small cylinder around the crack tip, equations (1)

and (2) still provide the dominant terms in the relations defining stress and displacement far from the crack tip, and the non-linear behaviour near the crack tip can also be shown to depend primarily on k, [4]. More elaborate relationships must be used to describe the fracture behaviour of specimens in which the material and loading conditions are such that the non-linear behaviour extends for a considerable distance from the crack tip, but for the work considered here, the value of k characterizes the system. Much more work has been done on loadings of k_I type than of the other two types. All the simulations done in the present work are concerned with k_I loadings only so the subscript I will be dropped hereafter and k will refer to k_I unless otherwise noted.

The basic premise of linear elastic fracture mechanics was first stated by Griffith, [5], and is that fracture will occur if the total energy of the system composed of the fracturing material and the applied loads decreases as the crack extends. This energy criterion can be stated in terms of k. The rate of change of the elastic strain energy and the potential energy of the loads per unit area extension of the crack is referred to as G. For a plane strain crack in a linear elastic, isotropic solid,

$$G = \frac{1 - \nu^2}{E} k^2 \qquad (3)$$

where, E = Young's modulus, and
ν = Poisson's ratio

The total energy change of the system per unit of new crack area is G plus the change in energy caused by the addition of two unit areas of free surface with surface energy, γ. The Griffith criterion states that fracture will occur when $G > 2\gamma$. Equation (3) allows the determination of the Griffith stress intensity factor, k_G, corresponding to $G = 2\gamma$. According to Griffith, the crack will extend if $k > k_G$, and recede if $k < k_G$. Receding cracks cannot usually be observed since crack face oxidation and the movement of the crack past heterogeneities in the material which act as pinning points prevent this. It can occaisionally be observed with very pure materials and inert atmospheres, however, [6]. The crack should be stable only for $k = k_G$ by the Griffith analysis. Other models indicate that the stress intensity factor for a propagating crack may differ from this value. To indicate this, the stress intensity factor for a propagating crack in a theoretical model or in experimental results will be called the critical stress intensity factor, k_c. In the Griffith model, $k_c = k_G$, but this may not always be true. Atomic level simulations predict two critical stress intensity factors. The crack will propagate when $k > k_+$, will recede when $k < k_-$, and is stable when $k_- < k < k_+$. In the remainder of the thesis, either k_- or k_+ may be referred to as the critical stress intensity factor, k_c, when there is no confusion about which is intended.

The area of microstructural fracture mechanics is concerned with the behaviour of the region in the material close enough to the crack tip that equations (1) and (2) begin to break down. There are several

levels on which this may be studied. The material may be considered to behave as an elastic-plastic solid and the stress field at the crack tip can be derived on this basis, [7]. On a finer scale, microstructural detail may be added to the analysis. For example, plasticity effects may be examined by considering the behaviour of individual Volterra dislocations and their interaction with the crack tip stress field, [8]. At the finest level, the material may be modelled to atomic detail, as described in the previous chapter.

One of the most interesting points to which microstructural theories address themselves is the competition between brittle and ductile fracture. Fracture by void nucleation and growth controlled by vacancy diffusion at high temperatures has been treated in [9] and [10]. In tough materials at lower temperatures, the classical view is that fracture proceeds by a ductile hole growth mechanism. As shown in [7] and [8], a crack in a material, treated as an elastic-plastic or rigid-plastic continuum, induces a maximum triaxial tension at a point slightly ahead of the crack tip, rather than at it as predicted by equation (1). A cavity is thought to nucleate at this point and the crack grows by necking of the material between the cavity and the old crack tip. This mechanism was discovered experimentally by Crussard, et al, [11]. Further details of this mechanism can be found in [12] and [13]. At still lower (cryogenic) temperatures, plastic flow is inhibited because dislocation glide speeds decrease as temperature falls. As a result, the fracture of many materials which are ductile at higher temperatures could be purely brittle, with atomically sharp

cracks, at low temperatures. Some controversy exists over this, however.

A simple argument on this point is that the tensile stress at the tip of an atomically sharp crack must be at the theoretical limiting tensile stress which the bonds of the material can support. If the maximum shear stress near the tip is calculated for this loading condition and compared to the theoretical limiting shear stress for the material, it may be argued that the crack will blunt by shearing if the limiting shear stress is reached before the limiting tensile stress. By this argument, most materials will fail to sustain atomically sharp cracks. Kelly, Tyson and Cottrell, [14], made detailed calculations for this theory and concluded that diamond, NaCl and silica could support atomically sharp cracks and fail by purely brittle fracture, but that most other materials could not. They recognized, however, that this argument is very elementary and that more detailed study should be made on this matter.

Because atomic level details of materials are difficult to derive in a direct way by experiment, more information on this point had to be provided by more elaborate theoretical treatment. This has recently shown that purely brittle fracture should be much more common than was previously considered. Computer simulation calculations which will be described fully below indicate that atomically sharp cracks should be able to exist in many materials. Other, purely theoretical work by Rice and Thomson, [15], have continued the work of Kelly, et al. Rice and Thomson use the linear elastic continuum mechanics stress

fields around crack tips and Volterra dislocations to examine their interaction. They find that a dislocation which has been punched out of a crack tip will be reattracted to the tip if it is within a critical distance, ξ_c, from the crack tip. ξ_c is derived from the macroscopic properties of the material. As for the crack tip behaviour described by equations (1) and (2), the Volterra stress field for a dislocation breaks down close to the dislocation center. The region in which this break down occurs is known as the dislocation core. Rice and Thomson propose that if ξ_c is less than the dislocation core size (or "core cut-off distance"), any dislocations which form will be repelled from the tip and the crack could spontaneously blunt. If ξ_c is greater than the core cut-off, dislocations which formed would be reattracted to the crack tip and blunting would not occur. On this basis, they find that many materials could maintain atomically sharp cracks. All the covalent and ionic crystals and some of the bcc and hcp metals studied are apparently stable with respect to this. The fcc metals appear unstable and should blunt. Interestingly, they find bcc α-iron to be a borderline case. This is the material which has been most studied by computer simulations with, so far, inconclusive results. Rice and Thomson recognize, however, that "a complete resolution of this problem must rely on a discrete lattice calculation involving realistic non-linear force fields", [15].

If this question of brittle-ductile competition can be answered, it would permit a much deeper understanding of fracture properties. Obviously, the theoretical and physical descriptions of fracture by

atomically sharp cracks and by the ductile hole growth mechanism
described above are very different and it is important to know when each
are applicable. Thomson, [16], has proposed a crack model in which both
are necessary. He argues that even if fracture appears to be taking
place by ductile failure, the discrete nature of the dislocation
processes which cause the associated plastic flow mean that, at the very
finest (atomic) scale, the crack tip could still be brittle with slip
being concentrated on localized slip bands which intersect dislocation
sources. These would be necessary to produce plastic flow if the crack
tip itself could not spontaneously generate dislocations. The
seperation between dislocations, even in a very highly strain hardened
metal averages greater than about 15 nm (1 nm = 1.E-9 m) and can be
10000 nm in annealed metals, [17]. This can be seen to be much larger
than a typical lattice parameter distance of 0.286 nm for bcc α-iron.
This indicates that, unless the crack tip itself can generate
dislocations, the crack will behave in an atomically sharp fashion as a
result of the discrete nature of the plastic effects. Sufficiently far
from the crack tip, the stresses may be averaged over large enough
regions of the material that this discrete nature can be ignored and
elastic-plastic continuum theory can be applied. Still farther from the
tip, the stresses fall into the elastic range and equations (1) and (2)
again describe the situation. Figure 4 is a schematic illustration of
the Thomson model.

Although not formally presented in the form of Rice and
Thomson's theory, [15], the interaction of the crack tip stress field

STRESS

DISCRETE | PLASTIC | ELASTIC
ATOMIC | CONTINUUM | CONTINUUM
REGION | REGION | REGION

X_1
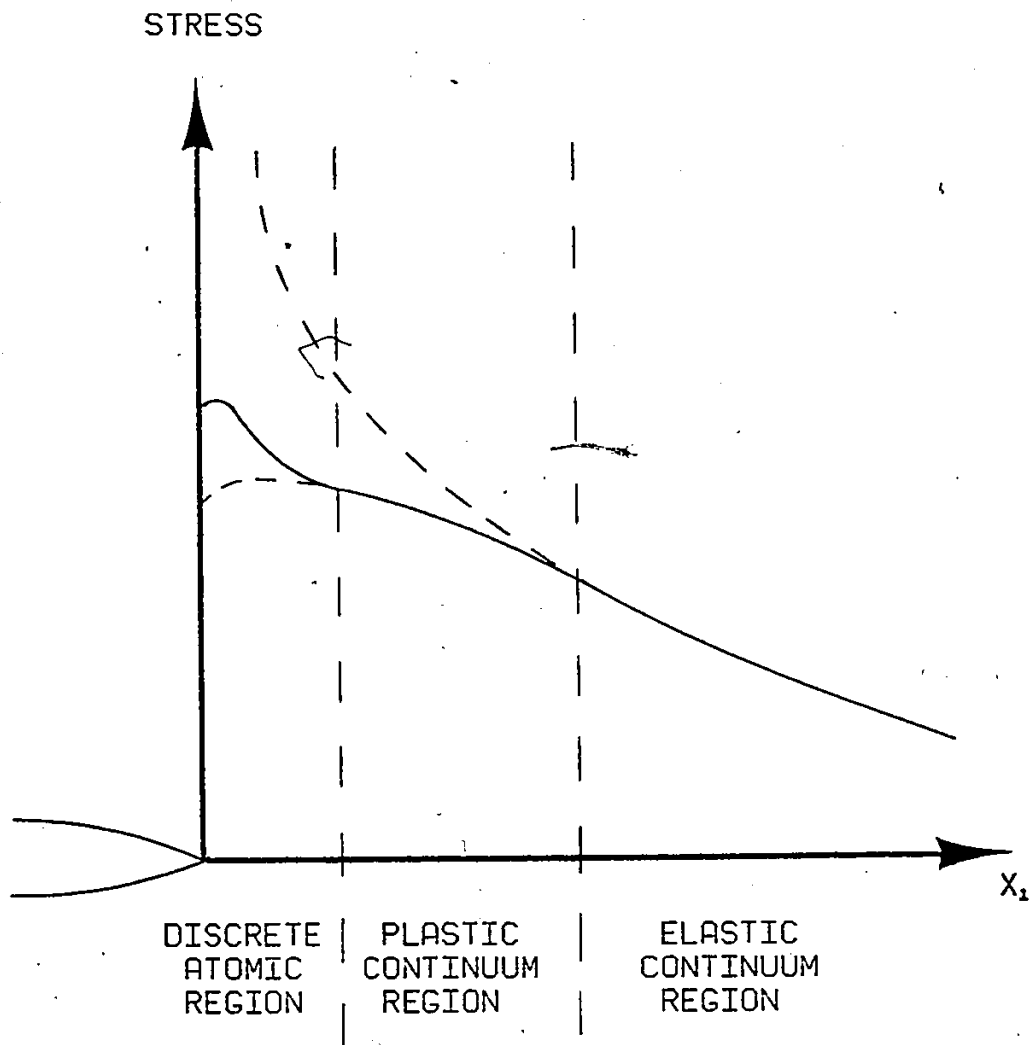
Figure 4.   Schematic illustration of Thomson's model, [16].
             In the discrete atomic regions, the dislocation
             population is too small for the material to behave
             plastically and the forces can approach the ultimate
             bond strengths.

with a cloud of dislocations has been the basis of several theories which attempt to predict the most likely cleavage plane of crystals. Ayres and Stein, [18], calculated the resolved shear stress on all slip planes around a crack in a bcc metal for various cleavage planes. By assuming that cleavage was most likely on the plane for which the resulting dislocation activity is minimized, they could correctly predict (001) plane cleavage in bcc crystals. They also predict that the [Ī10] crack line direction cleavage should be easier than [010]. Pharr et al, [19], have recently criticized some details of the Ayres-Stein treatment but a modification which they propose does not seem to provide better results. The authors of these theories apparently consider that the dislocations are pre-existing, ie. not punched out of the crack tip. Cleavage planes can also be predicted theoretically by means of direct bond counting. Tyson, [20], has done this but there are some significant discrepancies between the predictions of this theory and experimental results.

The work of this thesis is concerned with some aspects of the behaviour of the region governed by the atomically sharp crack properties in a model such as that of Fig. 4. It considers the most likely cleavage planes, the easiest fracture directions on these planes, and the question of the possibility of the crack blunting by dislocation emission by means of a discrete atomic simulation. The material studied is a bcc crystal with many properties chosen to correspond with those of α-iron. The model is still incomplete so that no final conclusions can be reached, but the analysis is carried out to greater detail than had

been done in any previous work and some very interesting behaviour was
observed.

3.2 Microstructural Fracture Mechanics - Experimental

Many of the papers discussed above contain, or refer to,
experimental results to illustrate the theories proposed. These will
not be discussed in further detail here since they bear only indirectly
on the work in this thesis. Some experimental studies which more
directly concern themselves with the work will, however, be discussed in
this section. The area considered is the fracture properties of single
crystal bcc metals, especially with regard to the competition between
brittle and ductile fracture and the effect of the direction of the
crack line of two dimensional cracks -- points which are studied in this
thesis.

As stated above, the model material chosen for the present study
is similar to bcc α-iron. This was chosen not only because of its
technological importance, but also because the interatomic potential on
which it is based (which will be discussed more fully below in
section 3.4) has taken on the status of a standard which is being
studied in considerable depth by many researchers. It has some
properties which are in disagreement with those of iron, however, so
that it cannot be thought of as a true model of iron. It should,
rather, be considered a model material which can be studied by computer
simulation, as real materials can be studied experimentally, in order to
determine the relation between their macroscopic and microscopic

properties. Thus, it cannot be expected to reproduce the behaviour of iron exactly, but, on the other hand, it should show results which can be compared, at least qualitatively, with the properties of bcc materials in general. This view of the role of computer simulation is also useful since the number of experimental results which can be directly compared to the model results for any one material is quite small. This is a consequence of the difficulty of performing experiments which are able to give a direct indication of atomic scale events. Theoretical and computer simulation calculations are proceeding up from this level, while experimental observations are working down to this level, but at the moment they can be compared in only a few points. Considerably more work is needed in these areas before the topic can be considered understood.

Whether or not a material fractures in a perfectly brittle fashion with an atomically sharp crack can be determined experimentally by, for example, measuring the load needed to cleave a crystal of the material, obtaining the corresponding surface energy from the method described with equation (3), and comparing this to the true, thermodynamic surface energy measured by other means. If significant non-linear behaviour has occured and the crack has not propagated in a truely brittle fashion, it will be found that the apparent surface energy measured by cleavage is much higher than the true surface energy. The difference represents the irreversible work done by the crack, for example, the work involved in moving dislocations or in generating a cloud of microcracks around the macroscopic crack tip. The true surface

energy may be measured by several means. One possibility is to measure the creep properties of a wire of material at high temperatures. The surface tension and corresponding surface energy of the material may be obtained from this, [21]. Other ways of estimating the likelihood of brittle fracture involve examining the appearance of the crack face and the shape of the load-displacement curve for the cracked specimen.

Experimental results appear to indicate that α-iron behaves in a perfectly brittle fashion at low temperatures. Most work has been done on an iron - 3% silicon alloy apparently because of the ease with which large single crystals of this material can be grown. This is a bcc crystal in which some silicon atoms replace iron atoms in the α-iron lattice. Cracks in these studies always propagated on (001) type planes. Gilman, [22], found the apparent surface energy of this material in cleavage tests at various temperatures. This was greater than 240 J/m^2 at 195 K, 25 J/m^2 at 77 K, and 1.36 J/m^2 at 23 K. The value of 1.36 J/m^2 is based on only one specimen but it is close to the true, thermodynamic surface energy of iron which is about 2 J/m^2, [23]. There is obviously a great deal of extra work, representing plastic deformation at 195 K. By examining the crack surface appearance, Gilman concluded that most of the excess work in the 77 K specimens was due to the formation of twins around the crack rather than dislocation processes. Twinning was apparently also inhibited at the lowest temperature studied.

Tetelman and Robertson, [24], have also studied the fracture properties of this material experimentally. They induced fracture by

charging the crystals with hydrogen. This then was precipitated out of the crystal and the resulting gas pressure formed and expanded very small internal cracks. They found that at temperatures greater than 1000 K, a great deal of dislocation activity could be observed involving [111] dislocations around (001)[110] cracks (2 dimensional cracks with crack plane (001), and crack line direction [110]). They could not determine whether the dislocations were emitted by the crack tip or were from surrounding dislocation sources. By examining the load-displacement curve and the appearance of the crack face, they concluded that fracture was completely brittle at 77 K, but they did not study fracture at this temperature in as great detail as did Gilman, [22]. More evidence for the twinning process described by Gilman was found by Berry, [25]. He examined the appearance of the crack faces in iron - 3% silicon crystals fractured at 77 K and concluded also that twinning on (112) planes was the main mode of inelastic deformation. In conclusion, then it appears that iron-silicon behaves in a brittle fashion at very low temperatures (23 K from Gilman). At higher temperatures (77 K) some inelastic deformation is observed, but it is mainly due to twinning. At still higher temperatures (room temperature and above) the apparent surface energy from Gilman and the direct observation of dislocations by Tetelman and Robertson indicate that a great deal of inelastic behaviour occurs including dislocation processes. Whether these dislocations are emitted by the crack tip or are from surrounding dislocation sources has not been determined.

Another bcc metal which has been studied to some extent is
tungsten. Hull and Beardmore, [26], studied the speed of propagation of
cracks in tungsten single crystals by means of the shape of Wallner
lines and river lines on the fractured surfaces. Wallner lines are
ripples in the crack surface caused by the interaction of the moving
crack tip with passing acoustic waves. The acoustic waves are generated
by the same moving crack as it passes surface or internal flaws or
heterogeneities in the crystal. The speed of the crack tip can be
determined from these lines by the method described in [26]. River
lines are steps in the crack faces. They probably represent the lines
of the twins described in [25]. They may be used to determine the crack
speed in a similar manner to that for the Wallner lines. Hull and
Beardmore were able to measure speeds by Wallner lines on crystals
fractured at low temperatures (20 K and 77 K) since obscuring river lines
were rare. This indicates that the twinning process was suppressed at
low temperatures for this material as for iron-silicon. River lines
were more easily observed on crystals fractured at higher temperatures
(77 K, 201 K and 300 K) and these were used to measure crack speeds for
these crystals. The cracks always propagated on (001) planes. Crack
speeds were measured for cracks having crack lines in [010] and [110]
directions. The results appear to indicate that for the higher
temperature crystals, the [010] crack was fastest. The ratio of [110]
speed to [010] speed ranged from about 0.5 to 1 in various specimens.
For the lower temperature crystals, however, it appears that the [110]
crack may have been faster. Of two specimens fractured at 20 K, one
showed the [110] crack to be about twice the speed of the [010], the

other showed them to be about the same. The second specimen was fractured accidentally, so this result may not be as reliable as the first. At 77 K, some results showed [010] fastest, some [110] fastest. It appears then, that at high temperatures, plasticity effects become important and [010] cracks are faster than [110]. At low temperatures, plasticity effects are reduced and [110] cracks are faster. It can be seen from the above detailed description, however, that there is a great deal of scatter in experimental results in this area, and that the number of results which are available is usually too small for meaningful statistics to be drawn. This is a consequence of the difficulty of performing experiments which require the production of pure, single crystals, cryogenic temperatures, stiff testing machines and the examination of microscopic properties of the crack faces. It must, thus, be expected that any agreement between theory and experiment can be only tentative at the present time.

Further experimental results on tungsten are provided by Liu and Bilello, [27]. They also fractured tungsten single crystals at 77 K and in the two crack directions and measured the apparent surface energy. Their initial cracks were created by electric spark discharge. Their results are shown in Table 1. Again the large scatter in the results is obvious. Liu and Bilello comment on the variation of initial crack shapes from the long plane strain geometry most common with the large cracks, to semicircular, most common with the small ones. This is one obvious cause for the scatter in the results and may be obscuring any true material properties. Cordwell and Hull, [28], performed similar

Table 1. Experimental Results of Liu and Bilello, [27], for tungsten.

Crack Direction	Crack Length (μm)	Fracture Stress (MPa)	Critical Stress Intensity Factor ($\mathrm{MNm}^{-3/2}$)
[010]	98	195	2.00
"	204	149	2.21
"	160	133	1.75
"	206	99	1.48
"	300	96	1.73
"	216	82	1.25
"	190	70	1.01
"	494	43	1.00
[110]	190	60	0.86
"	200	69	1.02
"	150	51	0.65

Average critical stress intensity factor is

1.554 $\mathrm{MNm}^{-3/2}$ for the [010] direction, and

0.843 $\mathrm{MNm}^{-3/2}$ for the [110] direction,

corresponding to surface energies of

8.6 $\mathrm{J/m}^2$ for the [010] direction, and

2.5 $\mathrm{J/m}^2$ for the [110] direction.

The above table assumes isotropy with elastic constants $E = 0.409$ TPa,

and $\nu = 0.278$, [15].

experiments, but for the [010] direction only. They give a further

discussion of the effects of crack shapes. Liu and Bilello found

evidence of dislocation activity around the crack tip. They could not

determine whether or not the crack was atomically sharp, however. They

examined their results in the light of a theory similar to that of Ayres

and Stein, [18], in order to calculate the effects of the dislocation

activity on the values of apparent surface energy which they measured.

They estimated from this theory that the true, thermodynamic tungsten

surface energy is about 3 J/m². This compares with estimates ranging

from 1.7 J/m², [28], to 7.8 J/m², [29], by other workers using other

methods. Table 1 shows calculated values for critical stress intensity

factor and corresponding surface energy obtained by ignoring any

correction for dislocation activity and assuming that the geometry is

that of a long crack in plane strain. The effect of the geometry of the

crack could be as much as 50% on these values. In any case, it is clear

that the effect of crack tip plasticity is fairly small at this

temperature since the apparent surface energy calculated in this manner

is close to the true thermodynamic value. It would be expected that its

effect would be even smaller at lower temperatures. When the critical

stress intensity factors of Table 1 are averaged for the two crack

directions independently and used to calculate a surface energy, the

[010] average is 8.6 J/m², while the [110] is 2.5 J/m². Many effects

could be responsible for this. It may be a random result of the

experimental errors. The number of results available is insufficient

for any statistical certainty to be possible for these values. The

effect of crack geometry may be important. Liu and Bilello indicate

that the initial crack shapes were the same in each direction but the
size effect mentioned earlier may have some significance. The effect
may be due to the different slip systems available in the two cases,
resulting in different corrections to the surface energy for plasticity
effects. Alternatively the differences, if real, could be due to a real,
crystallographic effect at the atomic level of the crack. The work
presented later in this thesis predicts such an effect. It must be
emphasized, however, that experimental verification of such a result
must be considered very tentative at this time.

Both Hull and Beardmore, [26], and Liu and Bilello, [27],
comment on the different appearance of the fracture surface for the two
crack line directions, especially at higher temperatures. This is
probably due mainly to the different plasticity processes operable in
the two cases. No quantitative information can be derived from this
which pertains to the present work, but it does provide another
indication that the crystallographic direction of the crack is important
in determining its macroscopic behaviour.

In summary, it appears that experimental results indicate that
fracture in single crystal iron-silicon and tungsten, taken as sample
bcc metals, occurs on (001) planes, that both behave in a purely brittle
fashion at very low temperatures, and that there are differences in
fracture properties between cracks having crack line directions of [010]
and [110]. The [110] crack appears to propagate at a lower stress
intensity factor than the [010] and to propagate at a faster speed at
very low temperatures. The experimental results from which these

conclusions are drawn, however, have a great deal of uncertainty. Further experimental work must be performed before they can be confidently accepted. Nevertheless, the model calculations which are described later in this thesis will be compared to them and this will indicate that there is general agreement between these two sets of results.

3.3 Discrete Atomic Simulation - General

In this section, a brief review will be made of the broad area of discrete atomic computer simulation of materials. This will provide an indication of the range of problems to which this basic method of modelling is applicable and of the type of results which can be expected in each area. A more detailed, but older, review can be found in [30], by Beeler. A great deal of work in the area of the simulation of defects in solids is reported in the conference proceedings, [31].

The basic philosophy of computer simulation of materials with atomic detail may be stated as follows. A material model is constructed which consists of atoms interacting with each other by means of an interatomic potential. This model is then examined by computer simulation to observe its behaviour. The correspondence between the model and a real material may be close. In this case, great pains are taken to produce a potential which has a close similarity to that which actually exists for the real material being simulated, and the behaviour of the computer model should, then, reproduce the behaviour of the real material accurately. On the other hand, a simpler, more general

potential may be chosen which does not have a close resemblance to that for any real material, but which can be expected to possess some of the properties common to a range of real materials. In this case, the computer simulations are thought of as experiments performed on these model materials which have the great advantage of being much more easily observed than real materials. Studies of this type shed light on the general relationships that exist between the microscopic and macroscopic properties of materials of a class similar to the model material. Models of this type may also be used to test theories which propose to explain the properties of real materials on the microlevel such as that of Rice and Thomson, [15], described above. If the theory is applicable to a wide range of real materials, it should also be applicable to the computer model material and it is usually easier to test on these. At the present state of the art, accurate interatomic potentials are difficult to derive for most real materials, so that computer simulations tend more toward the latter than the former type.

One of the earliest applications of computer modelling was in the study of liquids. Rahman, [32], studied a model of liquid argon using a Lennard-Jones interatomic potential (the properties of the various interatomic potentials which have been used will be discussed below). He found good agreement with experimental values for the self-diffusion coefficient and its variation with temperature. The position pair distribution function also showed reasonable agreement with that derived from x-ray data. The inert gas liquids are relatively simple to model. More difficult is a liquid such as water. Rahman and

Stillinger, [33], have studied a model of liquid water using a very
special interatomic potential which took account of the polar properties
of the water molecule and could therefore account for their rotational
as well as translational degrees of freedom. They could obtain good
agreement with experimental data for the position distribution function.
The self-diffusion coefficient was in error by about 50%. Dipole
relaxation times appeared to be within the range of the error in nuclear
magnetic resonance experiments. Considering the complexity of molecular
interactions in water, the overall results indicated that the method was
useful in the study of such liquids but that more work would be needed
to derive accurate interatomic potentials.

As with liquids, the rare gas solids are also relatively easy to
model. Dickey and Paskin, [34], modelled solid krypton and neon
lattices. They observed thermal vibrations of the crystals and derived
statistical mechanics properties of the lattices from the results. They
found that the normal mode distribution showed good agreement with
experiment and with other theories that can be applied at low
temperatures. Comparison of dispersion curves with those obtained from
neutron diffraction studies showed reasonable agreement for krypton but
were less acceptable for neon. Quantum effects may have obscured the
results.

Johnson and White, [35], have modelled the surfaces of metal
crystals. The results appear reasonable and are in general agreement
with calculations by other methods but experimental results are

insufficient at the present to give an accurate evaluation.

Johnson, [36], has studied interstitials and vacancies in α-iron. He gives computer predicted structures for the stable interstitials and di-vacancies. The interstitial migration energy appears reasonable compared to experimental values.

Considerable work has been done on the modelling of dislocations in solids. The classical theory of dislocations may be found in Hirth and Lothe, [37]. Doyama and Cotterill, [38], examined the [110] edge dislocation in copper, an fcc crystal, by computer simulation. They found appreciable out of plane displacements not predicted by continuum theory. The dislocation core energy was comparable to experimental values. The same authors also studied a screw dislocation, [39], and obtained similar results. Chang and Graham, [40], modelled the [111] edge dislocation in bcc α-iron. They made an estimate of the Peierls barrier for dislocation motion by moving the dislocation in a somewhat artificial fashion. They estimated the barrier to correspond to a stress of 0.54 MPa, compared to an experimental value of 0.45 to 0.48 MPa. Chang, [41], also studied the [111] screw dislocation and found an asymmetry in the Peierls barrier similar to that observed experimentally. Bullough and Perrin, [42], studied the [111] and [100] edge dislocations in α-iron. The core energy they predict is in the range of the experimental data available. They find that the appearance of the atomic motions during the relaxation process indicates that the [100] edge may act as a nascent crack in the material. This was confirmed with another model by Gehlen, et al, [43]. Improved models

with flexible boundary schemes followed (the next section describes
these boundary schemes in detail). Gehlen, et al, [44], found that
there was an elliptical expansion associated with the [100] edge
dislocation and that this might be detectable by a suitable experiment
although this has not been done for iron. Hoagland, et al, [45],
modelled dislocations in potassium chloride. With a flexible boundary
scheme, they could move the dislocation by the application of an
external stress, something which had not been possible previously, and
thus could get an estimate of the Peierls barrier based on a more
physically acceptable argument than that used by Chang, [40,41]. The
agreement with experiment was reasonable although there was some
difficulty in pinpointing the value of the barrier with the model.

Some work has been done on the simulation of grain boundaries.
Hasson, and Goux [46], studied the energy, entropy and likely
orientation of grain boundaries in aluminum and found reasonable
agreement with experiment. Johannesson and Tholen, [47], studied the
mechanics of grain boundary sliding. A review of grain boundary studies
can be found in [48].

The effect on solids of nuclear radiation and shock waves has
also been studied by computer simulation. Gibson, et al, [49], obtained
threshold energies, damage zones and information on the types of defects
generated in copper by nuclear radiation. They claimed the results
appeared reasonable but detailed experimental information was not
available for comparison. Paskin and Dienes, [50], studied the effect
of a shock wave passing through an inert gas solid. They found that the

temperature rise at the shock front was higher than expected indicating
that the transfer of kinetic energy to the material was more efficient
than that possible by adiabatic compression heating. Comparison of the
pressure-volume relationship at the shock front with the experimental
values for solid neon appeared acceptable.

Computer simulation studies applied to various defects could
eventually shed light on many aspects of material behaviour:

1) Accurate knowledge of defect core structure, energy and entropy
   could allow the determination of the equilibrium concentration of
   defects in materials produced under various conditions. This is
   important in the production of very pure, nearly perfect crystals
   for use in electronics components, for example. There is some
   evidence that the stress induced in crystals by gravity while they
   are growing can affect defect concentration, [51]. This is one of
   the arguments in favour of space manufacturing facilities.

2) Models which indicate the conditions under which defects will move
   through the lattice can allow the calculation of slow crack growth
   effects, [72], for example.

3) Volume expansion associated with dislocations shown by these
   models, [44], could result in a hydrostatic stress dependence for
   yielding.

4) Studies of damage caused by nuclear radiation, [49], is important for nuclear engineering.

5) The generation and scattering of acoustic waves by defects is important to non-destructive testing methods such as acoustic emission. The level of knowledge of the microstructural significance of an acoustic emission event seems quite elementary at the present time. Estimates of the number of dislocations in motion which could produce a detectable acoustic output range from one, [52], to several hundred, [53]. Atomic simulation studies could illuminate this topic.

6) The interaction of defects is a very important subject. For example, it would be interesting to discover the conditions under which a dislocation would be emitted from a crack tip since this affects brittle-ductile transition properties. Work in this area has been limited because of the difficulty of constructing adequate models.

This section has provided a broad discussion of the area of atomic level computer simulation of materials in order to indicate the range of problems which can be studied with this technique. A more detailed discussion of the simulation of cracks has been postponed to later in this chapter. This allows, first, a discussion of interatomic potentials and boundary condition schemes for simulation modelling.

3.4 Discrete Atomic Simulation - Interatomic Potentials

This section provides information on the interatomic potentials which have been used in computer simulations.

The force-position relation existing between the atoms in a fluid or crystal may be described by an interatomic potential, ϕ. In the most general case, ϕ is a function of all positions,

$$\phi = \phi(\bar{r}_1, \bar{r}_2, \bar{r}_3, \ldots, \bar{r}_n) \tag{4}$$

where $\bar{r}_i$ is the position vector of atom i, and there are a total of n atoms in the complete crystal. The force on atom i is then given by

$$\bar{F}_i = \frac{\partial \phi}{\partial \bar{r}_i} \tag{5}$$

Even if a formula could be determined to describe this force-position relation, it would undoubtedly be too complex for use in simulations such as the ones being described here because of limitations on computer cost. As a result, simplifications have to be made to describe the bonding behaviour. The bonds for many materials, including the inert gas solids and most metals, are generally taken to be pairwise bonds with no bending stiffness. They thus behave as a set of springs supporting axial forces only connecting the mass points representing the atoms. For this case, the total force on atom i, $\bar{F}_i$, is the sum of a set of forces, $\bar{F}_{ij}$, where j extends over all neighbours of i and

$$\overline{F}_{ij} = \frac{\partial \phi(r)}{\partial r} \frac{\overline{r}}{r}$$ (6)

where $\overline{r} = r_i - r_j$, and $r = |\overline{r}|$. The function $\phi(r)$ is the interatomic

potential for a single bond. Because of its restriction to atom pair

bonding and the fact that it is a function of r only (and, therefore,

results in radial forces only) it is referred to as a pairwise, central

potential. In order to contain computer costs, it is taken to have a

finite cut-off distance. Typical cut-off distances which have been used

allow the inclusion of nearest neighbours only in the noble gas solids,

the fcc metals such as copper, and the hcp metals such as zinc; up to

sixth nearest neighbours in the bcc alkali metals; and up to second

nearest neighbours in bcc α-iron. Simulations of liquids and gases

generally use similar potentials to those described above, ie. pairwise,

central potentials.

The relation between the first order elastic constants and the

interatomic potential was first developed by Fuchs, [54], for various

crystal structures. Johnson, [55,56], gives formulas for the second

order elastic constants. These have not been used extensively in

interatomic potential generation, but should find application in the

future. The first order elastic constants for a material with the

symmetry properties of a cubic crystal may be defined as, [57],

$$\begin{Bmatrix} \sigma_1 \\ \sigma_2 \\ \sigma_3 \\ \sigma_4 \\ \sigma_5 \\ \sigma_6 \end{Bmatrix} = \begin{bmatrix} C_{11} & C_{12} & C_{12} & 0 & 0 & 0 \\ C_{12} & C_{11} & C_{12} & 0 & 0 & 0 \\ C_{12} & C_{12} & C_{11} & 0 & 0 & 0 \\ 0 & 0 & 0 & C_{44} & 0 & 0 \\ 0 & 0 & 0 & 0 & C_{44} & 0 \\ 0 & 0 & 0 & 0 & 0 & C_{44} \end{bmatrix} \begin{Bmatrix} \varepsilon_1 \\ \varepsilon_2 \\ \varepsilon_3 \\ \varepsilon_4 \\ \varepsilon_5 \\ \varepsilon_6 \end{Bmatrix} \qquad (7)$$

provided that the x_1, x_2, x_3 axes are along the symmetry axes of the crystal. In equation (7), $\sigma_1 = \sigma_{11}$, $\sigma_2 = \sigma_{22}$, $\sigma_3 = \sigma_{33}$, $\sigma_4 = \sigma_{23}$, $\sigma_5 = \sigma_{31}$, $\sigma_6 = \sigma_{12}$ in the more usual notation. The strains, ε_i, are defined similarly, with engineering shear strain used. If

$$C_{11} = C_{12} + 2C_{44} \qquad (8)$$

then the material is isotropic. This is not usually the case for real materials.

The Cauchy relation is defined as

$$C_{12} = C_{44} \qquad (9)$$

It may be shown that central potentials in crystals in which every atom is a center of symmetry and which is under no external hydrostatic pressure to maintain non-equilibrium interatomic bonds, lead to the Cauchy relation. This also is not generally true of real materials.

The relation between the elastic constants and the interatomic potential for the case of a bcc crystal in which first and second nearest neighbour interactions by central, pairwise potentials only are

considered. (the case studied in this thesis) is, [36],

$$C_{11} - C_{12} = \frac{2}{3r_2} \left(\frac{6}{r_1} \phi'_1 + 3\phi''_2 + \frac{3}{r_2} \phi'_2 \right)$$

$$C_{44} = \frac{2}{3r_2} \left(\phi''_1 + \frac{2}{r_1} \phi'_1 + \frac{3}{r_2} \phi'_2 \right) \qquad (10)$$

$$B = \frac{2}{3r_2} \left(\phi''_1 - \frac{2}{r_1} \phi'_1 + \phi''_2 - \frac{2}{r_2} \phi'_2 \right)$$

where the primes indicate differentiation with respect to r, subscript 1 refers to evaluation at the nearest neighbour distance, and subscript 2 at the second nearest neighbour distance. B in equation (10) is the bulk modulus for the material,

$$B = (C_{11} + 2C_{12})/3 \qquad (11)$$

As stated above, the Cauchy relation, (9), must hold for such a material unless it is under an artificially applied external pressure which enables the interatomic bonds to be out of equilibrium at the perfect crystal position. The pressure required to maintain equilibrium of such a crystal is

$$P = (C_{12} - C_{44})/2 \qquad (12)$$

There are many possibilities for the detailed form of the function $\phi(r)$. One of the earliest used, [49], was the Born-Mayer potential. It is of the form

$$\phi(r) = A \ e^{(r-r_o)/\rho} \tag{13}$$

where A, r_o and ρ are parameters adjusted to fit known properties of the material such as the elastic constants. The force generated by this potential is always repulsive and requires the addition of hydrostatic pressure to maintain equilibrium of the lattice. A more commonly used potential is the Lennard-Jones potential,

$$\phi(r) = A \ r^{-m} - B \ r^{-n} \tag{14}$$

where A, m and n are parameters chosen as described above. The most commonly used values of m and n are 12 and 6, respectively. This form of equation (14) reproduces the theoretically exact behaviour of the inert gas solids at large distances and has been used extensively in these studies, [32,34,50]. It has occaisionally been used to model metals, usually with different values of m and n. The Morse potential has been used more often for metals. It is of the form

$$\phi(r) = A \ \{ \ e^{-2\alpha(r-r_o)} - 2e^{\alpha(r-r_o)} \ \} \tag{15}$$

where A, α and r_o are the adjustable parameters. This form has some theoretical basis for its large distance behaviour when applied to metals. Girifalco and Weizer, [58], give Morse potential parameters for a wide range of metals derived by fitting to the energy of vaporization, lattice parameter and bulk compressiblity.

The type of potential most often used for metals in computer simulations is a purely empirical potential, usually a polynomial, fit

to various known material properties. Johnson, [59], presented two

potentials for iron based on this approach. Each consists of three

splines (3rd order polynomials) applicable over different ranges of r.

Table 2 gives the formulae of the two Johnson potentials. Both go to

zero between the second and third nearest neighbour distances. Both are

fit to first order elastic constant data. The Johnson-II potential is

fit to the full value of the elastic constants of iron. Since these do

not obey the Cauchy relation, (9), an external stress given by (12) is

required to maintain the crystal in equilibrium. The Johnson-I

potential has been fit to altered values of the elastic constants which

do obey the Cauchy relations and eliminate the need for the external

pressure. This simplifies the modelling procedure. The Johnson-I

potential appears to have taken on the status of a standard potential

for model simulations. It has been used extensively for the study of

interstitials and vacancies, [36,59], dislocations, [42,43], and cracks,

[65,68,76]. It can thus be considered a model material of the second

type described in the previous section. Because of this status, the

Johnson-I potential was chosen for the work in this thesis even though

it does not model real α-iron exactly. Figure 5 shows the Johnson-I

potential. The general shape of this potential function is similar to

that of the other potentials discussed above although the exact

numerical values differ of course. Also shown in Fig. 5 are the bond

force, $F = \partial\phi/\partial r$, and spring constant, $s = \partial^2\phi/\partial r^2$, as functions of r.

The empirical potential approach seems to offer the best method

of deriving these functions at the present. Potentials for a number of

Table 2.   Johnson Interatomic Potentials, [59].

Potential is given by $\phi(r) = A(r-B)^3 + Cr + D$ with constants given below.

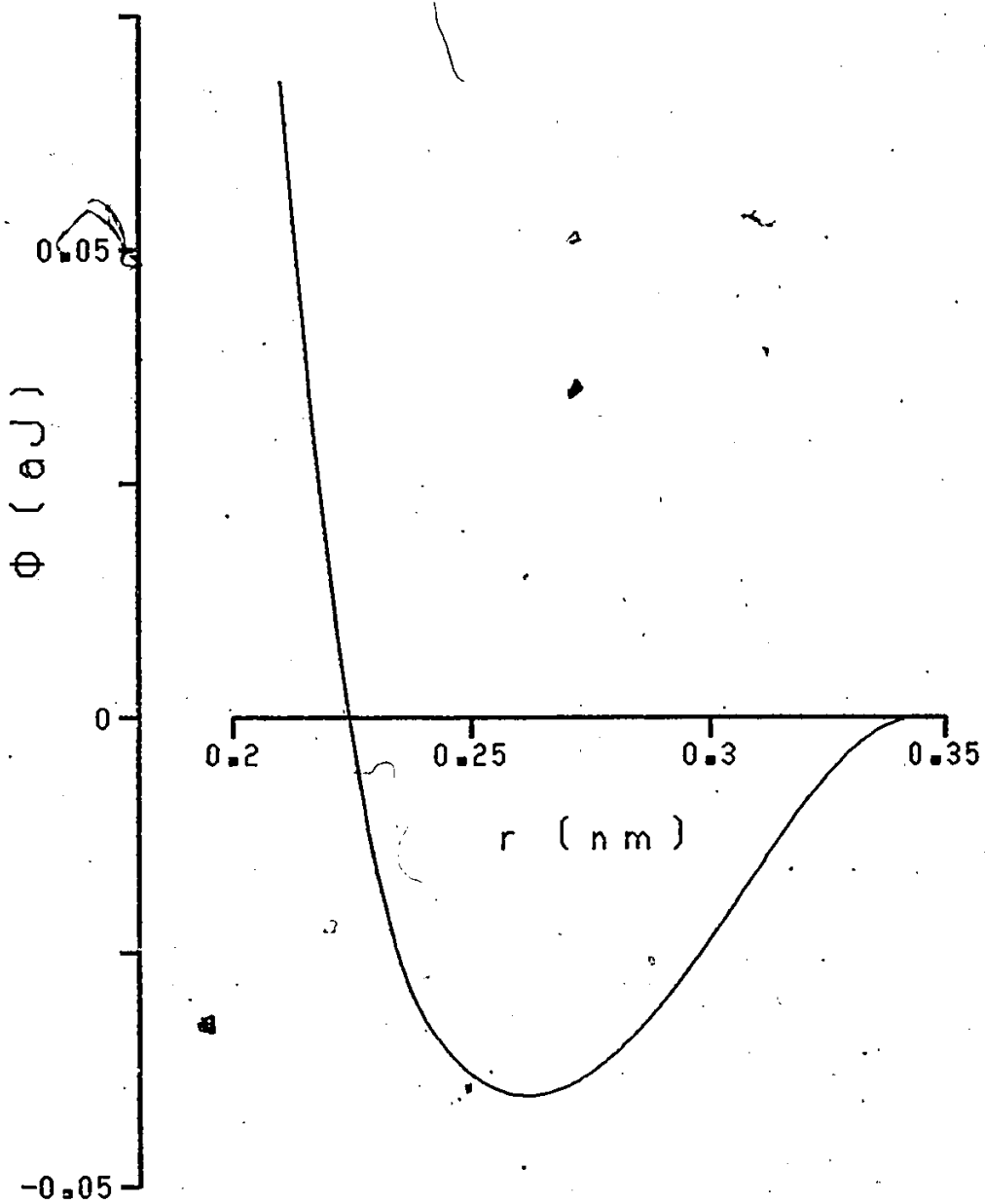| Potential	Range (nm)	A (aJ/nm³)	B (nm)	C (aJ/nm)	D (aJ)
I	<0.24	-351.82	0.30979	4.33215	-1.19139
I	0.24-0.3	-102.41	0.31158	0.76559	-0.25338
I	0.3-0.344	-178.64	0.30664	0.74800	-0.24800
I	>0.344	0	0	0	0
II	<0.24	-756.03	0.25699	-0.63393	0.12962
II	0.24-0.3	-142.09	0.30833	0.70114	-0.23241
II	0.3-0.344	-169.41	0.30698	0.69637	-0.23096
II	>0.344	0	0	0	0

Figure 5(a).   Johnson-I potential, [59].
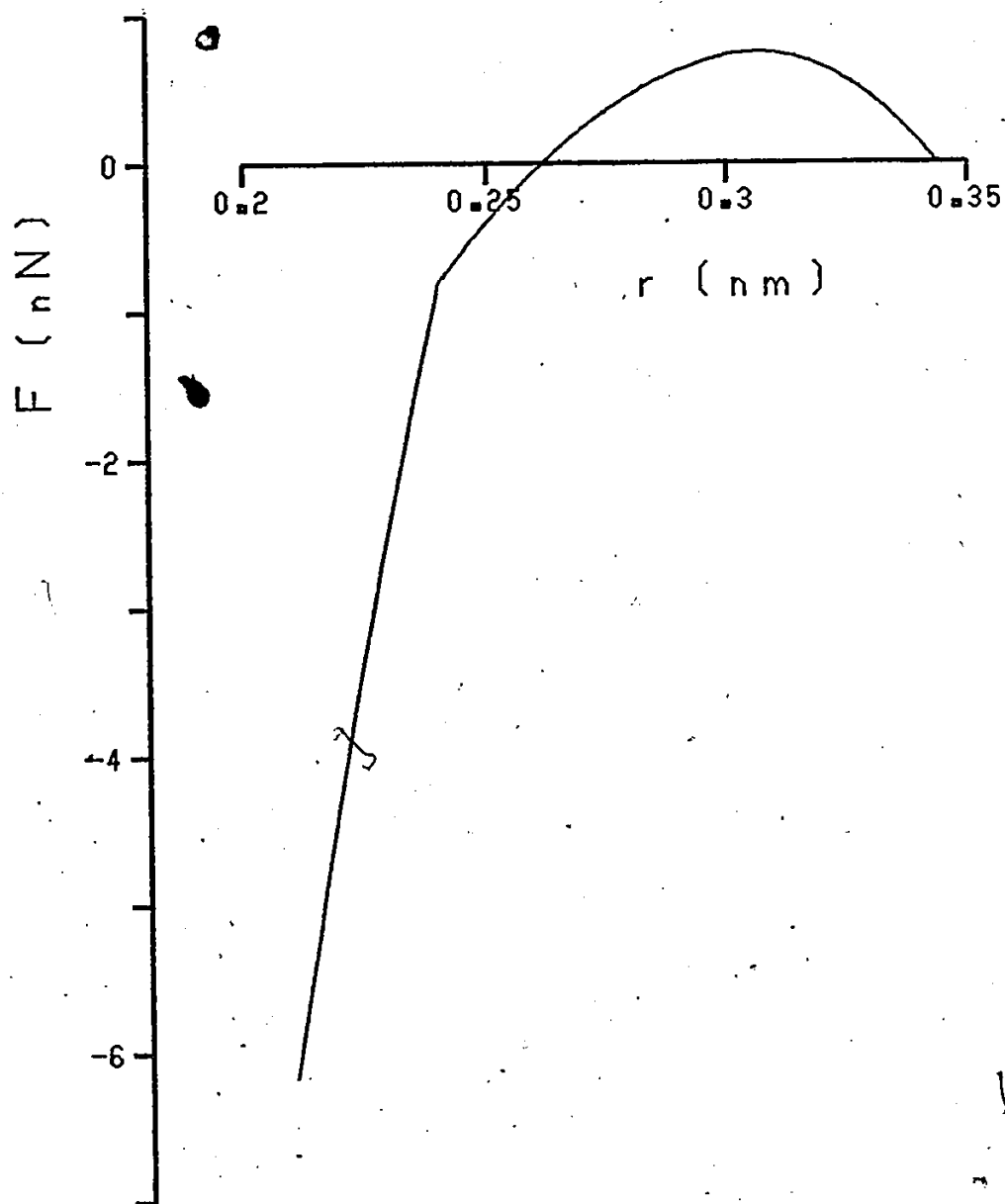   Potential, ∅, vs bond length, r.

Figure 5(b).   Johnson-I potential, [59].
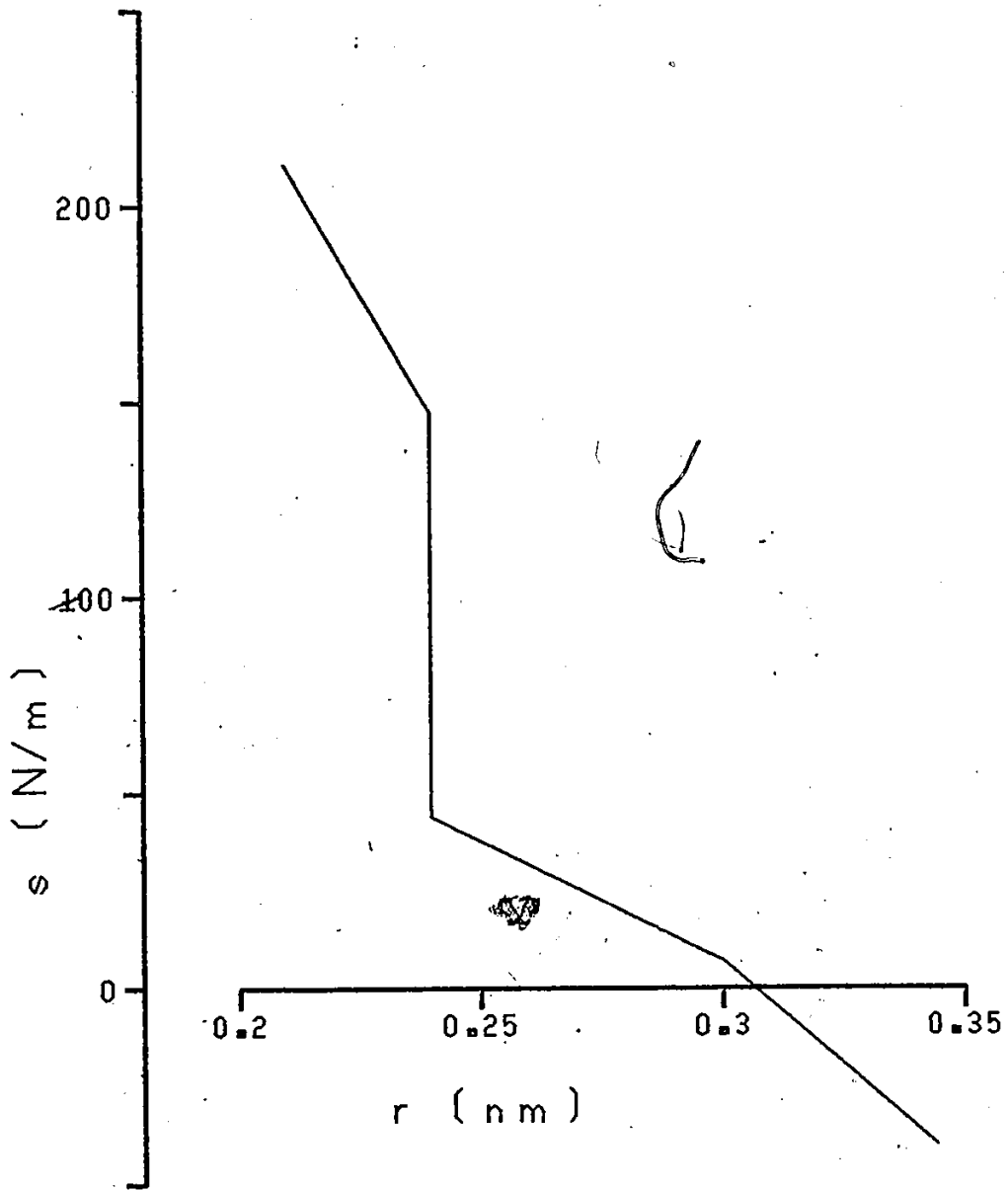   Bond force, F, vs bond length, r.

Figure 5(c).   Johnson-I potential, [59].
Spring constant, s, vs bond length, r.

materials derived in this manner are given by Johnson and Wilson, [60].
Some work is underway which could eventually enable their derivation on
more theoretically acceptable grounds, however. This could provide
better modelling of the long range, volume dependent effects which are
inadequately described by existing short range potentials such as that
of Johnson. The most important of these methods seems to be the
application of pseudopotentials, [61]. Few models have as yet been
constructed using these types of potentials, however.

Some materials cannot be described with any degree of accuracy
by pairwise central potentials, such as those described above. The
bonds of covalent crystals, such as diamond for example, have
significant bending stiffness. They have been described, [69], by
potentials which consider each atom to be bonded to its four nearest
neighbours. The bonds support axial forces which depend on their
length, as for the potentials above, but now, in addition, they are
provided with bending stiffness as well. The tangential forces which
they support are functions of the angles between adjacent bonds to the
atom. The functional forms for the potentials are taken to be
extensions of those described above. Another example of this type of
potential is that used by Rahman, [33], to model liquid water which
accounts for the dipole moment of the water molecule.

It is apparent that the level of understanding of interatomic
potentials is quite elementary at the present time. The absence of
better potentials is one of the prime problems of computer simulations
of the type considered here. It can be expected that more experimental

work will improve the situation in the future. The use of existing

potentials in computer simulations is not without purpose, however.

They do provide some significant correspondence to those for particular

real materials and can certainly provide a general view of the possible

nature of a class of real materials. In addition, disagreements between

the model results and real experimental results, which are inevitable at

the current level of understanding of this subject, can provide an

indication of the direction in which the potentials should be altered in

order to more accurately model real materials.

3.5 Discrete Atomic Simulation - Boundary Schemes

This section describes in detail the types of boundary condition

schemes which have been used in atomic simulations. This is an

important aspect of a computer model, especially in the study of solid

defects which generate large stresses such as crack tips. The previous

chapter contained a brief description of the boundary problem for these

types of studies. It consists of specifying the behaviour of the

continuum area and of the interaction between the continuum and discrete

areas in the model of Fig. 2.

The most primitive type of boundary scheme applicable to the

study of defects in solids involves setting the continuum to the

position determined by the linear elastic solution for the defect which

is being studied. Because single crystals of materials are usually not

isotropic, anisotropic solutions should be used. An example of these is

that for a crack tip in [62]. The continuum carries the embedded atoms

with it to new positions but there is no further interaction between the discrete and continuum areas. These rigid boundary conditions were used in some of the earliest studies, [43,64,68,69]. The resulting solutions showed anomalies. For example, the external stress needed to move a dislocation or crack appeared to be many times that observed experimentally. Flexible boundary schemes were introduced to make the models more realistic. These provide a mechanism by which the discrete and continuum areas may interact. In order to allow this, the forces applied to the atoms embedded in the continuum by interatomic bonds to their free neighbours must be able to distort the continuum.

Several techniques have been used to get the response of the continuum to these forces. The displacement field of the continuum may be described by a set of higher order linear elastic solutions for the defect being modelled. The potential energy of the complete system is then minimized with respect to the positions of all free atoms and with respect to the magnitudes of these higher order terms by a variational technique. This method implies that both the atomic and continuum degrees of freedom are treated identically in the solution procedure. Such an approach is possible for many problems. Vacancies and intestitials have been examined this way by Johnson, [36], dislocations, [63], and crack tips, [75], by Sinclair. The number of terms that has been used to describe the continuum ranges from one, [36], to six, [75]. The effectiveness of this method depends on how well the displacements of the continuum can be described by functions of this type. This will be examined later in this thesis for

the case of crack tips.

Alternatively, the continuum may be considered to be an infinite solid with a hole which contains the discrete region. The force on the embedded atoms is considered to be distributed over the inner surface of this hole. The response of the continuum is obtained from linear elasticity by means of Fourier series or Green's function expansions for the loads and displacements. Examples of the former are [44] and [45], for dislocations with eight terms in the series; of the latter are [45], for dislocations and [76] for crack tips. The complexity of this approach and correpondingly high computer cost, implies that the response of the continuum can only be calculated at relatively long time intervals compared to that of the free atoms. This can cause stability problems, [44].

The boundary schemes described above have several disadvantages. Among these are their analytical conplexity and the difficulty of accounting for unusual geometries and non-linear effects in the continuum. This will be discussed more fully later in this thesis when the new boundary scheme presented in this work is described.

3.6 Discrete Atomic Simulation - Crack Tips

The boundary condition scheme presented in this thesis is applied to the problem of the crack tip in bcc α-iron modelled by the Johnson-I potential. This section contains a review of previous work which has been done on the simulation of cracks in solids by atomic

level computer modelling.

The earliest simulations of cracks used rigid boundary conditions. None of these could show crack propagation even under very high loads. The first appears to be the work of Chang, [64]. He modelled two dimensional cracks in bcc and fcc iron as vacancy sheets. This is probably unrealistic and all later models assumed the crack to be a cleavage plane. He studied cracks of various orientations. By comparing the shear and tensile "stresses" (defined in terms of bond forces for the discrete lattice) in a manner similar to that of Kelley, et al, [14], he felt that the chance of the crack spontaneously blunting by emitting dislocations was high for all crack planes except (001). No such blunting could be observed in the model, however. He studied (001) plane cracks with [010] crack line direction, as well as cracks on other planes in the bcc material.

Gehlen and Kanninen, [65], studied this crack using the Johnson-I potential and, again, rigid boundary conditions. They assumed the crack to be a true cleavage between adjacent crystal planes. They found, also, that the crack would not propagate. By means of an energy argument, they estimated the critical stress intensity factor, k_c, to be about 1.13 k_G, where k_G is the Griffith stress intensity factor predicted by continuum theory for this case. However, because of the inability to actually observe the crack propagating under stress, it was impossible to confirm this value.

Gehlen, et al, [66], allowed the lattice of the previous crack

to vibrate in a manner which simulated the effects of thermal motions of
the atoms. It was thought that this thermal activation might be an
important effect and that the crack should propagate more easily under
this condition than near absolute zero, which the previous simulations
had considered. They found, however, that again no crack propagation
could be observed. It was long felt that the effect of jogs in the
crack face could also be important in promoting crack propagation. The
stress needed to move such a jog parallel to the crack face should be
considerably smaller than that needed to cause the crack to extend as a
unit perpendicular to its direction. Kanninen and Gehlen, [67,68],
modelled such a crack. Because of the much larger number of free atoms
necessary in such a three dimensional model, computer costs for such
models are quite high and, therefore, such studies are rare. They did
find that the jog could move easily at stresses only slightly greater
than k_G. The question of whether or not such jogs were necessary for
crack propagation, however, remained unanswered.

The other materials in which cracks have been computer modelled
are the diamond structure crystals such as silicon. Sinclair and
Lawn, [69], performed this work for two dimensional cracks with rigid
boundary conditions. Again they could not obtain crack propagation.

The first study to obtain crack propagation as a result of the
action of an external stress appears to be that of Hsieh and
Thomson, [70]. They used a model which was a very severe simplification
of a real material. This was a square, two dimensional lattice with
bonds having both stretching and bending stiffness. The potential for

these bonds was quadratic, ie. the force-distance relation was linear, with a sharp cut-off. The model used by Hsieh and Thomson differs from those which have been described previously in that they used a "lattice statics" model as opposed to the "molecular dynamics" type of model already described. The lattice statics technique was developed as a means to calculate the vibration modes and frequencies in crystals for use in analyzing neutron and x-ray diffraction data. It involves writing the equilibrium equations for the atoms in the lattice and Fourier transforming them into a space of wavenumbers representing sinusoidal components in the displacements of the particles. The equations are solved in the wavenumber space and transformed back into real space to obtain the solution. This method has the advantage that the final equations are much more easily solved than those of molecular dynamics models because they are fewer in number or, at least, uncoupled to a large extent. The algebraic work involved in setting up the equations is large; however, except for the simplest cases. The method does permit the model to extend to infinity and, as a result of this, the boundary problem of molecular dynamics models is eliminated, and crack propagation could be observed. Cracks in this model were stable over a considerable range of stress intensity factors, k, around the Griffith value. Hsieh and Thomson called this the lattice trapping effect, and the limiting k values, the lattice trapping limits. The crack will extend if $k > k_+$, the upper limit, and recede if $k < k_-$, the lower limit. The ratio k_+/k_- could be as high as 2.5 in this model. A molecular dynamics model using a similar interatomic potential to that of Hsieh and Thomson in a triangular two dimensional lattice is given by

Ashurst and Hoover, [71].

Lawn, [72], using the lattice trapping concept, analyzed the problem of slow crack growth or "crack creep". This is the phenomenon observed in many materials of slow extension of a crack under constant stress until it becomes large enough to precipitate a catastrophic failure of the material. Lawn assumed that cracks would propagate by thermal and chemical activation over the lattice trapping barrier. He got reasonable correspondence between this theory and experimental results on the fracture of synthetic sapphire in a water vapour environment, but at the expense of lumping many unknown constants into one empirically derived one. This made an experimental determination of the size of the lattice trapping limits impossible.

Some later experiments by Wilkins and Dutton, [73], on the rate of closure of microcracks in glass during annealing indicated that lattice trapping limits might be even wider than those predicted by Hsieh and Thomson, [70]. Esterling, [74], extended their model to allow for some non-linearity of the interatomic force law and found that a more realistic force law than the sudden snapping one of Hsieh and Thomson gave narrower lattice trapping limits. Sinclair, [75], extended his model of silicon to include a flexible boundary scheme using higher order elasticity solution crack tip terms to describe the behaviour of the continuum. He used a more realistic non-linear force law than that used by Hsieh and Thomson and found the lattice trapping limits to be such that $k_+/k_- = 1.1$ to 1.4 These results indicated the importance of including realistic force and crystal structures in the

calculations and, as a result, the difficulties of the lattice statics

approach to these problems has practically eliminated it as a viable

modelling technique.

The iron crack has proven more difficult to model apparently

because the material is less easily fractured and because of the

possible complication of dislocation nucleation at the crack tip which

is very unlikely in silicon. This means that the strains in the

continuum region can be quite large and the modelling of the continuum

becomes very important in determining the results. Gehlen, et al, [76],

applied a flexible boundary scheme to the (001)[010] iron crack. This

involved modelling the crack as a parallelipiped of dislocations and

using this to describe the behaviour of the continuum by Green's

functions. Because of the complexity of the equations involved,

isotropic elasticity theory was used although the crystal is

anisotropic. Using this model, crack propagation could be observed at a

critical stress intensity factor of about 3 k_G. The crack propagated

along the (101) plane, however, rather than the (001) plane

experimentally observed. Gehlen, [77], later extended this model to

include anisotropic behaviour of the continuum. (001) plane fracture

could then be observed at k = 2.78 k_G. Personal communication with this

group, however, indicates that they now feel that there may have been an

analytical mistake in the construction of this model and they do not now

have great confidence in the results. Thus, the difficulty of

constructing suitable boundary schemes for these problems and the

complexity of the current approaches is evident. This difficulty is

related to the very high level of strain in the vicinity of the crack tip, as opposed to that for other defects such as dislocations. This means that the area of crystal significantly affected by the non-linear behaviour around the crack tip extends well beyond the discrete regions that can be accommodated in present computers. This indicates the need for a boundary scheme which is both more accurate and easier to implement than the ones which have been used previously so that work in this area can continue. It is hoped that the scheme presented in this thesis will prove of some use in this work.

This literature survey has provided an overview of the area of computer modelling and of microstructural fracture mechanics theories. In addition, more detailed information has been given on modelling of cracks and the difficulties which have been encountered in this area. The fracture behaviour of the bcc metals has also been examined in some detail. This should provide sufficient background for a study of the work in the remaining chapters.

4 SOLUTION METHODS COMPARISON

Most atomic level computer simulations which have been done to
date are static simulations, using the nomenclature of Chapter 2,
ie. they are concerned only with the equilibrium state of the crystal
containing the defect being modelled. A literature survey indicated
that several techniques had been used to solve the equations defining
the equilibrium position. In addition, various integration schemes had
been used to solve the equations of motion of the system in dynamic
simulations. The efficiency of the solution method used to solve the
model is very important since the limiting factor in work of this type
is computer cost. If computer cost could be reduced, it would be
possible to solve, larger, more complex models which would improve the
accuracy of the results. In spite of this, there appears to be no
systematic comparison of the relative merits of different solution
methods for these problems in the literature. This chapter presents the
results of such a study with emphasis on solution methods for static
simulations.

Three solution methods are in general use for static solutions
and they will be referred to here as simultaneous quenching, individual
quenching, and the conjugate gradient method. All start with the model
near the final equilibrium position and continuously force it closer to
equilibrium. The starting position may be set by using the linear
elastic solution for the defect being analysed, for example.

Simultaneous quenching, [43], involves integrating the equations of motion of the model until the total kinetic energy of the system reaches a maximum. At this point, all velocities are set to zero and the procedure is then repeated. The procedure of setting the velocities to zero is known as quenching since, at the macroscopic level, this is equivalent to suddenly dropping the temperature to absolute zero. Each of these quenching operations removes some excess energy from the system and, thus, the system continually approaches equilibrium. Individual quenching, [45], is similar to this except that each atom is individually quenched, or stopped, when its kinetic energy is a maximum. The conjugate gradient method, [78], is an optimization technique which is used to find equilibrium positions defined as potential energy minima. Johnson, [36], used a simpler optimization routine for simple crystal defects but general experience with optimization procedures, [79], indicates that the conjugate gradient method should be better for complex problems, so Johnson's method was not considered.

This chapter presents a systematic comparison of the three static solution techniques described above by examining the solution time that was required for various problems. Prior to this, a comparison is presented of several integration schemes which may be used to solve the equations of motion of the model. This is necessary since both quenching procedures use these integrators and the maximum time step which may be used with them determines how well the quenching procedures will compare to the conjugate gradient scheme. Since this is the primary reason for this test, elaborations such as tunable

integrators, [80], or variable step sizes were not considered. In spite
of this, the results should be of interest for choosing an integration
scheme for use in dynamic problems as well.

4.1 Integration Scheme Tests

The pertinent quantity to be used in comparing the relative
merits of various integration schemes is the number of interatomic force
evaluations per unit model time, since almost all the computer cost is
involved in the calculation of these forces. Alternatively, the inverse
of this quantity, h/n, where h is the length of the time step used in
the integration procedure and n is the number of force evaluations per
step, may be compared and the computer cost is then inversely
proportional to h/n. For dynamic problems the limiting factor is the
accuracy of the integration procedure, which must be within the limits
of accuracy desired for the simulation. When the integration scheme is
used as part of a quenching operation for static solutions, accuracy is
not important unless it is very poor since any errors in the model state
introduced by the integration scheme will be eliminated, just as the
initial error is eliminated, as the model approaches equilibrium. This
can be seen from the results presented later which show that the rate of
decrease of system energy as the system approaches equilibrium is about
20 times the possible increase due to integration errors, even for the
worst case of solution scheme and integration method. The limiting
factor on h/n for static solutions is, then, the system stability limit
regardless of accuracy.

The relative merits of different integration schemes are problem dependent, [81], and very difficult to determine analytically. As a result, comparison must be made by numerical experiments and several tests of this type are available, [81,82], from which some general conclusions may be drawn. No tests appear to have been published, however, on an atomic simulation problem which has a large number of degrees of freedom and a range of small displacement eigenvalues and large displacement non-linearities typical of problems of this type. Beeler and Kulcinski, [83], describe such a comparison but it is only for a simple, one degree of freedom harmonic oscillator. The degree to which such a test is applicable to the general atomic simulation problem is questionable. Several schemes have been used in these simulations, by far the most common of which is a simple 2-step difference formula, [49]. This was compared to several others selected from the literature and the results are presented below. All the integration schemes tested are summarized in Appendix A.

To select methods which may be applicable, the characteristics of the model being solved must be considered. The differential equations to be solved are not stiff, since the time scale of interest is that of the smallest time constant, so this is not a difficulty. The equations are purely second order with no first order components, so only those methods developed particularly for this type of problem will be tested. Most published comparisons are for first order differential equations only but the results are probably qualitatively applicable to similar second order problems and these will be used as the basis for

selection.

As stated above most discrete atomic simulations have used a simple 2-step difference scheme. Many other simple difference schemes are possible, all more elaborate than the 2-step, and a 5-step one was chosen as representative of this class, [81]. The other main classes are the Runge-Kutta and the predictor-corrector methods. The general conclusions of Lapidus and Seinfeld, [81], for the Runge-Kutta methods are that, for the accuracy level needed here, which is relatively low compared to that needed for many other problems, the accuracy at a given value of h/n is nearly independent of the order of the integration scheme used (note that this does not refer to the order of the differential equation). Similarly the stability limits expressed as h/n are also nearly independent of order. As a result only one Runge-Kutta method, of 3rd order, was selected for the test, [84]. Lapidus and Seinfeld also concluded that, of the predictor-corrector methods, the Adams methods are best in general. The Adams methods are characterized by the number of steps used, p, and the number of iterations of the corrector, q. A comparison of different Adams methods on several problems, [82], led Hull and Creemer to conclude that as p increased, the error and stability decreased for a given computer cost. Thus it would be expected that a high p method would be better for accuracy in dynamic problems, while a low p would give greater stability for static problems. The effect of changes in q was less consistent, with q=1 better for some problems and q=2 better for others. A p=4 and a p=6 method were selected and both were tried with q=1 and 2. The two q=2

schemes were not found to be competitive in either accuracy or stability when tested on the problem described below and so will not be considered further. The Nordsieck, [84,85], modification of the Adams method was used since it permits simultaneous possession of the atom positions and their derivatives. This is useful in the individual quenching static solution method since the time at which an atom reaches its kinetic energy maximum can then be determined as the time at which $\bar{v} \cdot \bar{a}$ becomes negative, where $\bar{v}$ is the atom's velocity and $\bar{a}$ its acceleration. Also changes in the step size are easier to implement than for the basic Adams method and this may be of use in some problems, although it is not pursued here. The p=6, q=1 Nordsieck method has been used for atomic simulations, [83]. Finally a hybrid scheme developed especially for high efficiency with second order equations in problems of astronautics, [86], was tested. This has characteristics of both Runge-Kutta and predictor-corrector methods.

The tests were performed on the model crystal shown in Fig. 6 which represents two planes of atoms in bcc α-iron. The atomic motions are restrained to lie in these planes so the material may be considered to be in plane strain. The interatomic potential used is the Johnson-I potential, [59]. The time step lengths used could be scaled for other materials to a first approximation by $\sqrt{m/k}$ where m is the atomic mass and k is some effective spring constant of the bonds. Some experimentation may, of course, be necessary. The size of the models used in atomic simulations varies over a wide range, but the one used here is typical of the smallest which have been used. It contains 194
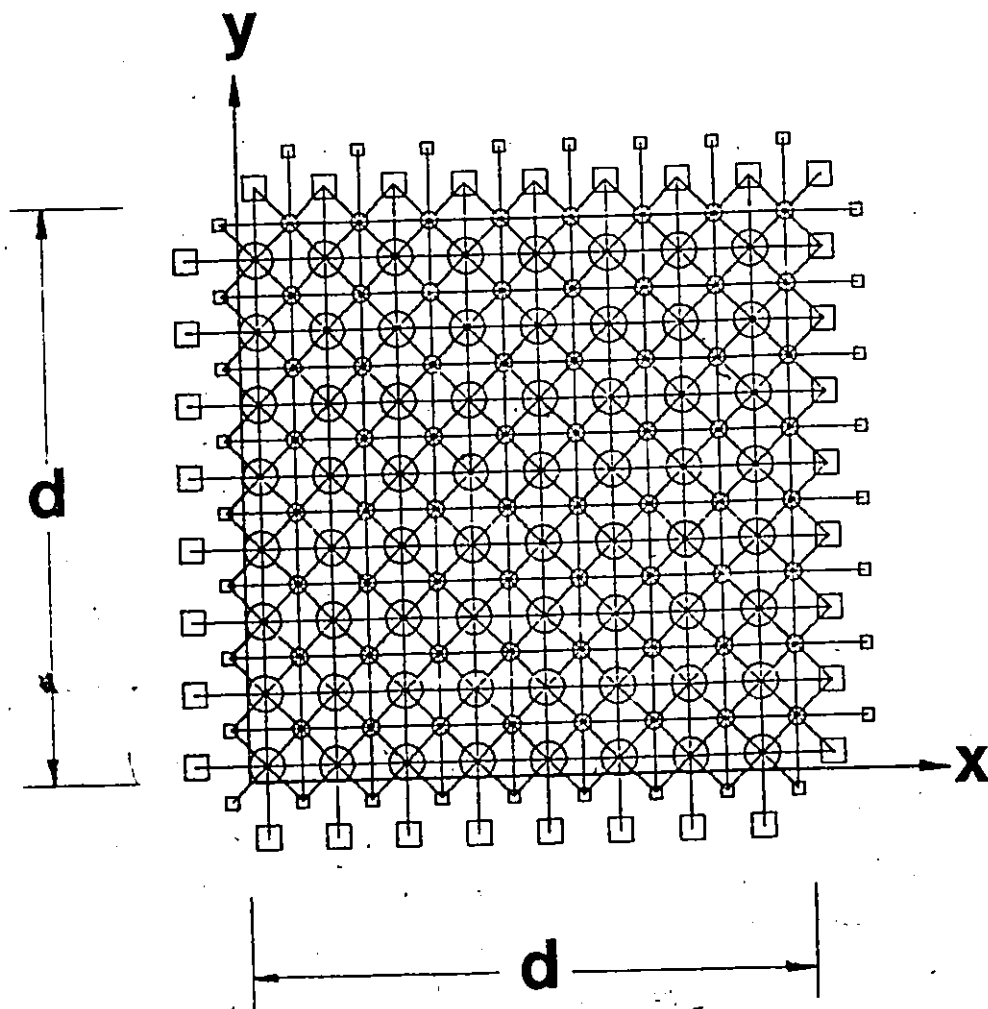
Figure 6.   Model crystal used in integration and solution scheme tests.
Scale = 3 cm to 1 nm. The free atoms are marked by circles,
embedded atoms by squares. The smaller markers are in a
plane below that of the larger. Interatomic bonds are
shown as straight lines.

atoms in total of which 128 are free to move. The 66 boundary atoms are

rigidly fixed at the positions needed to apply the desired boundary

loads to the model. In actual simulations some form of flexible

boundary scheme must be used to get accurate results, but as explained

in section 3.5, these either update the positions of the boundary atoms

only at long time intervals while holding them fixed between these

updates, [44, for example], or the boundary motions are defined by other

degrees of freedom which are treated in the same way as the atom

positions, [75, and the finite element boundary conditions presented

later in this thesis, for example]. Thus the computer time needed for a

model with rigid boundary-conditions is representative of that for a

model with flexible boundaries, so that the latter was not considered in

this test. The time for one evaluation of all interatomic forces for

the model of Fig. 6 was about 0.6 seconds on a CDC 6400 computer. This

time is proportional to model size and to the complexity of the

interatomic potential used. More complex potentials would be desireable

but they have been restricted by computer cost in the past. However,

sizes more than 10 times larger than that tested here have been used in

some cases, [75]. It is felt that changes in size should not affect the

relative merits of various integration schemes or static solution

methods although no tests were made of this. Future work could test

this point.

The integration schemes were compared by checking their

stability limits and the accuracy of energy conservation which they

maintained while simulating the thermal vibrations of the model of

Fig. 6. Energy conservation was checked since it is a single number characterizing the whole system accuracy, it is simple to evaluate, and it is often the physical property which is of primary interest, for example in thermodynamic simulations or for the evaluation of saddle point energies for defect motion. For this test, the atoms were first displaced from their equilibrium positions by normally distributed amounts such that the extra energy added to the system was equal to 1 aJ (1 aJ = 1.E-18 J). This is approximately the energy the crystal would possess at room temperature. It was chosen as being typical of the energies which might be examined in a thermodynamic analysis, as well as the energy excess which might be present in a model during the course of a static solution. For instance, it is about twice the excess energy which must be removed from the crystal for a crack problem at two times the Griffith stress intensity factor. The factor of two in energy should account for the presence of some bonds which are very highly stretched in such defect problems which do not appear in thermal vibrations.

The simulation was carried out with each integration scheme for a model time of 3500 fs (1 fs = 1.E-15 s). This time was chosen as the time needed for very accurate static solutions. This can be seen from the results of the static solution tests presented later. This length of time is also enough to permit a shear wave to propagate about 40 lattice parameters and, since the speed of crack propagation or dislocation motion is of this order of magnitude, it should be sufficient for dynamic studies of defect motion as well. For shorter

times, the stability limits may appear to be extended slightly since some cases appeared stable for several hundred fs before finally diverging. Each integration scheme was tested with step sizes of 3, 6, 9, 15, 21, 30 and 45 fs at least. The rate of increase of energy error with model time was roughly linear for almost all cases. The few exceptions were isolated and did not affect the relative standing of the methods involved. Thus comparing errors at the endpoint of the simulation is sufficient to rank the methods. This error is presented in the form r/(KT) where

r = energy error at the end of the simulation,

K = maximum system kinetic energy = 1 aJ, and

T = time of simulation = 3500 fs.

This is plotted against the measure of computer cost, h/n, both on logarithmic scales, in Fig. 7.

From Fig. 7 it can be seen that the p=4, q=1 Nordsieck method has the greatest stability and therefore should be best for static solutions. The commonly used 2-step difference formula is next best. It is, in fact; more accurate than the Nordsieck method over most of the range of step sizes but as stated earlier this factor is negligible for static solutions. In addition the Nordsieck method gives the velocity and acceleration of the atoms simultaneously while they are only available half a step length apart for the difference scheme. This makes programming individual quenching static solutions easier with the Nordsieck method. The Nordsieck scheme does use slightly more memory
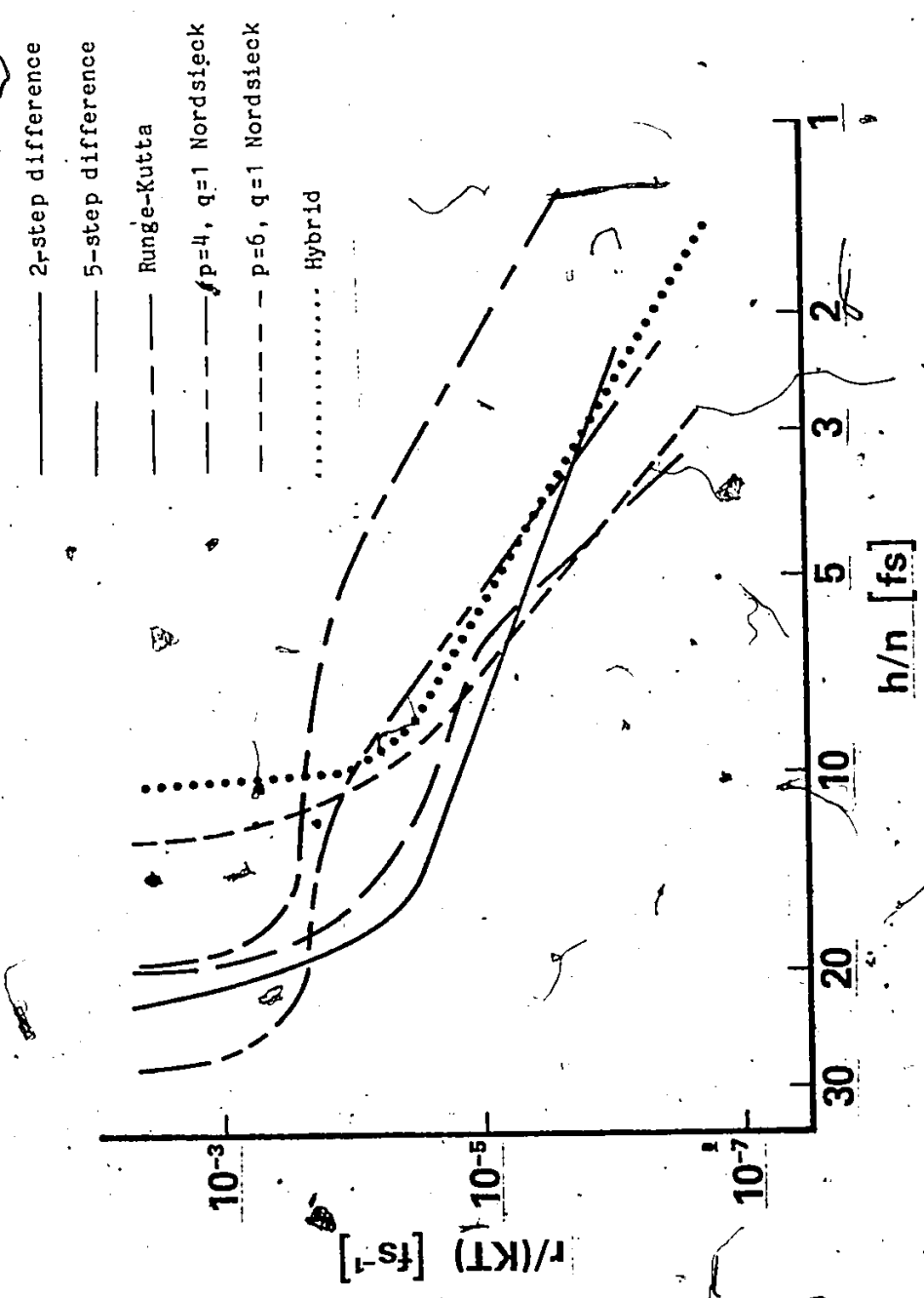
Figure 7.   Results of the integration scheme tests.

than the 2-step difference and this may be a problem in some cases. The 5-step difference and the Runge-Kutta methods are also acceptable while the hybrid scheme and the p=6, q=1 Nordsieck, which has been used in the past for these simulations, are significantly worse. Step sizes which have been used in simulations are not always stated in published work but the largest is apparently 17 fs, [43], used in a dislocation problem for the 2-step difference scheme. This is very near the stability limit found here for this method and confirms the general applicability of the results for different problems.

The best method to be used for a dynamic analysis depends on the accuracy level needed. An order of magnitude estimate for this may be made as follows. Suppose the material properties are known to 1% and it is desired that the integration scheme accuracy be comparable to this. If r/K = 0.01 at a time of 3500 fs, then r/(KT) = 2.9E-6 fs^{-1}. At this accuracy and higher, the p=6, q=1 Nordsieck and the 5-step difference schemes are best. At lower accuracies the 2-step difference becomes best with the 5-step difference very close. The others are generally within a factor of 1.5 of the best methods in computer cost except for the Runge-Kutta which is as much as five times costlier at some accuracies.

In conclusion, if a single method is desired for static and dynamic analyses, the 2-step or 5-step difference schemes are probably best. For static analyses alone, the p=4, q=1 Nordsieck is slightly better than the 2-step difference method. The integration time step used must be less than 20 fs for stability for the Nordsieck case and

10 fs should provide a sufficient safety margin to ensure stability under all conditions. No instabilities were observed using 10 fs on a wide variety of problems such as those presented later in the thesis, while instablility did occur occasionally when 20 fs was used, and once with 15 fs. For dynamic analyses, one of the difference schemes or the p=6, q=1 Nordsieck is best depending on the accuracy needed. The step length for any degree of accuracy can be read off Fig. 7 and scaled for other materials as mentioned above.

4.2 Static Solution Scheme Tests

In this section the three static solution methods will be compared. The model used is the same one used for the test of integration schemes and shown in Fig. 6. The computer time required to approach equilibrium was determined for four problems. In three of the problems the boundary atoms were fixed at the perfect crystal positions. The free atoms were given initial displacements which were sinusoidal in form:

$$u = A \sin(m \pi x/d) \sin(m \pi y/d)$$
$$v = B \sin(m \pi x/d) \sin(m \pi y/d)$$
(16)

where (u,v) is the displacement of the atom at (x,y). B was set equal to A/2 so that the displacement vectors did not lie along a high symmetry axis such as the [110] direction. The value of A was chosen so that the total energy which had to be removed from the crystal was 5 aJ. This is larger than the energy excess in most static solution problems so that the efficiency of the solution schemes over a wide range of

energy levels could be observed. Values of 1, 2 and 3 were used for m.

This form of test problem was chosen so that the effect of different

spatial frequencies in the initial position errors for static problems

could be determined. Also, since the final position which was sought

was the perfect crystal position, no problems of alternate minima were

encountered which can be seen in more complex problems. The final

problem on which the solution schemes were compared was a crack tip

problem. For this, the boundary atoms were set at the positions

specified by linear elastic fracture mechanics, as were the initial

positions of the free atoms. The system was then relaxed from this

position. The energy which had to be removed was about 0.063 aJ for a

stress intensity factor equal to the Griffith value.

The conjugate gradient method had to be modified in one way from

that presented by Sinclair and Fletcher, [78], in order to get efficient

convergence. It was found that the unmodified method hung up at

non-equilibrium points which it only slowly passed. To avoid this, the

series of conjugate directions had to be restarted periodically, much

more often than suggested by the tolerances of Sinclair and Fletcher. A

restart every 10 steps was satisfactory.

The results are shown in Figs. 8 to 14. Each figure gives the

results for one of the test problems. The horizontal axis in each plot

is a measure of computer time expended. This is expressed as the number

of interatomic force evaluations made. The integration scheme used for

the two quenching solution methods was the $p=4$, $q=1$ Nordsieck with a

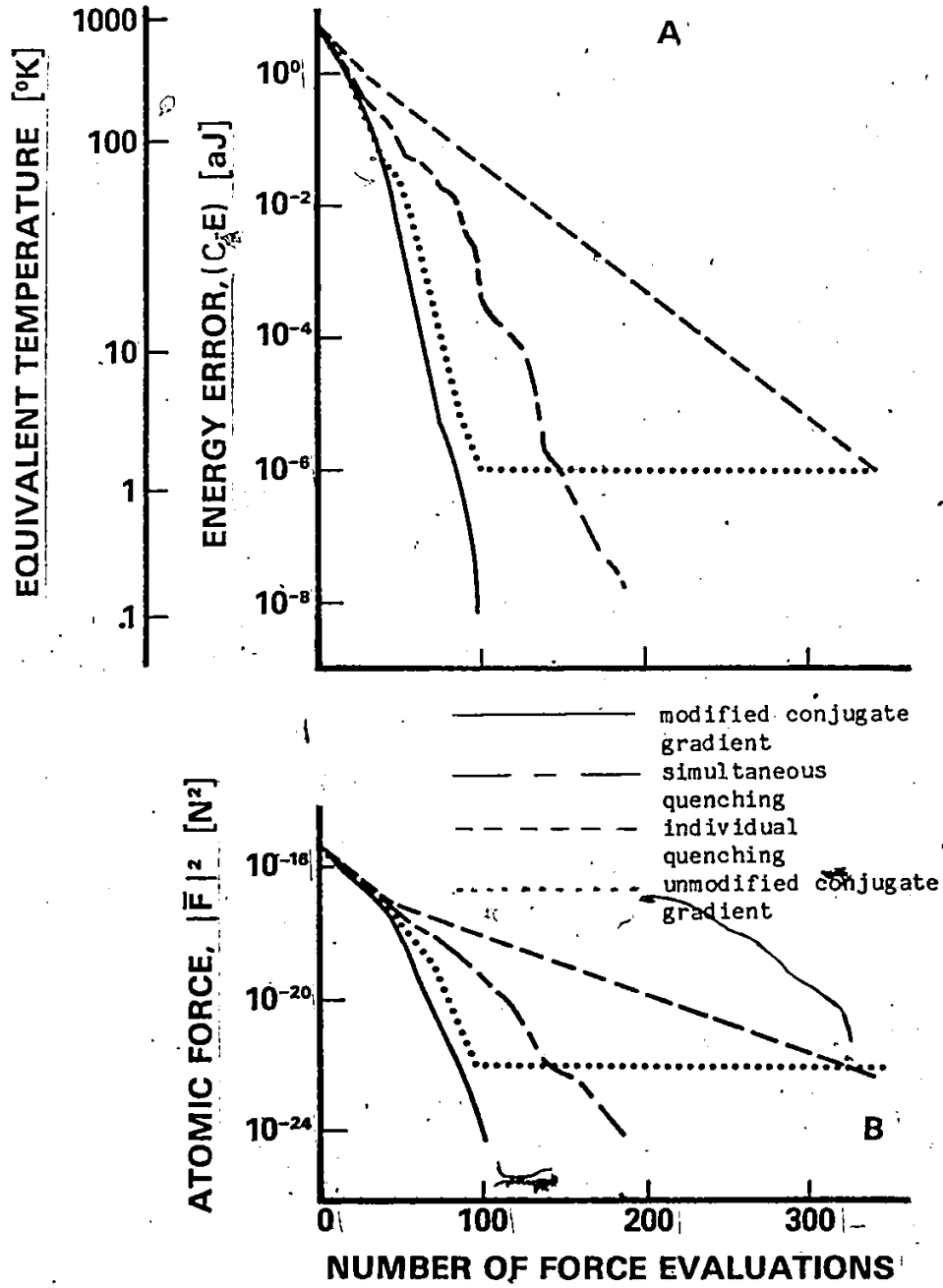time step of 10 fs. Increasing the step length would proportionally

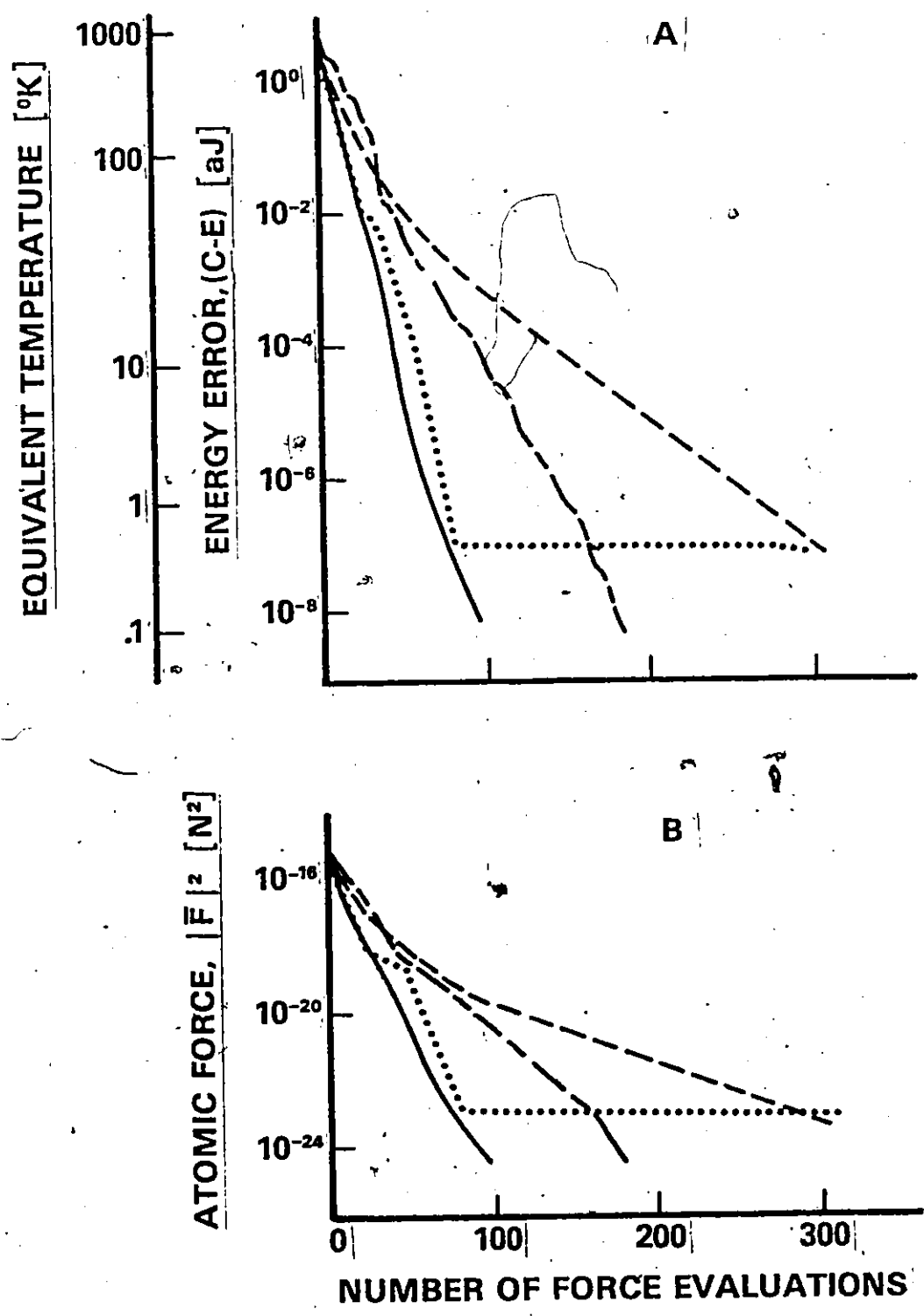Figure 8. Results of solution scheme tests. Sinusoidal initial displacement, m=1.
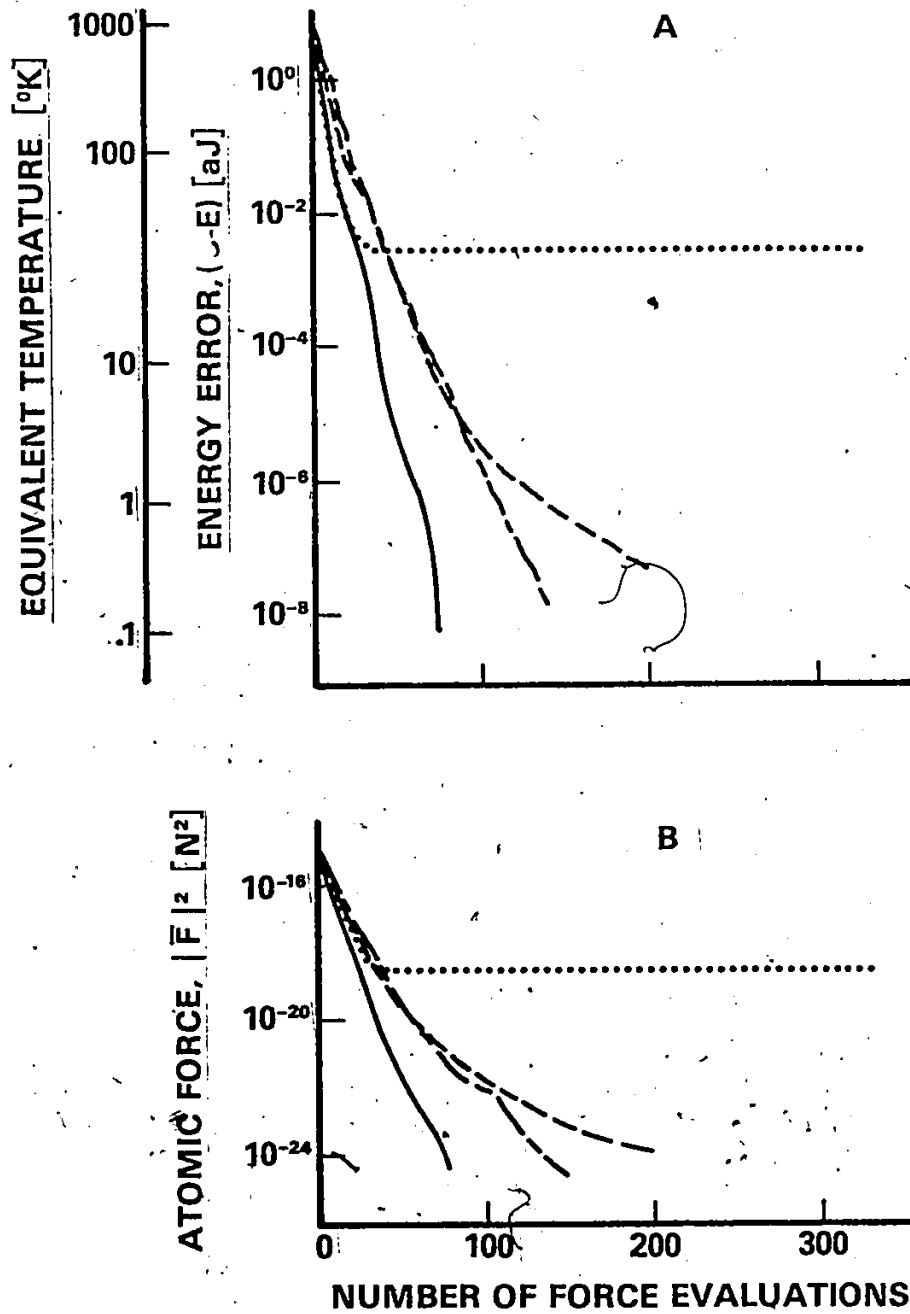
Figure 9.   Same as Figure 8 except m=2.

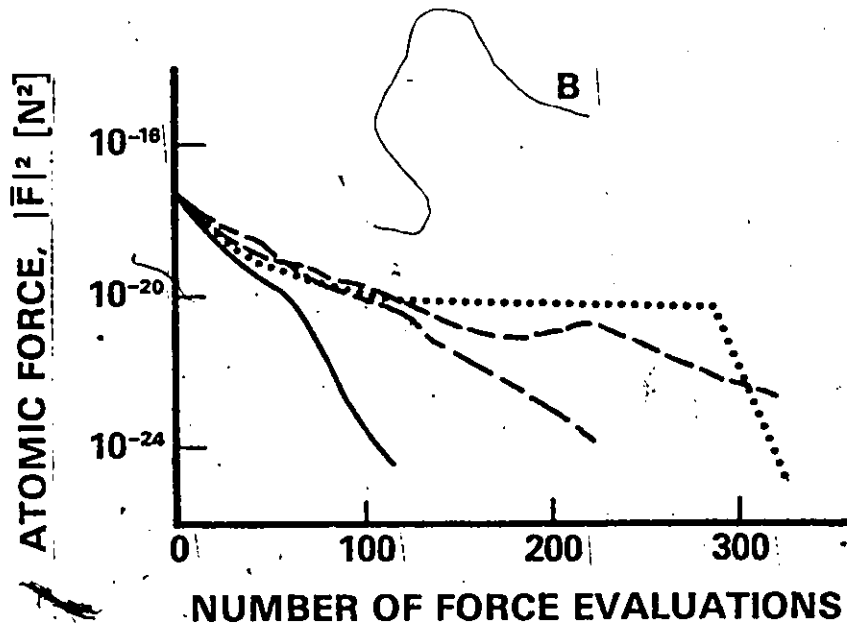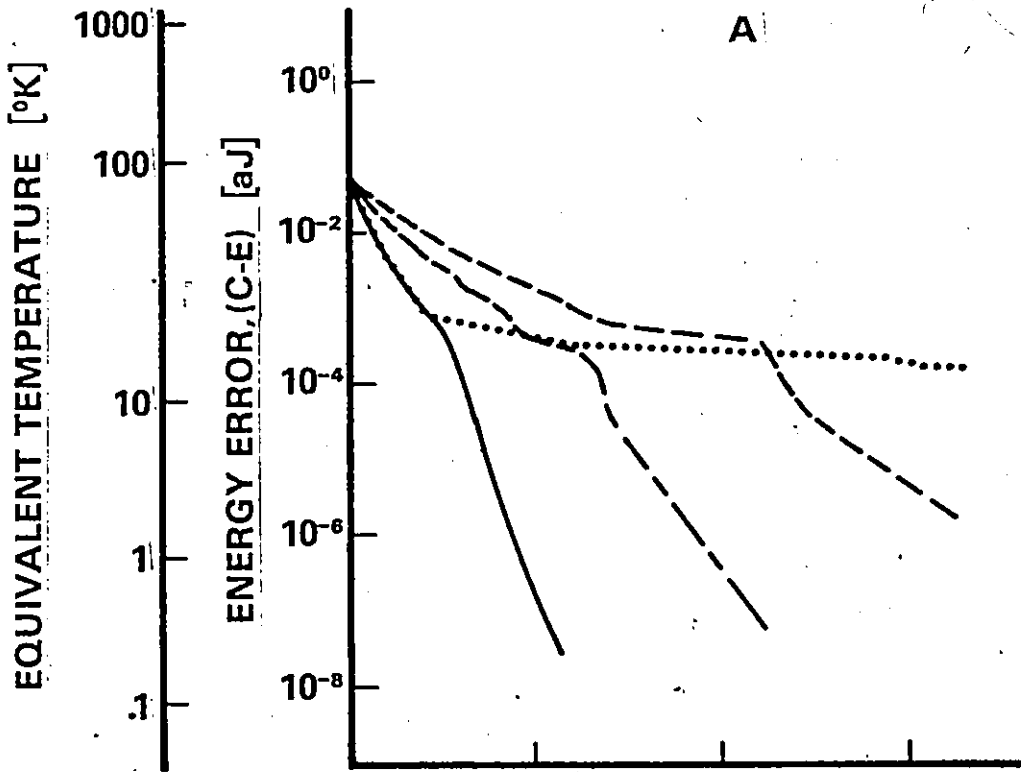Figure 10. Same as Figure 8 except m=3.

Figure 11.   Same as Figure 8 except for crack tip problem at the
              Griffith stress intensity factor.

decrease the computer time needed to reach a given level of accuracy for the two quenching methods thus making them more attractive vis-a-vis the conjugate gradient method. The test of integration schemes described above indicates that this could be done although by less than a factor of two. To do so would remove the safety factor on the stability limits of the integration and so would not be adviseable.

The energy error at a given point in the solution is expressed as (C-E) where

C = potential energy of the system in its current configuration, and

E = potential energy of the system at the final equilibrium configuration.

E was determined to sufficient accuracy from a very accurate solution for each case. The energy error may also be expressed as a temperature. This is the temperature which would correspond to the energy excess in the system if it were evenly distributed through the crystal. The temperature of a system such as that considered here is given by statistical thermodynamics as a function of the Hamiltonian of the system [87]. No attempt was made to calculate this for the present model. Experimental information for real iron is readily available, however, and since the Johnson-I potential has many properties similar to those of iron, this should be sufficiently accurate to indicate the order of magnitude of the energy in the system. Figure 12 shows the specific heat and enthalpy as a function of temperature for real
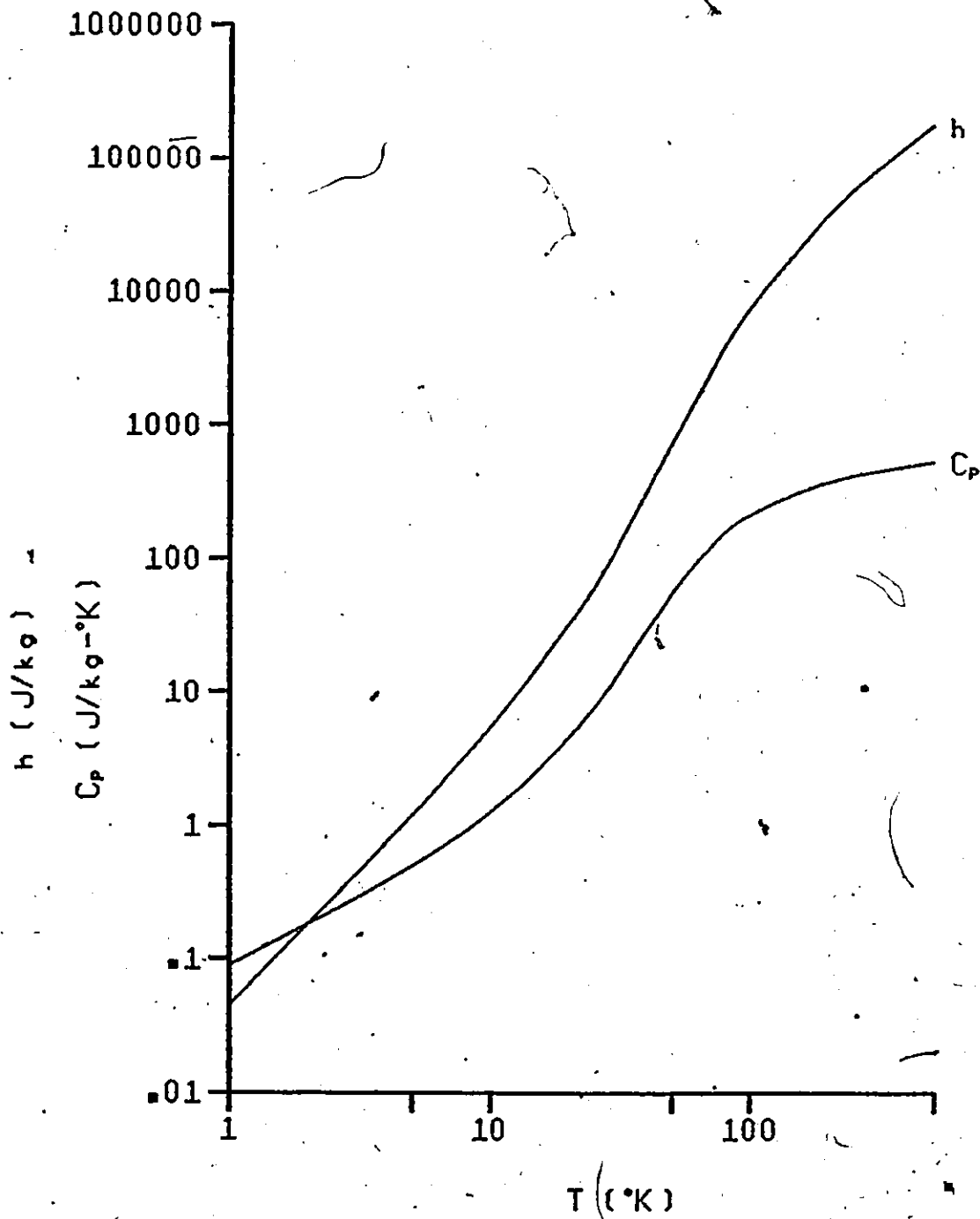
Figure 12.   Specific heat and enthalpy of iron vs temperature.

α-iron, [88,89].

Part (a) of each of Figs. 8 to 11 is a plot of this energy error
in the solution against computer time used. Part (b) of each figure is
a plot of the sum of the squares of the forces on all atoms, $|\bar{F}|^2$,
against computer time. At equilibrium, these should both be zero of
course.

The results show that for all cases, the errors decreased
approximately exponentially with computer time. This knowledge enables
a prediction to be made of the time required to reach a given accuracy
level once a solution has been started. This may be useful in
scheduling. In addition, for the sinusoidal initial displacement
problems, the modified conjugate gradient method was best, followed by
the simultaneous quenching and the individual quenching methods.
Increasing the integration step size for the simultaneous quenching
method could make it more efficient but not so much so that it would
become best without introducing the possibility of numerical
instability. The poor performance of the individual quenching was
surprising in view of its widespread use. It may do much better if more
than one atomic mass were present. This is a point which could be
examined in the future. The unmodified conjugate gradient method
reached stages in the solution at which the change in position of the
system during each step became very small. This causes the plateaus in
the energy and force curves which were not passed in the time studied.
For each method, the time to reach a given accuracy was shortest for the
highest spatial frequency, m=3, and largest for the lowest frequency,

m=1. Thus if any trade-off were possible, initial conditions should be chosen to minimize the large spatial frequencies in the initial errors. This may be of interest to proposals, [48], to combine the molecular dynamics models considered here with the lattice statics models described in section 3.6 . The change in solution speed as the spatial frequency changed was least for the modified conjugate gradient method and greatest for the individual quenching method.

For the crack tip problem, the curves are more complex but the same order of efficiency holds for the solution methods so this result is probably widely applicable. The plateaus in the unmodified conjugate gradient curves are again seen. The force magnitude plot of Fig. 11(b) shows that the plateau was passed and that a fairly accurate equilibrium position was achieved at about 320 force evaluations. The reason that the steep drop off was not observed in the energy plot of Fig. 11(a) is that the equilibrium position which was found by this method was different than that found by the others. The energy difference between the two equilibria is about 0.00017 aJ. If spread through the entire crystal this energy would represent a temperature of about 15 K. The curves for the other methods seem to have kinks at this point indicating that they too may have felt this alternate equilibrium point. This result would seem to confirm the statement of Beeler, [30], that "of all the methods available for computing defect equilibrium configurations, the artificial damping dynamic method [the quenching methods used here] is the only one which will certainly converge to the lowest energy configuration and not to some low-lying metastable configuration." That

this is not generally true, however, can be seen for the crack problem

at a stress intensity factor of twice the Griffith value. The crack

does not propagate because of the lattice trapping effect and the rigid

boundary conditions. The accuracy versus computer time curves are

similar to those already given and so will not be presented. In this

case, however, three different equilibria were found. The lowest in

this case was found by the two conjugate gradient methods. The

simultaneous quenching method converged to an equilibrium configuration

0.0005 aJ (35 K) above this and 'the independent quenching method to one

0.0136 aJ (60 K) above the conjugate gradient solution. Figure 13 shows

two of these equilibrium positions and the unbroken bonds in each case.

The differences can be seen mainly in the area between the crack tip and

the lower right corner of the model. These are real, seperate

equilibrium positions made possible by the presence of a non-linear

interatomic potential, and they are not merely artifacts of the solution

method used. The presence of these alternate equilibria may be

important in computer simulation studies. Saddle point energy for crack

propagation and thermally activated defect motion for example, may be

significantly different for the seperate equilibria. No solution method

apparently can be counted on to give true lowest energy configurations.

The problem considered here is of course a simple one and cannot be

considered representative of a true crack tip situation. The main

problems are the small size and the rigid boundaries, but improving

these points would increase the number of degrees of freedom and

increase the region of crystal affected by the non-linear crack tip

field, so that the number of alternate equilibria possible may increase.
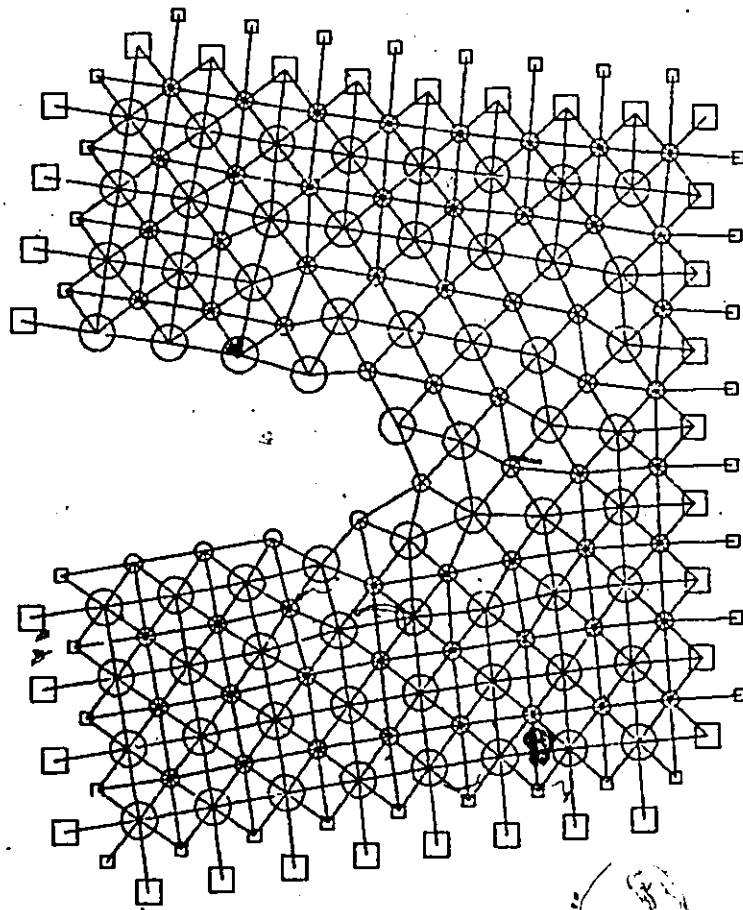
Figure 13.   Alternate equilibria at twice the Griffith stress
            intensity factor.
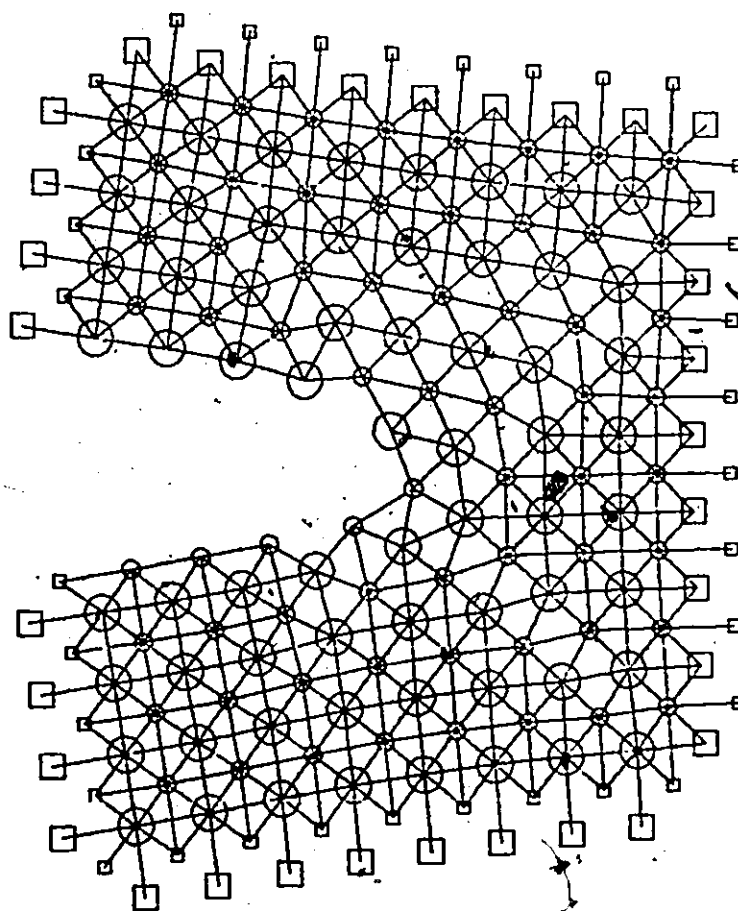   (a) ' modified conjugate gradient solution

Figure 13 (cont.)   Alternate equilibria at twice the Griffith stress
intensity factor.
(b)   individual quenching solution

The fact that alternate equilibria are so easily produced even for such a simple problem as this indicates that they may be more common than is usually considered.

The final point which will be considered is the relation between the energy error, $(C-E)'$, and the sum square of the atomic forces, $|\overline{F}|^2$, as the system approaches equilibrium during a static solution. The former quantity cannot, of course, be known before the solution is completed since E is the final equilibrium energy, but the latter is easily calculated at any time and it has in fact been used, [78], to determine the point at which the solution may be stopped. It can be used with all solution methods considered here. Other stopping criteria involving the use of kinetic energy in the system are more common for the quenching methods, [43,45], but these cannot be used for the conjugate gradient scheme. The criteria and the values used as tolerances in them have apparently been chosen fairly arbitrarily in the past. Figure 14 is a plot of $(C-E)$ versus $|\overline{F}|^2$ for all solution schemes on all problems tested here. A point is plotted for each after every 20 force evaluations. It can be seen that the force and energy are very strongly correlated for all cases. If a single interatomic bond is represented to a first approximation by a linear spring, we would have

$$e = f^2/(2s) \qquad (17)$$

where

e = potential energy in this spring,

f = force in the spring, and

s = spring constant of the bond.

If all springs were similar, the total energy above the equilibrium state and the sum square of all forces should behave in the same way. Figure 14 contains plots of the above equation for s's of 39.3 and 15.7 N/m. These are the spring constants for small displacements of the nearest and second nearest neighbour bonds in the model used here at their perfect crystal lengths. This can only be a very rough approximation to the true situation as a system such as the one used here approaches equilibrium of course. In crack problems for example, there is a general stretching of all bonds and a corresponding decrease in spring constant since the bonds are non-linear. Also, the fact that all springs are not alike even if no changes occurred would mean that no single value of s could characterize the system for all energies. Nevertheless, the correspondence between the observed points and the curves is quite good even for the crack problem. This ability to estimate the actual value of the energy error makes the force criterion an excellent one to use to determine when a solution has reached a sufficient level of accuracy.
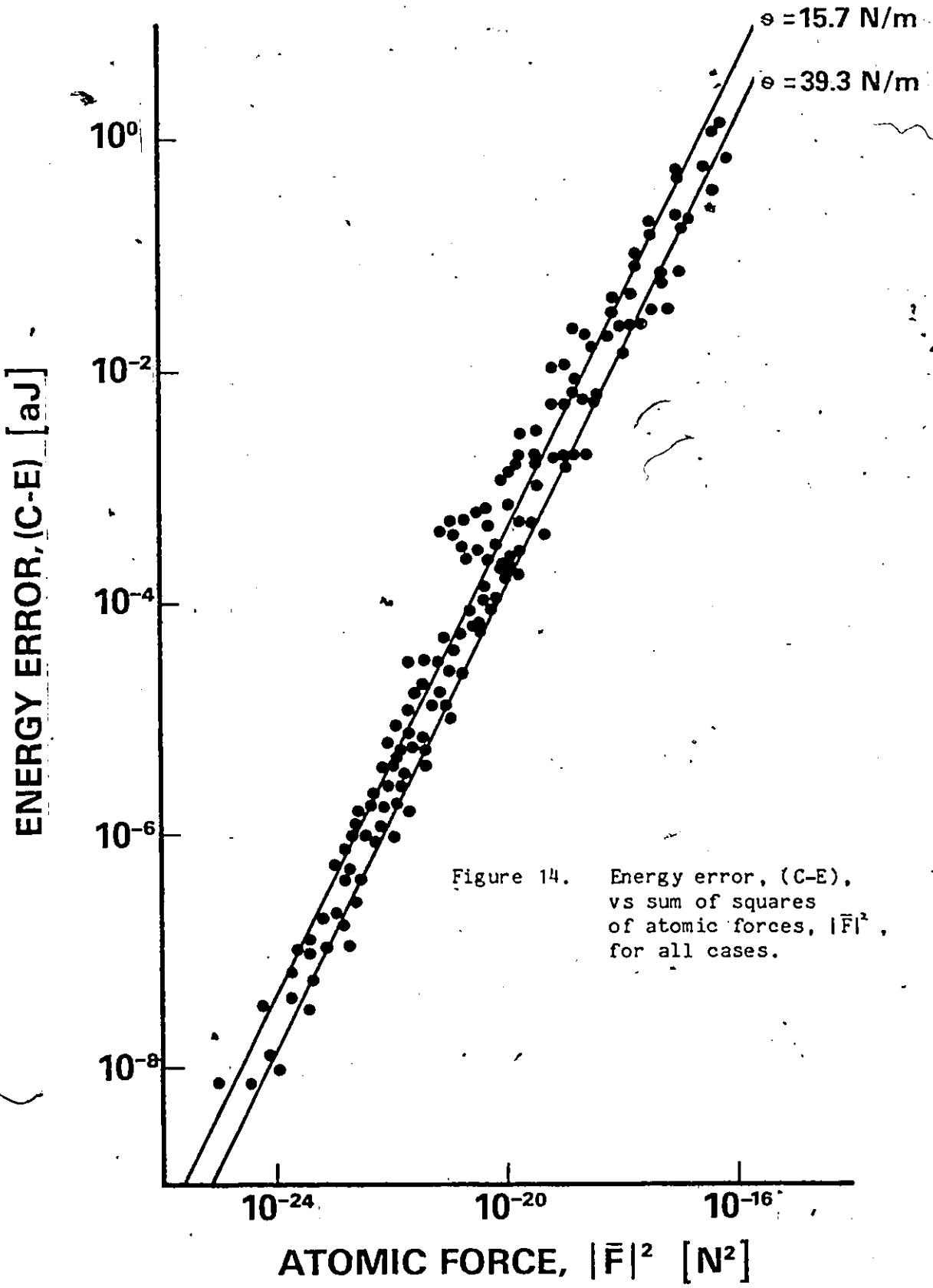
Figure 14. Energy error, (C-E),
vs sum of squares
of atomic forces, $|\bar{F}|^2$,
for all cases.

4.3 Conclusions

The tests presented in this chapter have shown that the selection of the optimum method for solution of an atomic simulation problem can result in a decrease of computer time used by factors of two or three over that required by other, often used, methods. For dynamic analyses where accurate solution of the equations of motion of the system is desired, the integration schemes which provide the best performance are the 2-step and 5-step difference formulas at low accuracies and the 5-step difference and p=6, q=1 Nordsieck at high accuracies. If one of the quenching methods are being used for static solutions, the p=4, q=1 Nordsieck is best, followed by the 2-step difference scheme. The integration step sizes may be chosen from Fig. 7.

For static solutions, the conjugate gradient optimization scheme has proven better for all test problems than either of the quenching methods. It was found, however, that the series of conjugate directions had to be restarted much more often than suggested by Sinclair and Fletcher in order to get efficient convergence (about every 10 steps). Simultaneous quenching was better than individual quenching for all cases. It may be that in problems where more than one atomic mass is present, individual quenching could be superior although this was not tested. For all solution methods, the higher spatial frequency components of the position errors were removed before the lower ones. This difference in speed was especially important for the quenching schemes, less so for the conjugate gradient method. The test problems

chosen here were fairly elementary but it is hoped that the results are
of general applicability. Future work could check the effect of model
size on solution efficiency and could determine if the addition of
flexible boundary schemes has any effect on it. The ease with which
alternate equilibrium positions were obtained indicates that this
problem may be of some importance. Judging by the limited experience
presented here, no static solution method appears to guarantee a true
lowest energy state. The differences in energy between the various
equilibria are fairly small but may become important when questions of
thermally activated defect motion are considered, for example. Further
exploration of this point would appear to be in order. No detailed
studies of the possibility of alternate minima were carried out in the
remainder of the work presented in this thesis. The computer time
necessary for solution of a typical problem, such as those used later,
is large enough that the cost of solving each by several different
methods, or with several different initial conditions, is prohibitive.
It may eventually be possible to produce a solution method which
unerringly converges to a true minimum in a reasonable amount of
computer time. At the moment, however, this would be very difficult and
it must be recognized that alternate minima, slightly different in
energy from those found, may exist. Finally, the use of the sum of the
squares of the unbalanced forces on all atoms appears to be a good
criterion to use to determine when sufficient accuracy has been reached
in a static solution.

5 FINITE ELEMENT BOUNDARY CONDITIONS

The accuracy of the boundary scheme used to analyze the continuum area of a computer simulation model, such as that shown in Fig. 2, has a very important effect on the accuracy of the final results. This has been indicated in sections 3.5 and 3.6 of the literature survey by, for example, a description of the failure of a crack to propagate when rigid boundary conditions were used. The types of flexible boundary schemes which have so far been employed in published work were also described. This chapter presents a description of a new boundary scheme employing the finite element method which appears to offer many advantages over previous methods. Tests of the new boundary scheme and a description of its advantages are also provided. The finite element method is described extensively elsewhere, [90, for example].

5.1 General Description

Figure 15 shows a typical model with finite element boundary conditions. It represents two planes of atoms of bcc α-Fe. The lattice parameter for this material is 0.286 nm. The crack shown lies in the (001) plane and has its crack line in the [010] direction. The model contains 308 free atoms, 82 embedded atoms, 175 nodes and 288 elements. Image planes of atoms above and below the two planes shown are established to provide the plane strain condition desired. These are
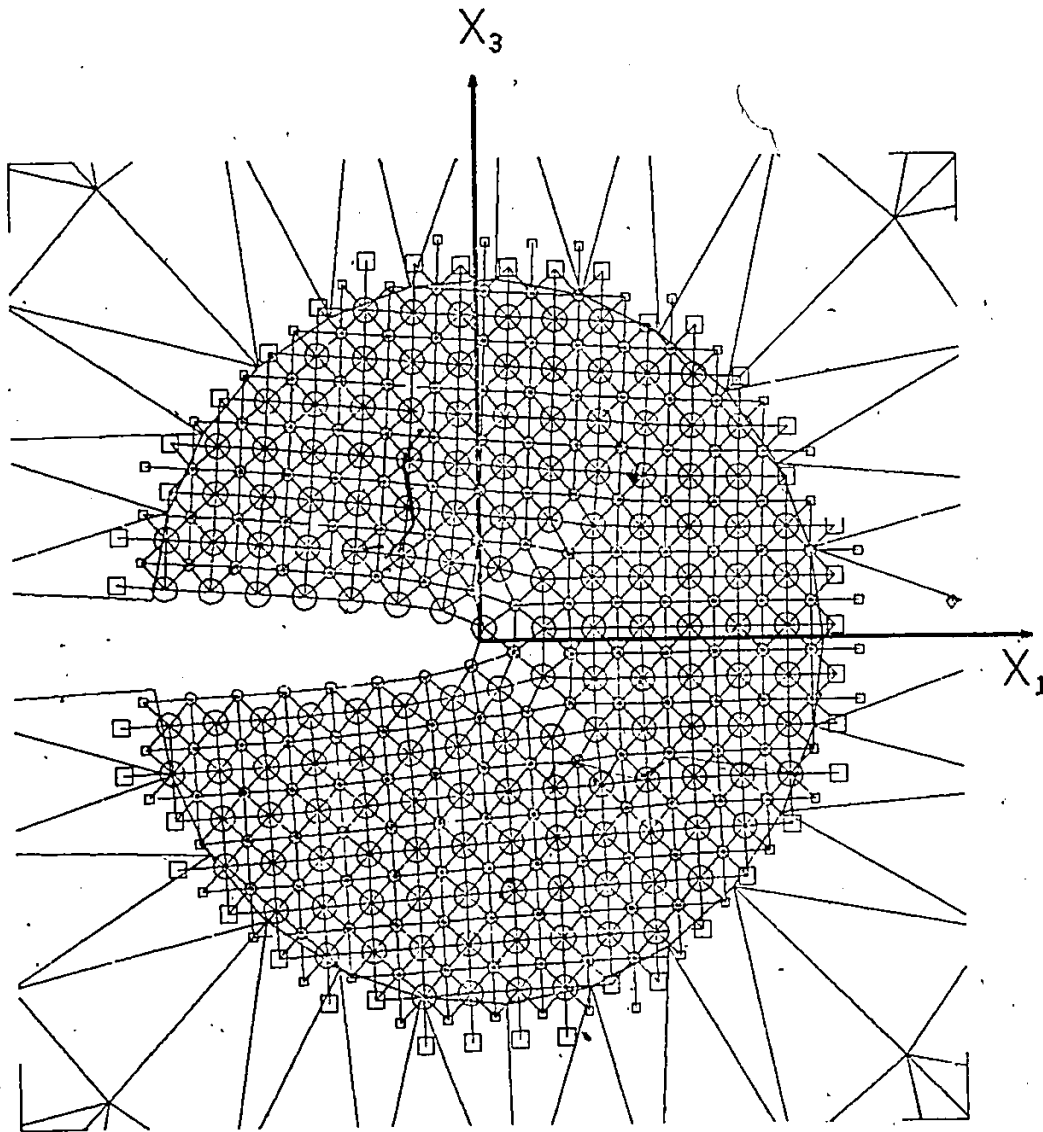
90

Figure 15. Model with finite element boundary conditions representing a (001)[010] crack in α-iron at $k = k_c$.
Scale is 2.5 cm to 1 nm.
The x_1 axis is [100], the x_3 axis is [001].
See Figure 6 for a description of the format of this plot.
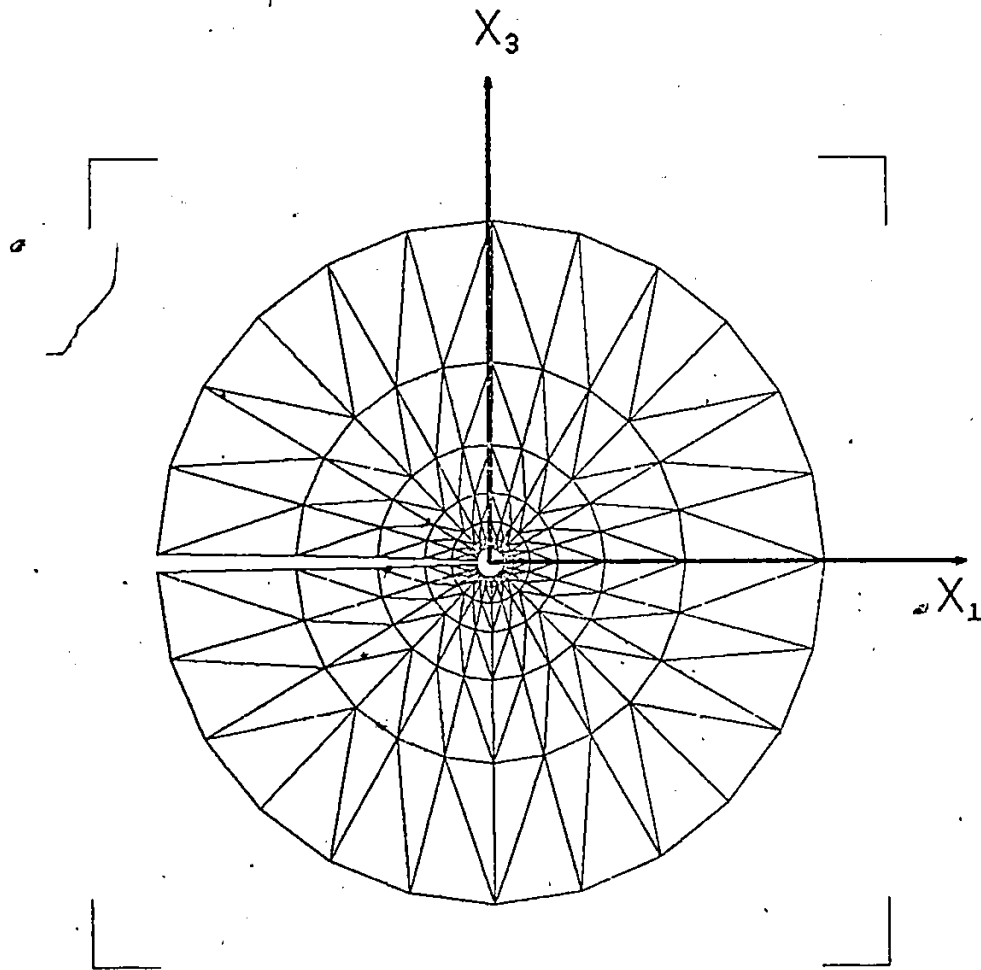(a) atomic area

Figure 15 (cont.)   Model with finite element boundary conditions.
                     Scale is 1 cm to 10 mm.
                     (b)   finite element area

moved with the corresponding atoms in the two active planes and their presence enables every atom in these two planes to have a complete set of bonds. In the present work, the free atoms are able to move in all three coordinate directions, while the nodes are restricted to movement in the x_1-x_3 plane.

The following nomenclature will be used in this chapter. A typical free atom will be referred to as atom i, a typical embedded atom by k. Quantities referring to free atoms will have subscript i, to embedded atoms will have subscript k. A typical node will be referred to as j, and quantities associated with this node will have subscript j. The coordinate directions will be described by subscript l, where l = 1,2, or 3. Forces on atoms are F, on nodes, Q. Thus, for example, the x_1 direction force on a typical free atom is F_{1i}, and the x_3 direction force on a typical node is Q_{3j}.

The degrees of freedom which completely describe the model are the x_1, x_2 and x_3 positions of all free atoms, $\{x_{1i}\}$, l = 1,2,3, and the x_1 and x_3 displacements from their perfect crystal positions of the nodes, $\{u_{1j}\}$, l = 1,3. Thus, the model of Fig. 15 has 924 degrees of freedom in the atomic area and 350 in the continuum. Forces corresponding to these degrees of freedom are $\{F_{1i}\}$ and $\{Q_{1j}\}$ respectively.

The $\{F_{1i}\}$ are determined by vector summation of the forces in all bonds to each free atom, i. These can be calculated from the $\{x_{1i}\}$, $\{x_{1k}\}$ and the interatomic potential. The $\{Q_{1j}\}$ have two components,

$\{Q_{1j}\}_1$ and $\{Q_{1j}\}_2$. The first is the nodal force due to the grid alone. If the continuum is considered to be linear, this is given by

$$\{Q_{1j}\}_1 = [K]\{u_{1j}\} \qquad (18)$$

where $[K]$ is the stiffness matrix for the finite element grid. The second component of the nodal force is due to the force on the embedded atoms caused by all bonds to them from the free atoms. This force, $\{F_{1k}\}$, is moved to the nodes by standard finite element techniques. The nodal force corresponding to any embedded atom, k, is

$$\{Q_{1j}\}_2 = [N]^T\{F_{1k}\} \qquad (19)$$

where $[N]$ is the shape function of the element containing atom k. Thus the total nodal force can be described as

$$\{Q_{1j}\} = \{Q_{1j}\}_1 + \{Q_{1j}\}_2 = [K]\{u_{1j}\} + [N]^T\{F_{1k}\} \qquad (20)$$

The embedded atoms move with the grid so that the displacement from its equilibrium position for atom k is given by $[N]\{u_{1j}\}$ where, again, $[N]$ is the shape function of the element containing atom k. Thus the positions of the embedded atoms are given by

$$\{x_{1k}\} = \{x_{1k}\}_0 + [N]\{u_{1j}\} \qquad (21)$$

where the $\{x_{1k}\}_0$ are the equilibrium positions of the embedded atoms.

A unique relationship has now been established between the degrees of freedom of the model and the corresponding forces. Given the displacements from equilibrium of the nodes, $\{u_{1j}\}$, the embedded atoms

are set to $\{x_{1k}\}$ by equation (21). This, together with the positions of the free atoms, $\{x_{1i}\}$, enables the forces on the free atoms, $\{F_{1i}\}$, and on the embedded atoms, $\{F_{1k}\}$, to be determined from the interatomic potential. The forces on the nodes, $\{Q_{1j}\}$, are now calculated by equation (20).

The method of linking the atomic and continuum areas described above is not completely straightforward since there is some ambiguity in determining the force on the embedded atoms. The method which has been used here is to keep all bonds from embedded to free atoms and to eliminate all bonds between embedded atoms. This implies that the finite element grid can account for the total stiffness of the material in the small ring around the atomic area which contains the embedded atoms. Another method might be to halve the strength of all embedded-to-embedded bonds and to halve the stiffness of the grid in this ring. Such elaborations were not felt to be warranted, however, and tests of the model on a uniaxial strain field described below indicated that the method used was probably adequate. Another problem is the non-uniform distribution of bonds crossing the border to the continuum area. A long flat border would have the correct number of bonds but corners of a rectangular atomic area and certain points on the border of a round atomic area have a non-uniform distribution. Again, the uniaxial strain tests indicated that the effect of this is also small. A third difficulty is the presence of non-zero bond forces in the model at the perfect crystal configuration. In this condition, the nearest neighbour bonds are in compression and the second nearest

neighbours are in equilibrating tension. The presence of these forces would lead to forces on the grid with wavelength equal to the lattice parameter. In the real crystal, these would be balanced by similar forces from bonds in the area of the crystal represented by the continuum region of the model. To balance these in the model, a set of additional forces, $\{F_{lk}\}_0$, are applied to the embedded atoms which balance the forces just described in the perfect crystal configuration. Figure 16 illustrates this point. Finally, the area of the model at the crack face is another ambiguous region. The bonds across the crack in the atomic area were cut and no other forces applied to the atoms there so that they are permitted to relax into a free surface arrangement with no account taken of possible bond redistribution at such a surface. The forces, $\{F_{lk}\}_0$, on the embedded atoms at the crack face were set so that no net force acted on the crack faces and no net force acted on the grid perpendicular to the grid-atomic area border in the perfect crystal configuration.

Any of the standard solution techniques for atomic simulation problems may now be employed to solve the model for its equilibrium position. The application of a variational technique is straightforward with the $\{x_{li}\}$ and $\{u_{lj}\}$ changed until $\{F_{li}\}$ and $\{Q_{lj}\}$ approach zero. Quenching type solution methods may also be used. The mass of each element may be lumped to its nodes (or a more elaborate consistent mass matrix may be established) and the equations of motion integrated and quenched at the appropriate times. Since only the final equilibrium position is of interest, the mass used has no importance except as it
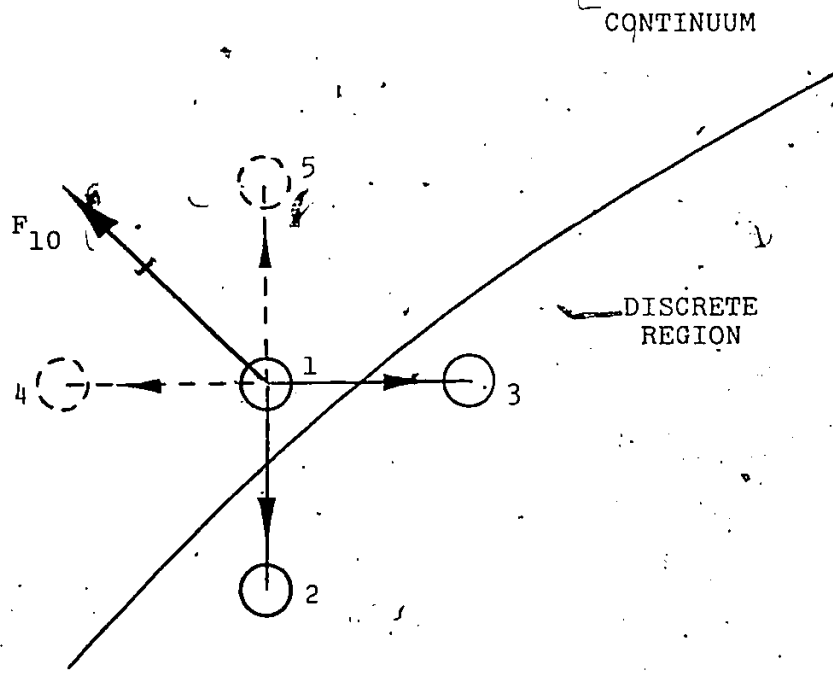
Figure 16. Schematic illustration of initial forces applied to embedded atoms. In the equilibrium configuration of the crystal, the sum of the forces in the four bonds to atom 1 would be zero. In the present model atoms 4 and 5 have been eliminated since they are entirely within the continuum. Force $\bar{F}_{10}$ (the sum of the forces in bonds 1-4 and 1-5) is added to atom 1 to simulate these forces.

affects the speed of convergence. It was found that scaling the mass of each node to the diagonal element of the stiffness matrix corresponding to this node gave good convergence without introducing any instability in the numerical integration process. A dynamic simulation would, of course, involve integrating the equations of motion of the model with the correct mass on each node.

Anisotropy is easily introduced when the stiffness matrix is calculated. Non-linearity may also be introduced into finite element analyses. The usual methods involve an incremental solution by means of tangent stiffness matrices corresponding to the current configuration at the end of each increment, [90]. This could be used here although, because of the nature of the two solution methods described above, a simpler technique is possible. The problem of finding the nodal forces, $\{Q_{1j}\}_1$, due to the grid, corresponding to given nodal displacements, $\{u_{1j}\}$, can be approached as follows: the nodal displacements of each element can be used to find the strain in the element; this strain can be used to find the corresponding non-linear stress from the crystal configuration and the interatomic potential; this stress can then be translated back into nodal forces by standard finite element techniques as

$$\{Q_{1j}\}_1 = \int_V [B]^T \{\sigma\} dV \tag{22}$$

where $\{\sigma\}$ is the vector of stresses in the element, and the integration is over the volume of the element containing the nodes $\{j\}$. Matrix $[B]$ relates strain, $\{\varepsilon\}$, to nodal displacements for the element, i.e.

$${\epsilon} = [B]{u_{1j}} \tag{23}$$

Equation (22) must be evaluated for each element and the force on each node due to each element containing this node summed. Both material and geometric non-linearities may be accounted for in this manner. The time for the evaluation of one set of nodal forces is proportional to the number of elements and independent of bandwidth in this case.

5.2 Non-Linear Stress-Strain Relationship

Material non-linearity has been included in the studies done in this thesis. This was found to be necessary as a result of the tests on the model under uniaxial strain. The manner in which the non-linear stress-strain relationship was calculated and the shape of this relation are described in this section.

A single atom surrounded by a set of all its neighbouring atoms was considered. In the case of the Johnson-I potential and bcc crystals used in this work, there were 14 neighbouring atoms, 8 nearest neighbours and 6 second nearest neighbours. A count was made of the number of bonds of each type which cross the three positive coordinate direction planes. Figure 17 snows the set of neighbouring atoms to the test atom, and Tables 3 and 4 give the count of bonds in each direction for the case of coordinate axes in the two directions used in this work.

The neighbouring atoms were moved with respect to the central atom to correspond to a given strain. The force in each bond was calculated from the interatomic potential. The total force per unit
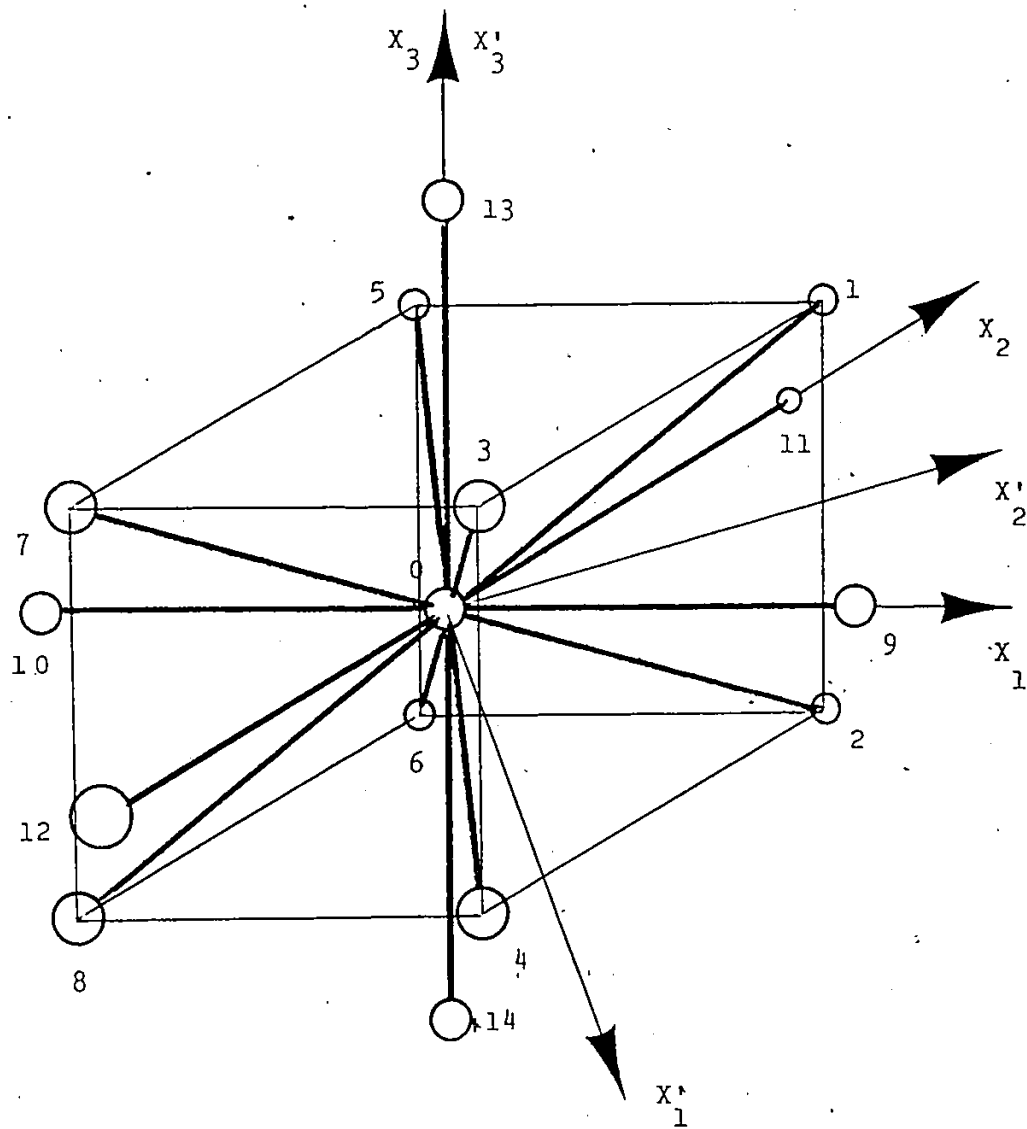
Figure 17.   Neighbouring atoms to test atom, 0, for non-linear stress
              calculation. The unprimed axes are used for the [010]
              crack model, the primed axes for the [110] crack model.

Table 3.   Bond count for non-linear stress calculation for [010] crack.

Atom numbers refer to Fig. 17.   This table gives the number of bonds similar to that to a given atom number per square nm of each positive coordinate plane for bcc α-iron.

Atom Number	x_1-plane (100)	x_2-plane (010)	x_3-plane (001)
1	12.23	12.23	12.23
2	12.23	12.23	0
3	12.23	0	12.23
4	12.23	0	0
5	0	12.23	12.23
6	0	12.23	0
7	0	0	12.23
8	0	0	0
9	24.45	0	0
10	0	0	0
11	0	24.45	0
12	0	0	0
13	0	0	24.45
14	0	0	0

Table 4.   Bond count for non-linear stress calculation for [110] crack.

Atom numbers refer to Fig. 17.   This table gives the number of
bonds similar to that to a given atom number per square nm of each
positive coordinate plane for bcc α-iron.

Atom Number	x_1-plane (110)	x_2-plane (110)	x_3-plane (001)
1	0	17.29	12.23
2	0	17.29	0
3	17.29	0	12.23
4	17.29	0	0
5	0	0	12.23
6	0	0	0
7	0	0	12.23
8	0	0	0
9	17.29	17.29	0
10	0	0	0
11	0	17.29	0
12	17.29	0	0
13	0	0	24.45
14	0	0	0

area and, therefore, the stresses were then calculated by summing the
components of the forces in each bond, weighted by the values in Table 3
or 4, and resolving these into direct and shear components. The
non-linear stress-strain relations corresponding to a given interatomic
potential could then be calculated. This procedure is carried out
whenever the stress corresponding to a given strain is needed. This is
done once per element for every force evaluation.

Figure 18 shows the plane strain and plane stress uniaxial
stress-strain curves for the model of α-iron used in this thesis. This
is the bcc material of Fig. 15 with the Johnson-I potential, Fig. 5.
The material is assumed to be oriented so that the coordinate directions
are [100] directions. Since no dislocation processes were considered,
no plastic yielding occurs and very high stresses are possible. Strains
in the continuum greater than 0.05 are possible in crack tip studies and
it can be seen that significant elastic non-linearity occurs in the
material at this strain level. This indicates that including
non-linearity in the continuum region of a simulation model should be
quite important in crack tip studies.

Figure 19 shows the extent of non-linearity in the material
under plane strain conditions, $\varepsilon_2 = 0$. This plot was created by
calculating the stress for given values of ε_1 and ε_3 with all other
strains zero. For each of the six stress values, the quantity
$(\sigma - \sigma_1)/\sigma_{max}$ was calculated where
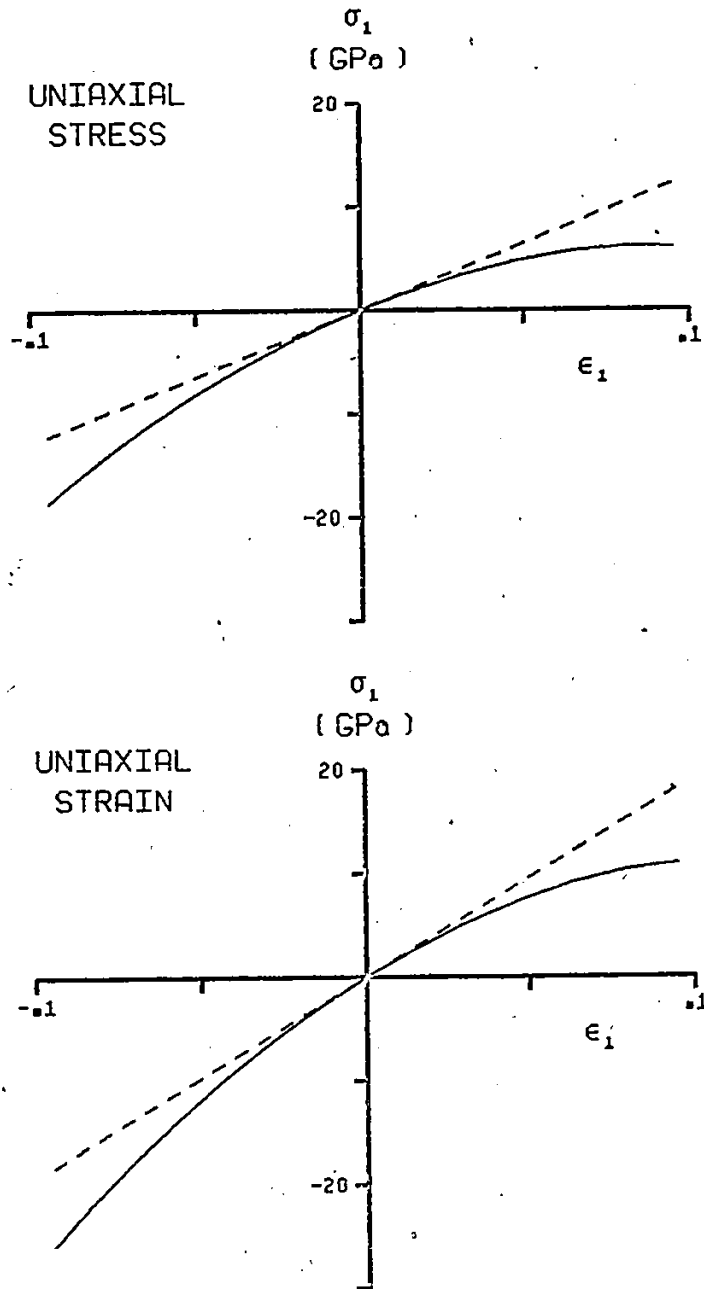
Figure 18.   Stress-strain curves for Johnson-I potential bcc iron at
             large strains (solid curve). Dotted line is derived from
             the small strain elastic constants.
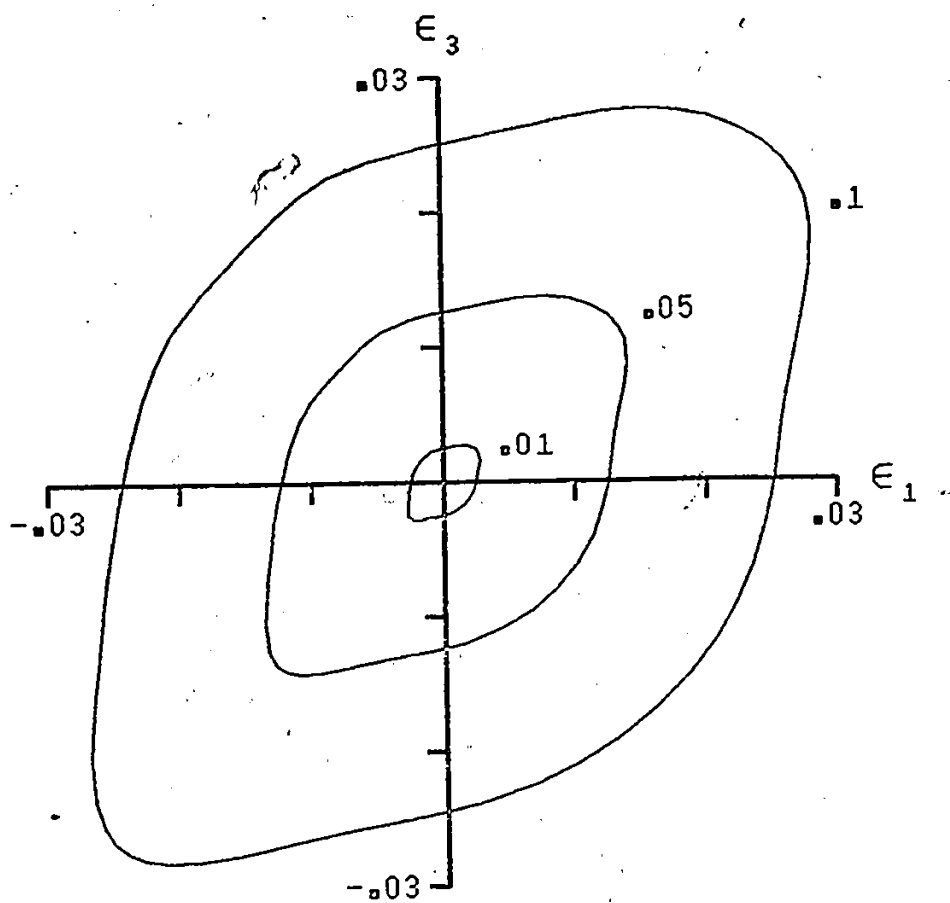
Figure 19.   Contours of constant non-linearity defined in section 5.2 .

σ — non-linear stress value for strain ε_1, ε_3,

σ_1 = stress value for ε_1, ε_3 if material were linear

with elastic constants equal to their small

strain values, and

σ_{max} = maximum of the six σ_1's.

The greatest of these values is plotted as the non-linearity. Again, it can be seen that it can be quite significant. As a result of this examination, it was felt that non-linearity would probably have to be included and the results of the next section confirmed this.

5.3 Uniaxial Strain Tests

In order to test the accuracy of the method of linking the grid and the atomic area and to examine the effect of including non-linearity of the grid, a model was solved under a very simple loading condition. This made a check possible of errors in the final atomic positions. The loading condition chosen was uniaxial strain.

The model shown in Fig. 20 was used. The outside edge of the grid shown in Fig. 20(b) was fixed at a position corresponding to uniform uniaxial strain, ε_1. ε_2 was zero because of the plane strain condition and ε_3 was set zero on the boundary. In the exact solution, the strain state should be constant everywhere. The model was solved for $\varepsilon_1 = 0.01$ and 0.05 for both linear and non-linear grids. The Johnson-I model of α-iron was used in all cases.
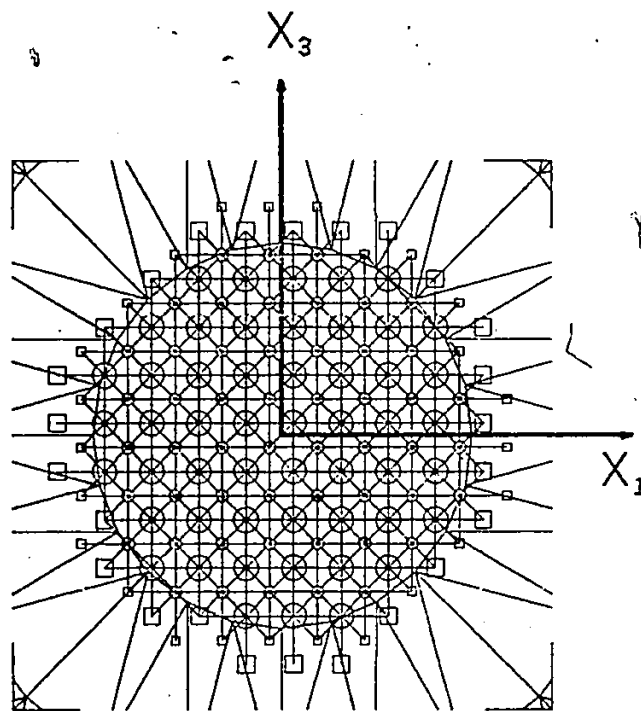
Figure 20. Model for uniaxial strain tests. Scale is 2.5 cm to 1 nm.
(a)   atomic area
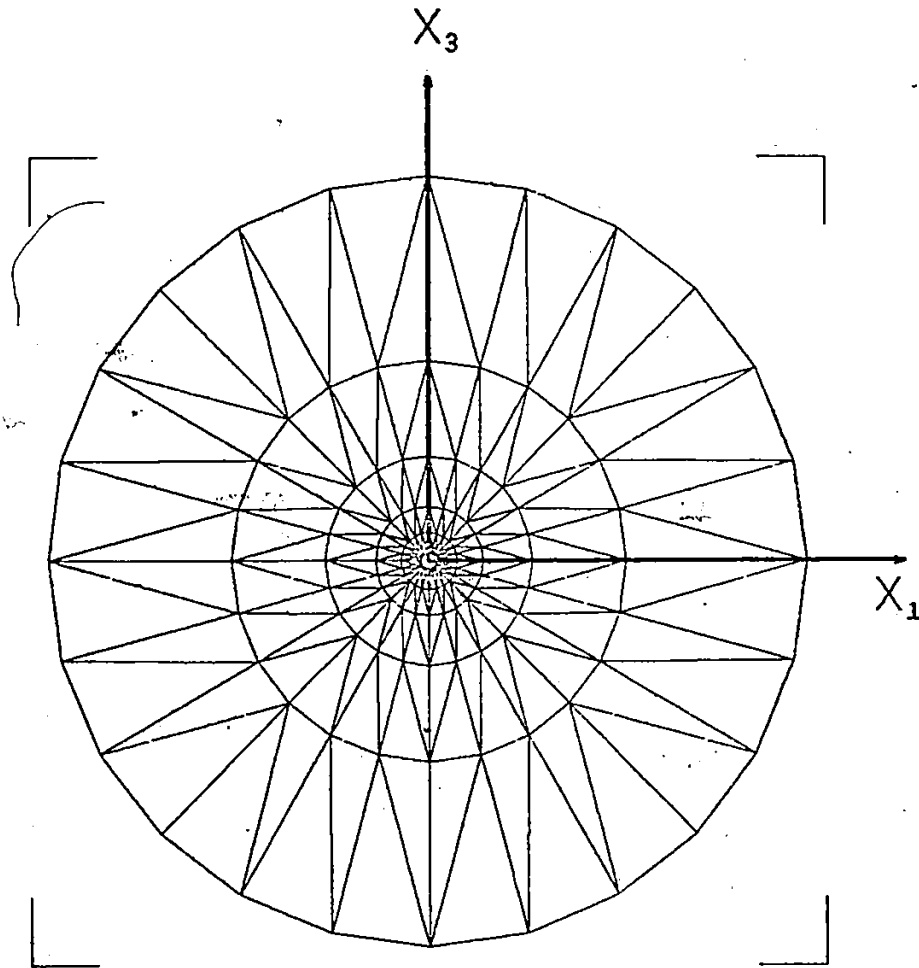
Figure 20 (cont.)   Model for uniaxial strain tests.
Scale is 1 cm to 10 nm.
(b)   finite element area

.The results are shown in Figs. 21 and 22. The error in position

of an atom in the x_1 and x_3 directions are δx_1 and δx_3 respectively.

The quantities plotted in Figs. 21 and 22 are

$(\delta x_1/x_1)$ $/\epsilon_1$ for the error in the x_1 direction, and

$(\delta x_3/x_3)$ $/\epsilon_1$ for the error in the x_3 direction.

These represent the fraction error in strain. These are pl̶̶̶r the

atoms around the largest square inscribed in the circular atomic area of

Fig. 20.

It can be seen that both grids are about equal in accuracy at

$\epsilon_1 = 0.01$, but that the non-linear grid is much better at $\epsilon_1 = 0.05$.

Since strains in excess of 0.05 appear in the continuum areas in some

crack tip studies, it was felt that the non-linear grid should be used

for all later work. The error with the linear grid is about .10% over

much of the area studied. In addition, it appears to be strongly

dependent on strain level so that it would be even higher at the strain

levels encountered in some simulations. Comparing Figs. 21 and 22

indicates that the error with the non-linear grid is virtually

independent of strain. This error is, then, probably the error due to

the non-uniform distribution of bonds as described in section 5.1 above.

It is less than 2% in all cases and is less than 1% over most of the

area studied. The models used later in this thesis are larger than that

of Fig. 20. It would be expected that larger models should be even more

accurate than this. It was felt that this was sufficiently accurate for

the present work, so no attempt was make to reduce this error.
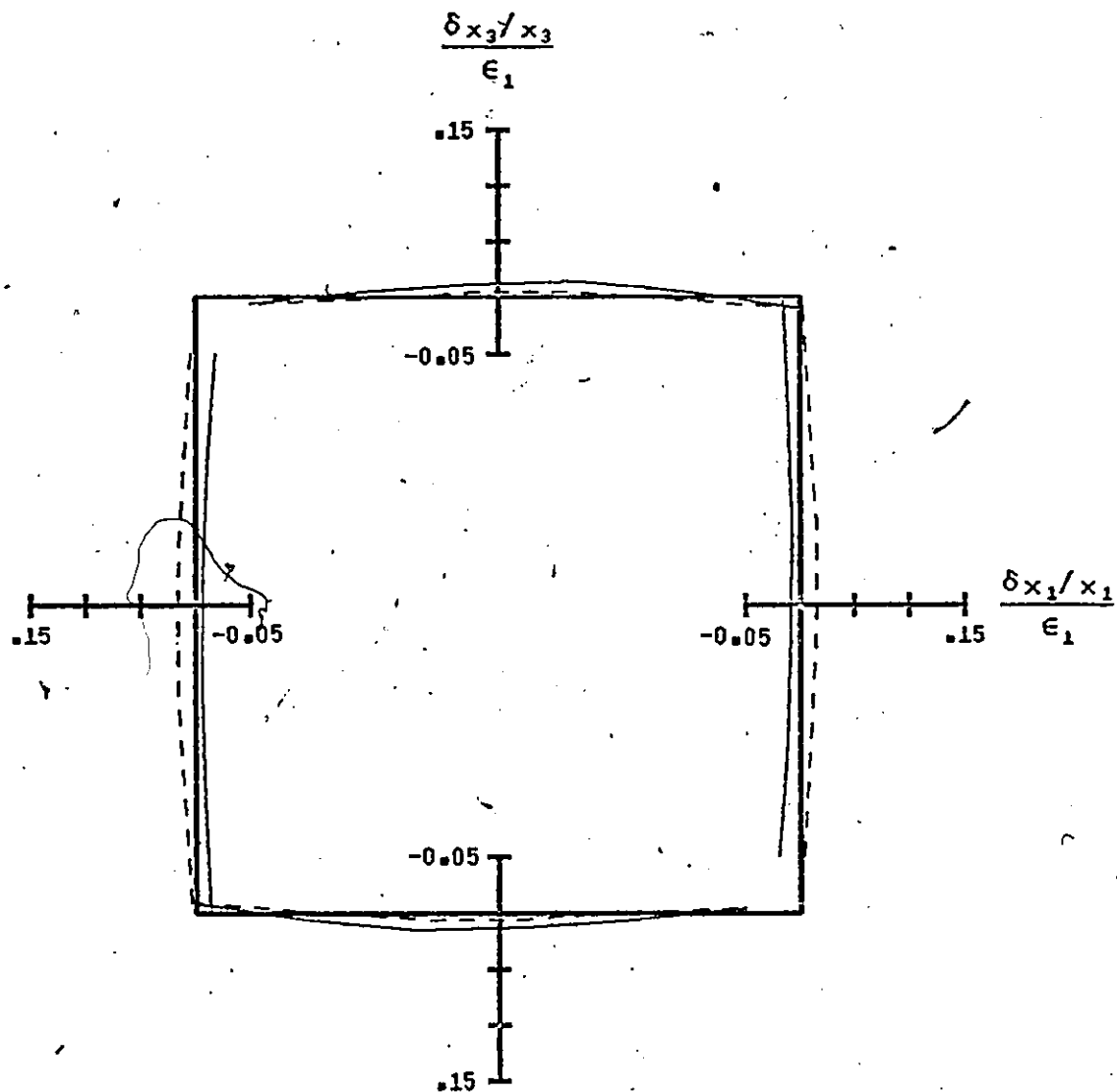
Figure 21.   Results of uniaxial strain tests. The square represents
the correct positions of the atoms considered. The solid
curve shows the deviation from these positions, x, for
the non-linear grid. The dashed curve shows the results
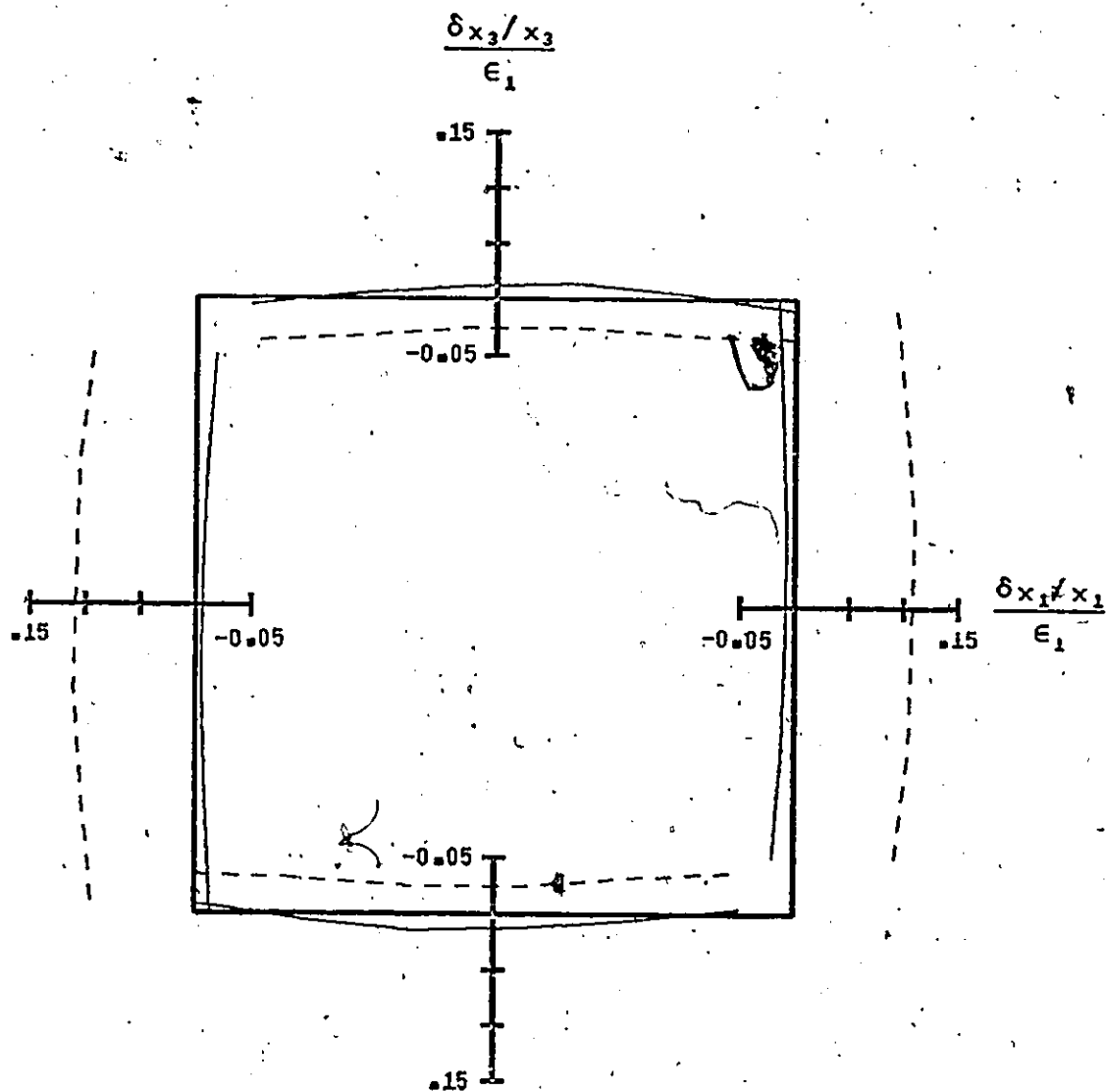for the linear grid. $\epsilon_1 = 0.01$.

$$\frac{\delta x_3 / x_3}{\epsilon_1}$$

.15

−0.05

−0.05

.15

−0.05

−0.05

.15

.15

$$\frac{\delta x_1 / x_1}{\epsilon_1}$$

Figure 22.   Same as Figure 21 except $\epsilon_1 = 0.05$.

5.4 Model Size and Boundary Condition Tests

This section describes some possibilities for loading the model at the outer edge of the finite element continuum area. The method chosen and some tests of the effect of changes in this, and in the number of degrees of freedom in the continuum area are described.

The external loads in a real crystal being fractured are applied at distances very large in comparison to the atomic spacing. This should be the case, also, in model crystals. In order to eliminate any confusing effect of the outer boundary, it would be most appropriate if these were set at infinity. It is possible to do this with finite elements by means of the so-called "boundary solution procedure", [90], but this did not appear necessary in the present case. Instead, standard finite elements were used and the outside edge of the continuum area was made very large compared to the size of the atomic area. The displacements of nodes at this outside boundary were then set at the linear elastic solution positions for the crack studied. Because the outside boundary is much larger than the size of the atomic area, the error caused by fixing these nodes is small. For the cases studied in Chapter 6, the radius of the outer boundary was set at 25 times that of the atomic area. This is the case that was illustrated in Fig. 15.

One estimate of the effect of this boundary may be made as follows. For the solutions obtained later in this thesis, some curve fitting was performed to determine whether the higher order linear elastic crack tip solutions could provide a good description of the

resulting displacement field. If any of the terms found from fitting the displacements near the crack tip are extended to the outer boundary, the change in displacement there would be about 0.003 of the total displacement, probably a negligible amount. Another way of estimating the effect of this is to solve a problem with a larger boundary and compare the results. Figure 23 shows a model with outer radius 50 times that of the atomic area or twice that of Fig. 15. At the Griffith stress intensity factor, the largest difference in position for any atom between the two cases was 0.003 nm, while the average difference was 0.001 nm. This compares to a maximum total displacement of 0.274 nm and an average total displacement of 0.167 nm. It was felt that this was sufficiently small so the smaller boundary was chosen for all work.

A test of the effect of grid coarseness was also performed. The model shown in Fig. 24 was solved at the Griffith stress intensity factor and compared to that in Fig. 15. Figure 24 contains 85 nodes compared to 175 in Fig. 15 and the former thus has about half as many degrees of freedom as the latter. For this test, the maximum position difference was 0.01 nm while the average was 0.005 nm. It was felt that the coarse grid might not have been sufficiently accurate so the finer one was used for all studies. Computer memory and cost limitations made the use of even finer grids or larger atomic areas inconvenient.
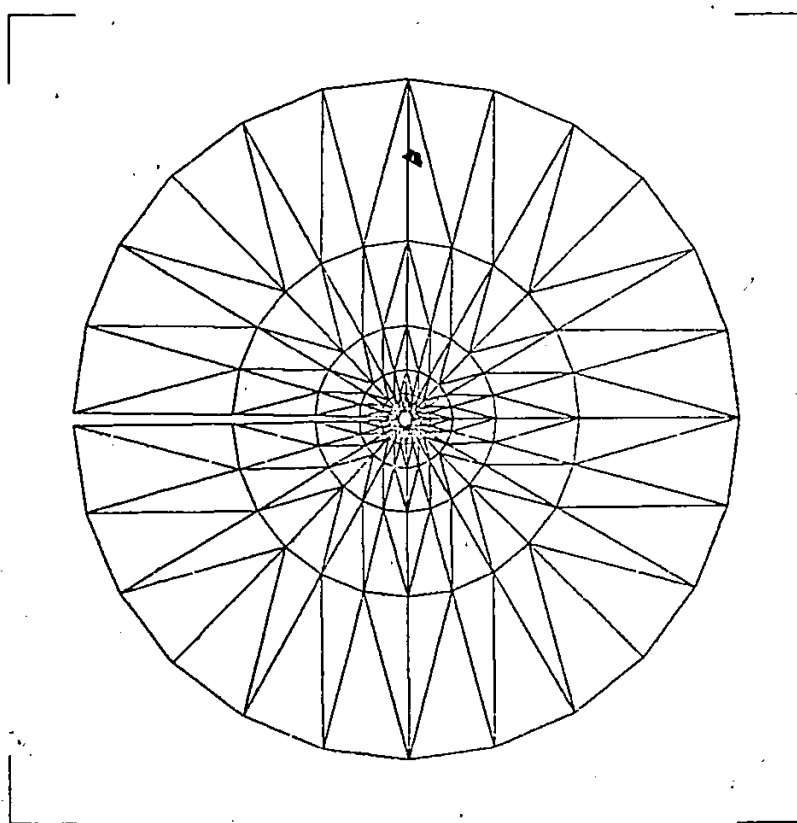
Figure 23. Model with outer radius 50 times atomic area radius.
Scale is 1 cm to 20 nm.
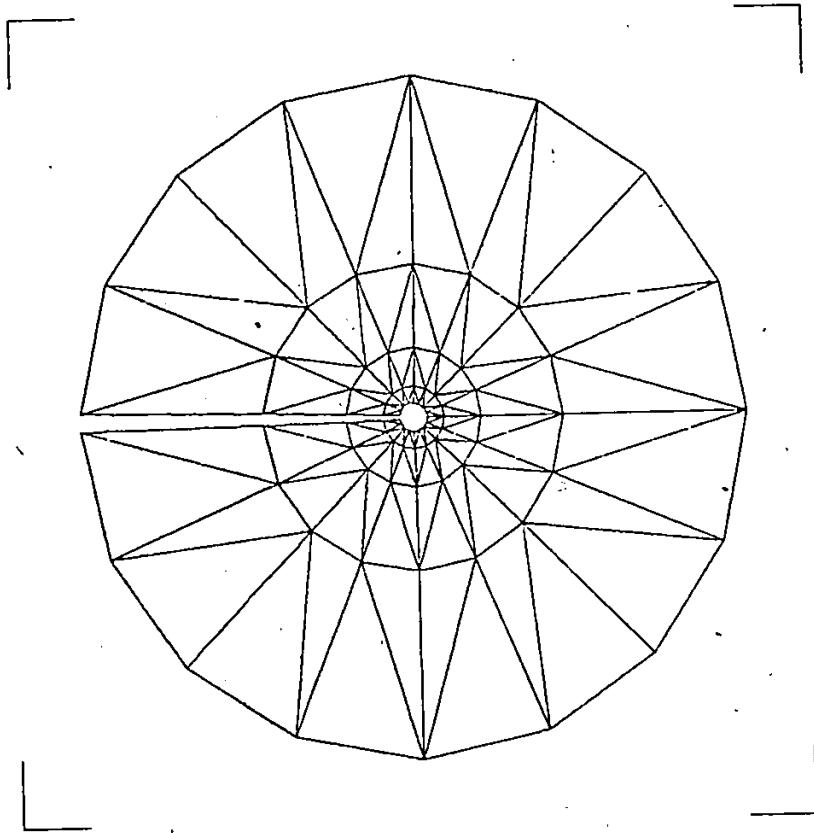
Figure 24.   Coarse grid model.   Scale is 1 cm to 10 nm.

5.5 Conclusions

This chapter has presented a description of a new boundary condition scheme for atomic simulation problems. In comparison to previous methods --

1) It is much simpler analytically. The previous methods are all very complicated to apply especially since anisotropic solutions should be used. As a result, the continuum has usually been modelled with only about ten degrees of freedom, often less. The finite element method can easily employ several hundred and still involve less set up and computer time as well as less chance of error.

2) All the solution techniques which can be applied to the atomic area of the model can also be applied to the finite element area. This eliminates instability problems encountered with the other methods caused by the more complicated solution process which must be used, [44].

3) Non-linearity may be added to the finite element area by fairly well known methods. This may be quite important in the study of some defects such as cracks, around which large stresses extend for a considerable distance into the continuum area. There is no tractable way of doing this with the other techniques at the moment.

4) A dynamic analysis as would be required for the study of defect motion including the resulting acoustic emission is straightforward by finite elements but very difficult with the previous methods.

5) Unusual geometries, such as a grain boundary junction, are much easier to handle.

6) Three dimensional models or three dimensional displacements in two dimensional models are possible by finite elements while the analytical solutions that would be necessary in order to use the other boundary schemes exist only for very special cases. These types of models will become more widely used as computer costs decrease in the future. Screw dislocations, for example, must be modelled in this manner.

Various options in the application of this boundary scheme have been described and those chosen for the work presented later in this thesis have been indicated. Some further extensions or problems yet to be completely resolved are

1) Models with more degrees of freedom in both the continuum and discrete areas are, of course, always desireable. Computer memory and solution time limitations have imposed the limits chosen in the problems examined in the present work. The tests described above indicate that they are probably not too restrictive.

2) There are some ambiguities in the mating of the discrete and
continuum areas. This problem is common to all currently existing
boundary schemes and not limited to the finite element approach.

3) Geometric non-linearity has not been accounted for in the finite
element analysis. This should be done in the future in order to
determine if its effect is significant.

4) The method of applying the boundary conditions to the outer edge of
the model could be improved by the use of the boundary solution
procedure which would allow the model to effectively extend to an
infinite radius.

6 APPLICATION OF FINITE ELEMENT BOUNDARY CONDITION SCHEME

The boundary condition scheme described in the previous chapter
has been applied to the (001) plane crack in an α-iron model using the
Johnson-I interatomic potential. This crack has been studied
previously, as described in the literature survey, but the results have
not been completely successful with the boundary schemes which have been
used. In the present work, two dimensional cracks with crack line
directions of [010] and [110] have been studied. The latter had
apparently never before been examined. The model results are presented
in various formats and are compared to the experimental results
available. These have already been described in the literature survey.

The perfect crystal configuration for the two models studied in
this chapter are shown in Figs. 25 and 26. Unless otherwise noted, all
plots in this chapter are at a scale of 2.5 cm to 1 nm. In both cases,
the cracks are introduced along the x_3 plane extending from the origin
in the negative x_1 direction. The crack line is in the x_2 direction,
ie. perpendicular to the plane of these figures.

6.1 Linear Elastic Crack Tip Boundary Conditions

As stated in section 5.4, the outer edge of the continuum region
of these models was set at the linear elastic crack tip solution
position for each case studied. This section describes how these may be
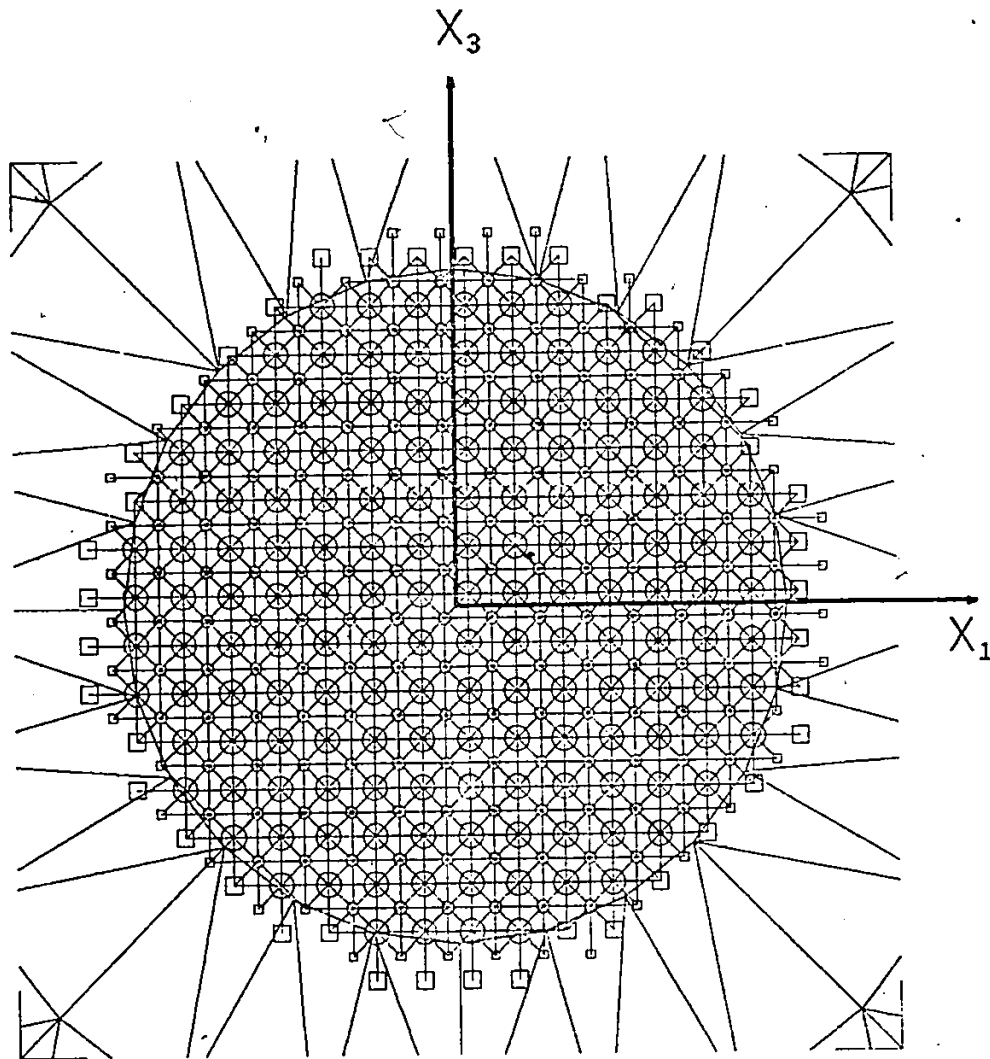
Figure 25.   Perfect crystal configuration for (001)[010] crack model.
See Figure 6 for a description of the format of this plot.
The x_1 axis is [100], the x_3 axis is [001].
(a)   atomic area
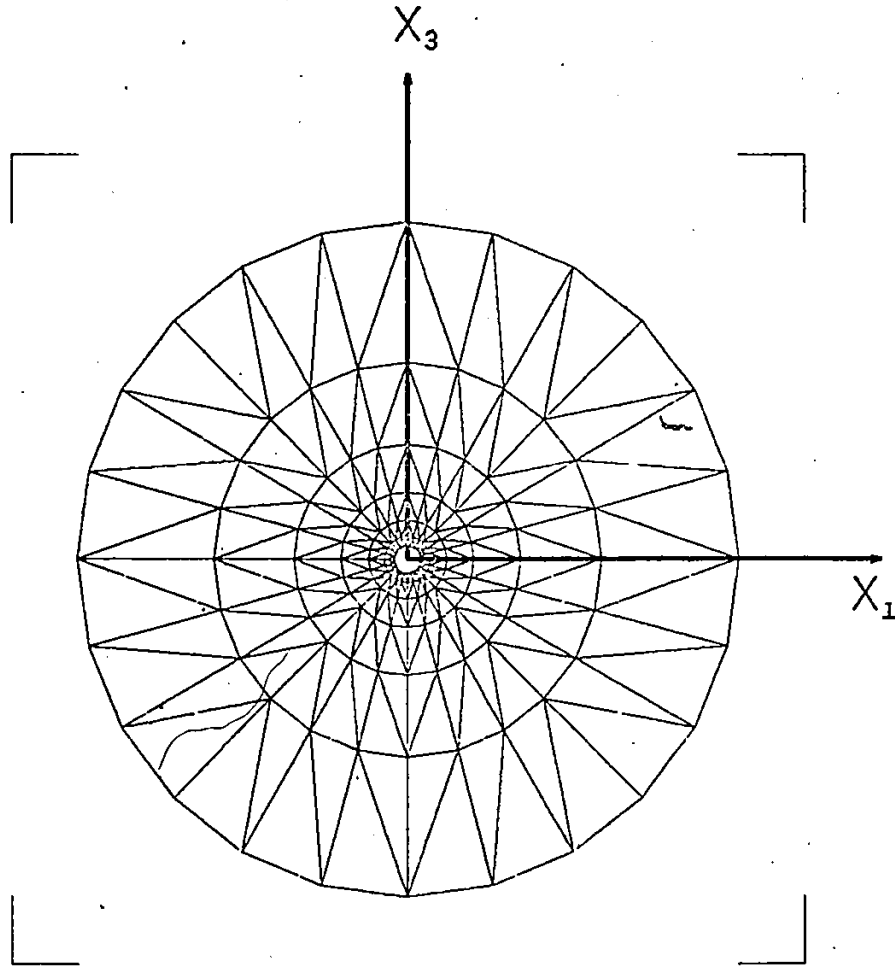
Figure 25 (cont.)   Perfect crystal configuration for (001)[010]
                    crack model.
                    Scale is 10 nm to 1 cm.
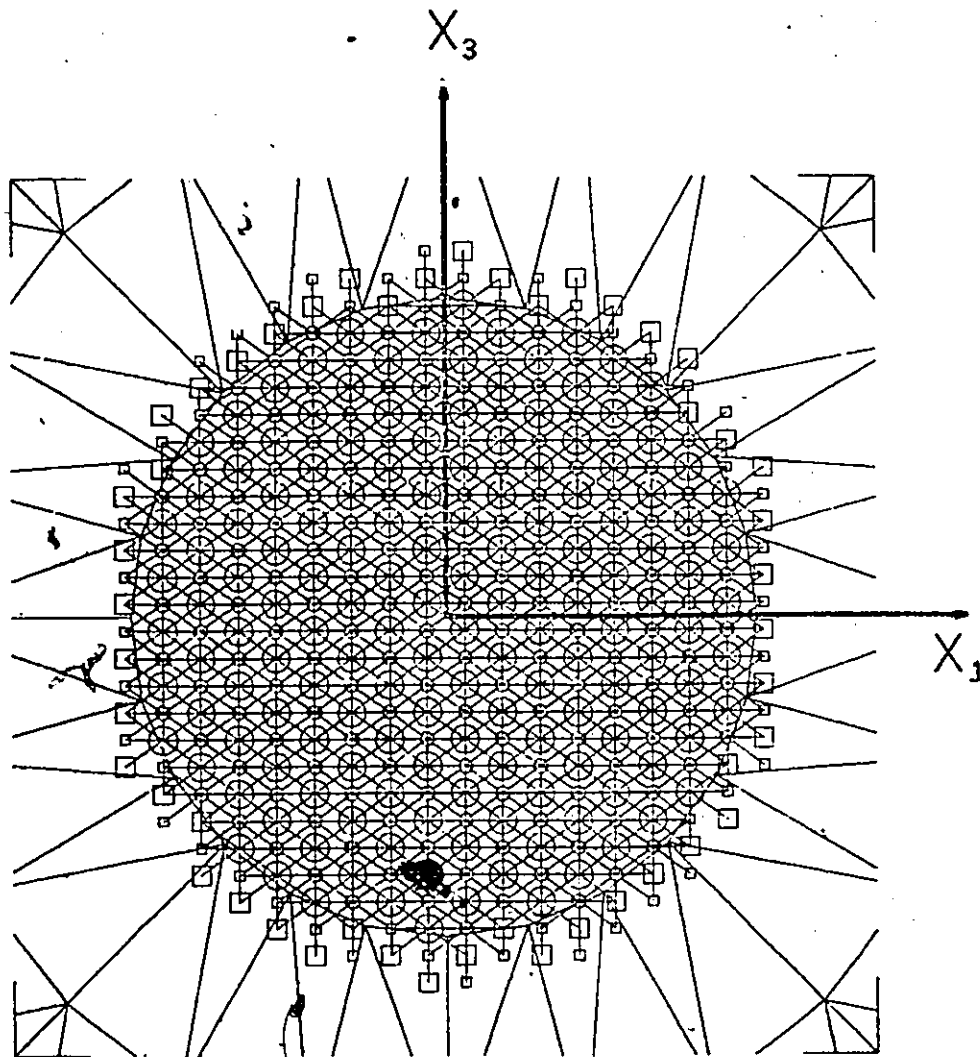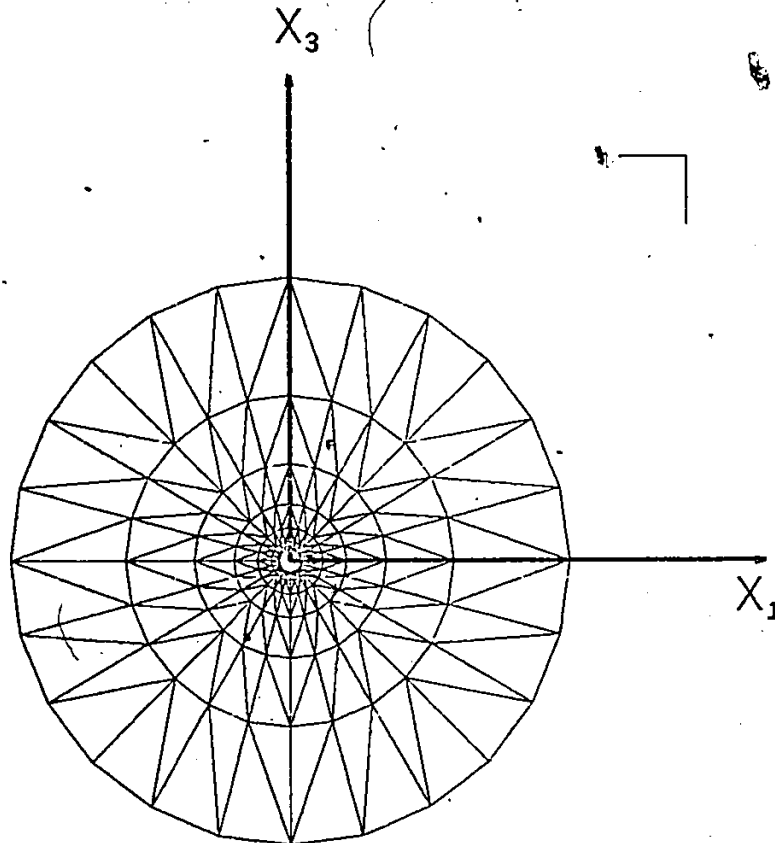   (b)   finite element area

Figure 26. Perfect crystal configuration for (001)[110] crack model.
The x_1 axis is [110], the x_3 axis is [001].
(a)   atomic area

Figure 26 (cont.) — Perfect crystal configuration for (001)[110]
crack model.
Scale is 10 nm to 1 cm.
(b)   finite element area

obtained, [62].

For an anisotropic material with mirror symmetry about the x_1-x_3 plane and plane strain in the x_2 direction (the cases studied here), the three in-plane strains may be given by

$$\begin{Bmatrix} \epsilon_1 \\ \epsilon_3 \\ \epsilon_5 \end{Bmatrix} = \begin{bmatrix} a_{11} & a_{13} & a_{15} \\ a_{13} & a_{33} & a_{35} \\ a_{15} & a_{35} & a_{55} \end{bmatrix} \begin{Bmatrix} \sigma_1 \\ \sigma_3 \\ \sigma_5 \end{Bmatrix} \tag{24}$$

where $\epsilon_1 = \epsilon_{11}$, $\epsilon_3 = \epsilon_{33}$, $\epsilon_5 = \epsilon_{31}$, $\sigma_1 = \sigma_{11}$, $\sigma_3 = \sigma_{33}$, $\sigma_5 = \sigma_{31}$, in the more usual notation and engineering shear strain is used. The linear elastic crack tip solution for this material is expressed in terms of two complex functions, $\phi_1(z_1)$ and $\phi_2(z_2)$ of the complex variables z_1 and z_2 where

$$z_1 = x_1 + \mu_1 x_2$$
$$z_2 = x_1 + \mu_2 x_2 \tag{25}$$

where μ_1 and μ_2 are obtained from the equation

$$a_{11}\mu^4 - 2a_{15}\mu^3 + (2a_{13} + a_{55})\mu^2 - 2a_{35}\mu + a_{33} = 0 \tag{26}$$

whose roots are μ_1, μ_1^*, μ_2, μ_2^* (complex conjugate pairs). The displacements are given by

$$u_1 = Re[p_1\phi_1(z_1) + p_2\phi_2(z_2)]$$
$$u_2 = 0 \tag{27}$$
$$u_3 = Re[q_1\phi_1(z_1) + q_2\phi_2(z_2)]$$

where

$$p_1 = a_{11}\mu_1^2 + a_{13} - a_{15}\mu_1 \qquad (28)$$

$$q_1 = a_{31}\mu_1 + a_{33}/\mu_1 - a_{35}$$

for $1 = 1,2$ and

$$\phi_1(z_1) = \frac{\mu_m}{\mu_m - \mu_1} k (2z_1)^{1/2} \qquad (29)$$

for stress intensity factor, k, where $1 = 1,2$ and $m = 2,1$ respectively. Equations (27) are used to set the boundary at the outer edge of the finite element grid. The energy release rate, G, corresponding to k for this case is given by

$$G = \pi \frac{k^2}{2} a_{33} Re \left[i \frac{\mu_1 + \mu_2}{\mu_1\mu_2} \right] \qquad (30)$$

$$= \pi k^2 \left(\frac{a_{11}a_{33}}{2} \right)^{1/2} \left[\left(\frac{a_{33}}{a_{11}} \right)^{1/2} + \frac{2a_{13} + a_{15}}{2a_{11}} \right]^{1/2}$$

It remains to find the matrix [a] in equation (24) and the energy release rate, G, at the Griffith stress intensity factor for the two cases studied in this chapter.

For the [010] crack, the coordinate axes are all in [100] type crystallographic directions. These are the axes of cubic symmetry for the bcc crystal and the elastic constants, [c] of equation (7) in section 3.4, are given by equation (10). For the Johnson-I potential, these are

$$c_{11} = .19225E12 \text{ Pa}$$

$$c_{12} = .09613E12 \text{ Pa} \qquad (31)$$

$$c_{14} = .09613E12 \text{ Pa}$$

The values of the a_{ij} for plane strain in the x_2 direction may be found by setting $\varepsilon_2 = \varepsilon_4 = \varepsilon_6 = 0$ in equation (7) and inverting the resulting equations. For this case, they become

$$a_{11} = a_{33} = 6.93565E-12 \text{ Pa}^{-1}$$

$$a_{13} = -3.46801E-12 \text{ Pa}^{-1} \qquad (32)$$

$$a_{55} = 10.40308E-12 \text{ Pa}^{-1}$$

$$a_{15} = a_{35} = 0$$

The elastic constants for the [110] crack may be obtained by rotating the constitutive equation given in equation (7) with the values given by equation (31). This may be done by setting one component of strain in the new coordinate system; using the constitutive equation with constants given by equation (31) in the old coordinate system; rotating the resulting stress tensor back to the new coordinates; and using this to form one column of the new [c] matrix. This leads to

$$[c] = \begin{bmatrix} .24031 & .04806 & .09613 & 0 & 0 & 0 \\ & .24031 & .09613 & 0 & 0 & 0 \\ & & .19225 & 0 & 0 & 0 \\ & & & .09613 & 0 & 0 \\ \text{SYM} & & & & .09613 & 0 \\ & & & & & .09613 \end{bmatrix}$$

$$X \ 10^{-12} \ Pa^{-1} \qquad (33)$$

where the x_1 and x_2 axes are of [110] type and the x_3 axis is of [100] type. The a_{ij} for plane strain in the x_2 direction now become

$$a_{11} = 5.20154E\text{-}12 \ Pa^{-1}$$

$$a_{13} = -2.60077E\text{-}12 \ Pa^{-1}$$

$$a_{33} = 6.50192E\text{-}12 \ Pa^{-1} \qquad (34)$$

$$a_{55} = 10.40308E\text{-}12 \ Pa^{-1}$$

$$a_{15} = a_{35} = 0$$

The surface energy, γ, for the (001) plane may be determined by counting the bonds which would have to be broken per unit area of new surface. These are four nearest neighbours and two second nearest neighbours per square lattice parameter. The energy of a nearest neighbour bond at the perfect crystal configuration is -0.0370375 aJ and of a second nearest neighbour is -0.0327080 aJ. The lattice parameter is 0.286 nm, leading to an energy of seperation of 2.615 J for 2 m^2 of new surface, or a surface energy of $\gamma = 1.307$ J/m^2. Substituting $G = 2\gamma$ for the Griffith stress intensity factor and the values of the a_{ij} given by equations (32) and (34) into equation (30) leads to

$k_G = 0.3896$ MNm$^{-3/2}$ for the [100] crack, and $k_G = 0.3989$ MNm$^{-3/2}$ for the [110] crack.

6.2 Lattice Trapping Limits and Crack Propagation Planes

Each of these cracks is stable over a range of stress intensity factors, k, rather than only at a single value of k as predicted by the Griffith theory. This is the lattice trapping effect. The lattice trapping limits and the planes on which the cracks propagated will be given in this section.

The models of Figs. 25 and 26 were loaded by setting the outside edge of the finite element region to the linear elastic solution positions given by equation (27). These were held fixed at these positions as described in section 5.4 . In order to reduce solution time, the positions of all other nodes and all atoms were also initially set at their linear elastic solution positions. This provided a reasonable approximation to the final positions. Quenching type solutions were attempted from this initial position with the equations of motion integrated by the 4th order Nordsieck scheme described in Chapter 4, using an integration time step of 10 fs. For the stress intensity factors used in this section, equilibrium positions could not be found because the crack propagated to the right for large k's and to the left for small k's.

Figure 27(a) shows the position of the [010] crack at a stress intensity factor of $k = 0.6\,k_G$ after a simulation for a model time of
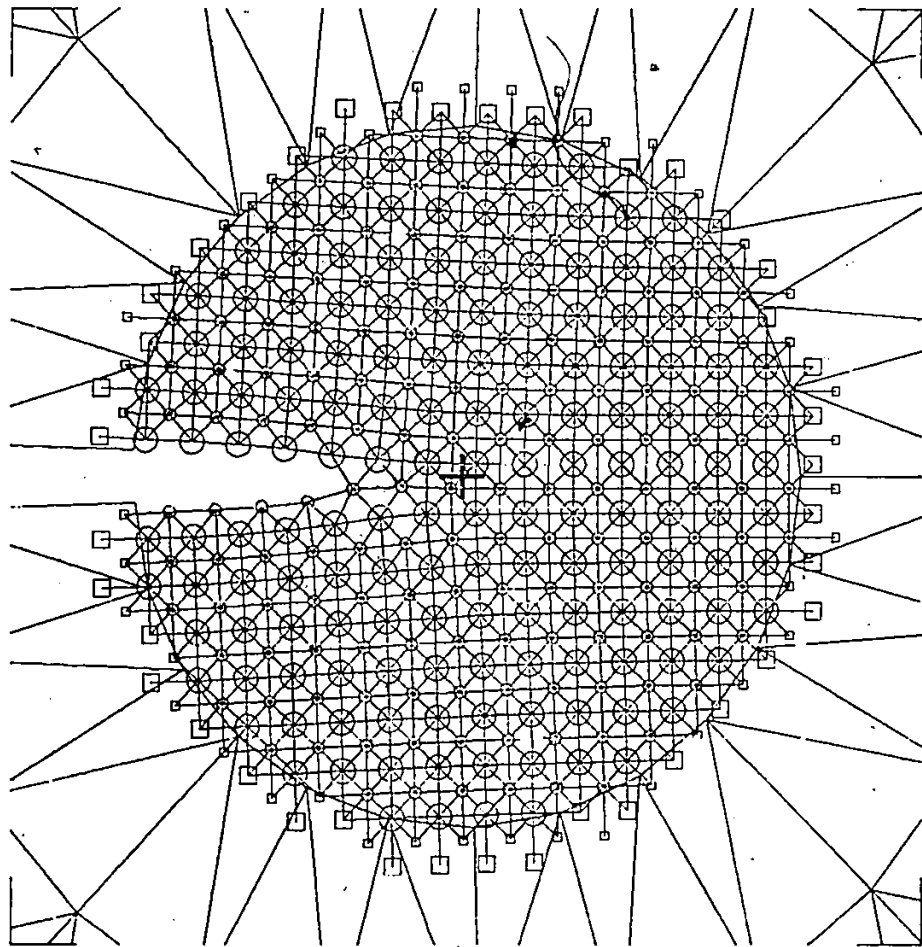
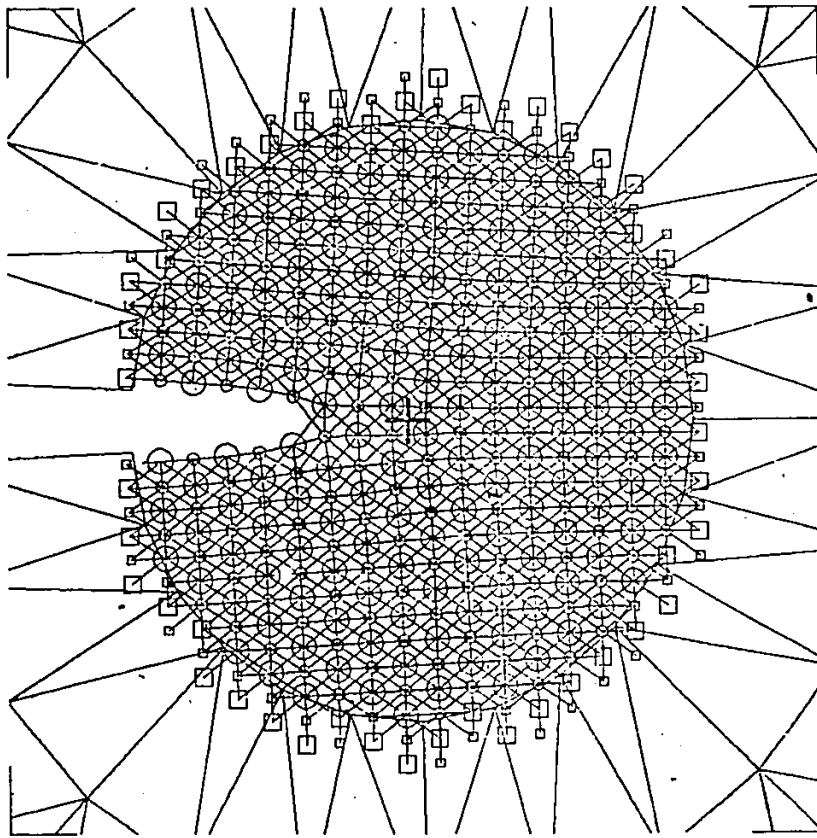Figure 27(a)   (001)[010] crack at k = 0.6 k_c after 750 fs.

Figure 27(b)   (001)[110] crack at k = 0.8 k_G after 750 fs.

750 fs. Figure 27(b) shows the [110] crack for k = 0.8 k_G, also after 750 fs. The original crack tip positions are shown as crosses. It can be seen that in both cases the crack moves to the left and closes up. This process is seldom observed in real materials, because oxidation of the crack face and the movement of the crack past heterogeneities in the material which act as pinning points restrict it. It may occasionally be observed in very pure materials in vacuum or inert gas atmospheres, [6].

More interesting is the response of the cracks to large loads. Fig. 28(a) shows the [010] crack at k = 3 k_G, and Fig. 28(b) shows the [110] crack at k = 1.3 k_G, both at model times of 1500 fs. It can be seen that in both cases, the cracks have moved to the right. In addition, both have propagated on the (001) plane and no dislocations were emitted. Twinning would be inhibited by the grid so it is not possible to say if this could spontaneously occur. Experimentally, twinning is apparently a result of shears caused by two cracks in close proximity, [25], so it would not be expected in the present model. A stress intensity factor of 3 k_G is well beyond the upper lattice trapping limit for the [010] crack. This crack propagated very slowly at lower stress intensity factors. The [110] crack, on the other hand, propagated at a comparable speed at 1.3 k_G, only slightly beyond its upper lattice trapping limit.

An attempt was made to determine the lattice trapping limits by means of the conjugate gradient method, [78]. This was not successful, however. Equilibrium positions could be easily located but the saddle
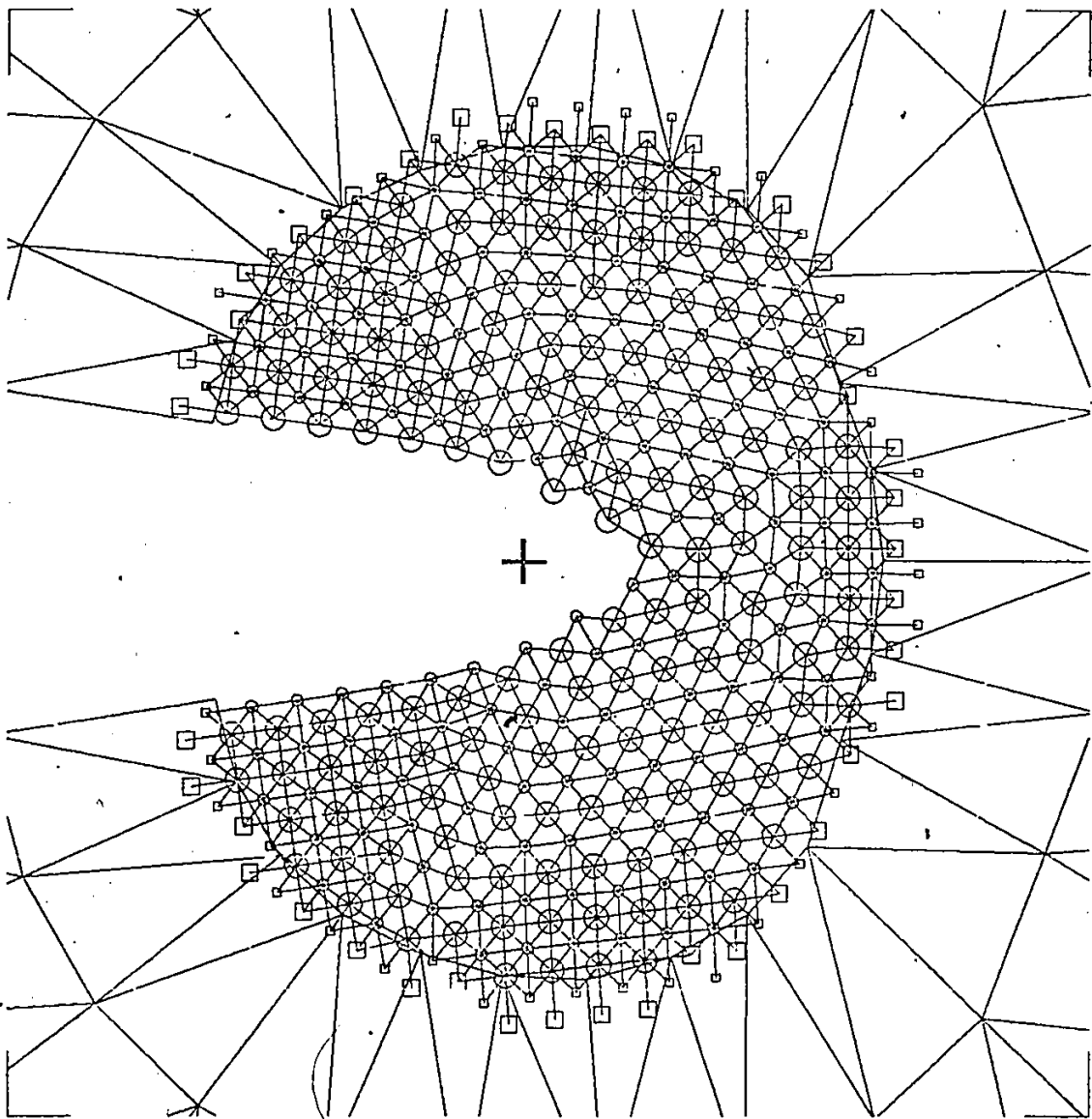
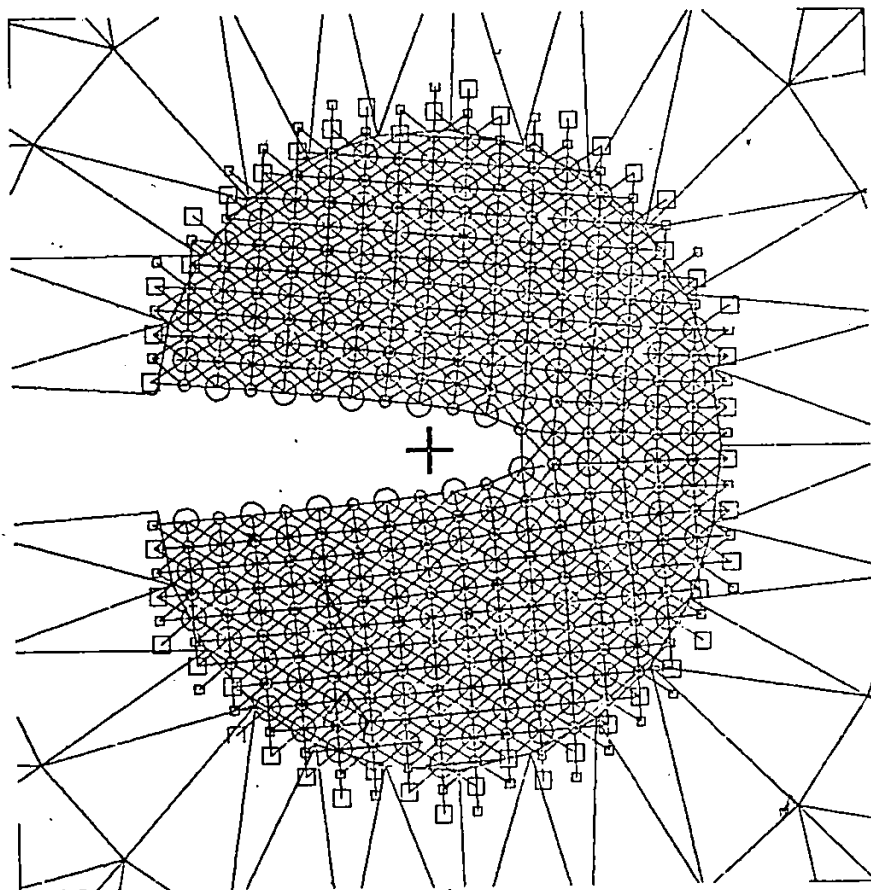Figure 28(a)   (001)[010] crack at k = 3 k_c after 1500 fs.

Figure 28(b)   (001)[110] crack at k = 1.3 k_G after 1500 fs.

point positions necessary for the determination of the lattice trapping

limits could not be found because of numerical instability. Other

workers, [91], have experienced similar difficulties with iron models

using other boundary schemes, although silicon models apparently perform

well, [75]. This may be due to the shape of the Johnson potential which

has a discontinuity in second derivative at the cut-off point.

As a result of this, the lattice trapping limits had to be

determined by finding the stress intensity factors at which no

equilibrium position could be found. These were

0.78 k_G and 1.42 k_G for the [010] crack, and

0.88 k_G and 1.12 k_G for the [110] crack.

It is felt that these values are correct to ±0.02 k_G. There is, thus, a

considerable difference between the two cracks. The [010] crack is

stable over a range of stress intensity factors nearly twice that of the

[110]. The [110] crack will propagate at a stress intensity factor of

0.81 that at which the [010] will propagate (when the above values are

corrected for the difference in k_G for the two cases).

If these results carry over to real materials, it would be

expected that they should apply only at low temperatures where the

complicating effect of dislocation or twinning processes could be

ignored. For this condition, the model predicts that

1)   both cracks should propagate on (001) planes,

2)   no dislocations should be emitted spontaneously from these cracks,

3)   the [110] crack should propagate at a lower stress intensity factor
     than the [010],

4)   the [110] crack should propagate faster than the [010].

The last point is an extension of the actual model observations.
Because of computer cost limitations, steady state crack propagation was
not reached for these cracks, while experimentally, steady state speeds
are measured. The differences in initial acceleration between the two
cracks at a given stress intensity factor is quite large, however, so
some experimental difference would probably be expected.

The experimental results pertaining to these observations have
already been discussed in section 3.2 of the literature survey.
Summarizing them here:
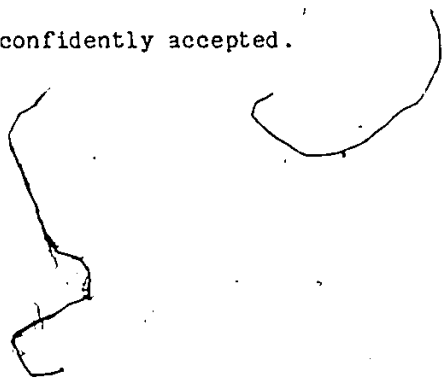
1)   All workers found that cracks propagated on (001) planes for iron
     and tungsten.

2)   Gilman, [22], and Tetelman and Robertson, [24], estimated that
     fracture of iron was completely brittle at the low temperatures
     corresponding to the model simulations described here, indicating
     that the effect of any dislocation activity must be small.

3)   Hull and Beardmore, [26], found that in tungsten at low
     temperatures the [110] crack probably propagated faster than the
     [010], although interpretation of the results is complicated by the

experimental scatter.

4) Liu and Bilello, [27], fractured tungsten in both directions
    considered here and measured the apparent surface energy. This
    showed some difference in the two directions which corresponds to
    the model predictions given here. The reality or cause of this
    difference is very difficult to confirm, however, because of the
    experimental difficulties.

It can be seen that the experimental results available appear to
correspond to the model predictions of the present work. Experiments of
this nature are very difficult, however, so this correspondence cannot
be accepted without question. The experimental difficulties and some
alternate explanations of the results have been described in the
literature survery.

In conclusion, then, the present model shows several interesting
results not seen in previous computer models. These are the clear cut
(001) plane fracture and the significant differences in lattice trapping
limits and crack acceleration rates between the [010] and [110] crack
line directions. Some confirmation of these effects from previously
published experimental work has been described but much more such work
is necessary before the model predictions can be confidently accepted.

6.3 Non-Linear Displacement Field - General

The positions of the atoms near a crack tip in static equilibrium are different from those given by the linear elastic crack tip solution which applies at greater distances. This is a result of the discrete nature of the lattice and the non-linearities caused by the interatomic potential and the geometry changes. In this section, the difference in position of an atom in the model solution and that position which it would occupy according to the linear elastic crack tip solution will be called that atom's non-linear displacement. This section presents a description of this non-linear displacement field. This will indicate the distance from the crack tip at which the linear elastic solution applies with reasonable accuracy and will provide a description of the shape of the actual displacements nearer to the crack tip for use in crack-crack, crack-dislocation, crack-vacancy, etc., interaction studies. In addition, some information on the possibility of dislocation emission from the crack tip may be derived from these results.

Equilibrium positions were obtained for various stress intensity factors for both crack directions. The outside edge of the model was fixed at the linear elastic solution position and all other nodes and atoms were initially set to these positions also. Static solutions were obtained by both the conjugate gradient method and simultaneous quenching. A systematic study was not done on models of the large size used here, as was performed for the smaller models in Chapter 4, but the results of Chapter 4 were confirmed qualitatively since the conjugate

gradient scheme appeared faster than simultaneous quenching. No
difficulties were experienced finding equilibrium positions with either
method indicating that both are suitable without modification with the
finite element boundary conditions.

The criterion used to stop the solution was that the sum square
of the unbalanced forces on all atoms should be less than 1.E-21 N^2.
This value was obtained from the results of Chapter 4 and the desire to
keep the excess energy in the crystal below that which would correspond
to the thermal energy due to a temperature of 5 K. From Fig. 12 and the
mass of the 308 free atoms in the present models, this energy is
approximately 2.4E-5 aJ. This is about 0.001 of the energy change in
the atomic area when it is quenched from an initial position set to
correspond to the linear elastic crack tip solution. Using this value
in Fig. 14 gives a corresponding sum-square atomic force of
about 1.E-21 N^2.

Figures 29 to 32 show the [010] crack at k = 0.8 k_G, k_G, 1.2 k_G,
and 1.4 k_G, respectively. Figures 33 to 35 show the [110] crack at
k = 0.9 k_G, k_G, and 1.1 k_G, respectively. Part (a) of each figure shows
the final equilibrium positions and the unbroken bonds for each case.
Part (b) shows the non-linear displacement of all atoms and nodes. Each
arrow represents the displacement of one of these from the position
given by linear elastic fracture mechanics. These displacements are
magnified 20 times. The remaining figure parts give these
displacements for atoms within rings 0.2 nm wide centered on radii of
0.5 nm, 1 nm, 1.5 nm, and 2 nm for the [010] crack and 0.5 nm, 1 nm, and

1.5 nm for the [110] crack (2 nm is larger than the radius of the atomic area for the [110] crack). The base of each arrow in these figure parts is on the circle of radius equal to the average radius of the ring. The angular position of the base of each arrow is fixed at the angular location of the corresponding atom or node in the perfect crystal configuration.

Some qualitative observations may be made from these results. As would be expected from the crystal structure, the non-linear displacement field is symmetrical about the crack plane for the [110] crack but not for the [010]. Moving the [010] crack tip by half a lattice parameter would result in equilibrium positions that are reflections in the crack plane compared to those cases given here. The magnitude of the non-linear displacements increases as k increases and decreases as distance from the crack tip increases. In both cases these displacements appear to be vaguely elliptical in form, with the atoms above and below the crack tip moving out, and those to the right and left of it moving in. This appears to be especially true for the [110] crack. The displacement field for the [010] case is more complicated, however. For this, there appears to be sudden changes in the displacements across the ($\bar{1}$01) and (101) planes at ±45° to the crack plane. These displacement changes appear as shears across these planes. This is what would be expected if dislocations were being nucleated at the crack tip. A discussion of this point is given below.
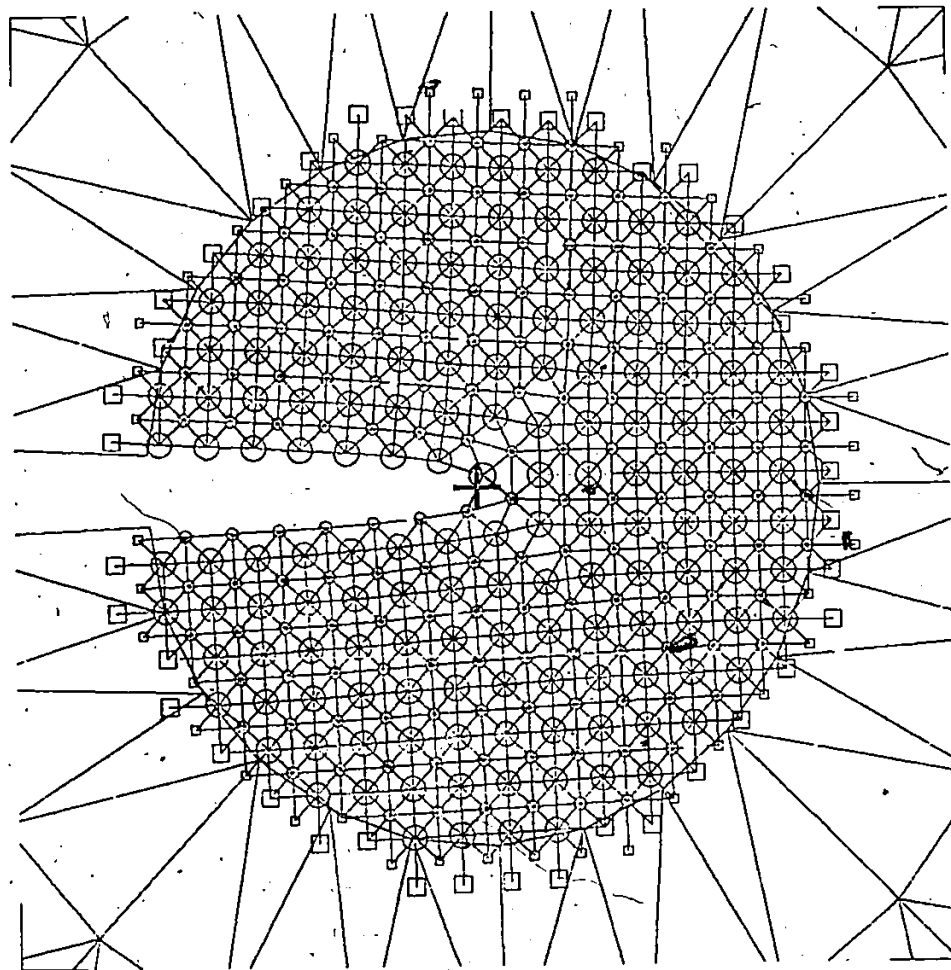
Figure 29(a)   Equilibrium position and unbroken bonds
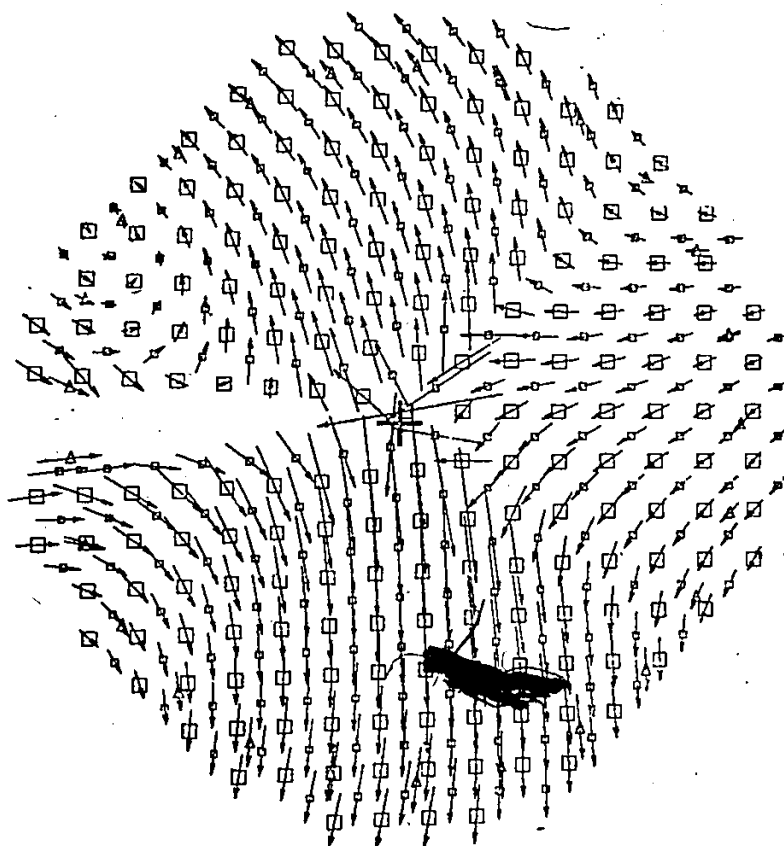for (001)[010] crack at k = 0.8 k_G.

Figure 29(b) Non-linear displacements magnified 20 times
for (001)[010] crack at k = 0.8 k_c.

(c)

(d)

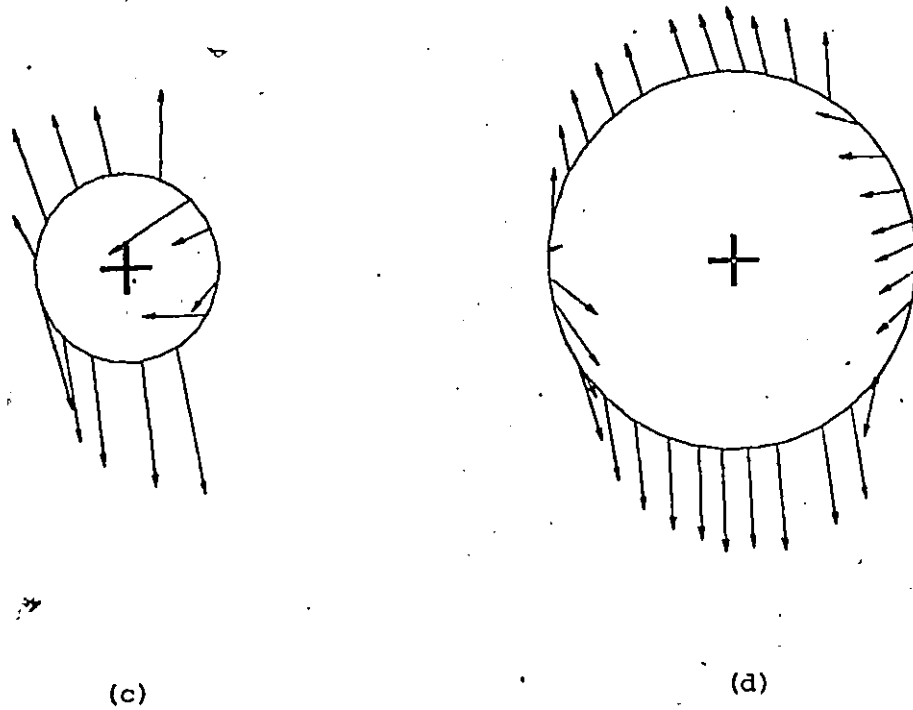Figure 29 (cont.)   Non-linear displacement magnified 20 times
                     for (001)[010] crack at k = 0.8 k$_c$,
                     (c)   radius, r, equals 0.4 to 0.6 nm.
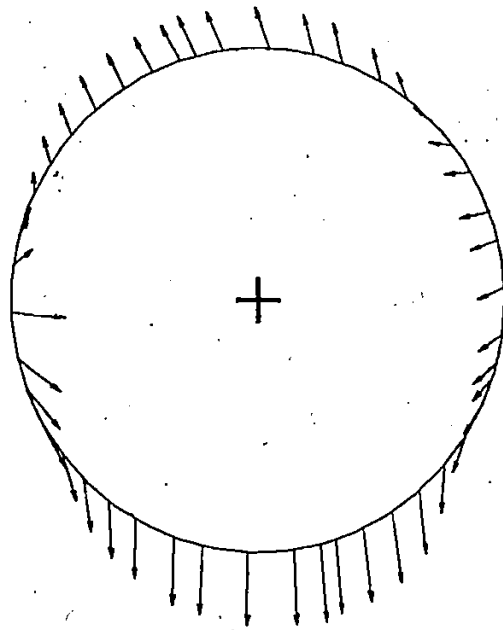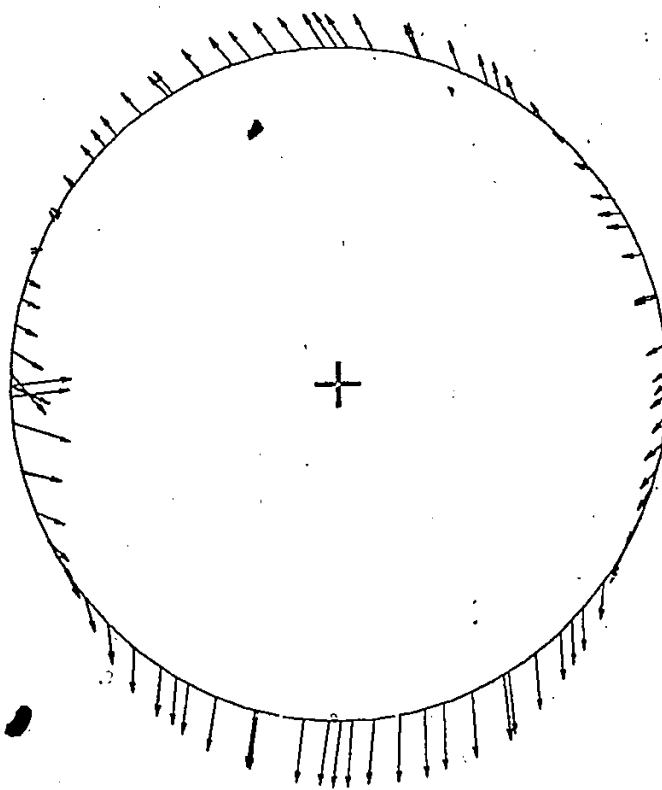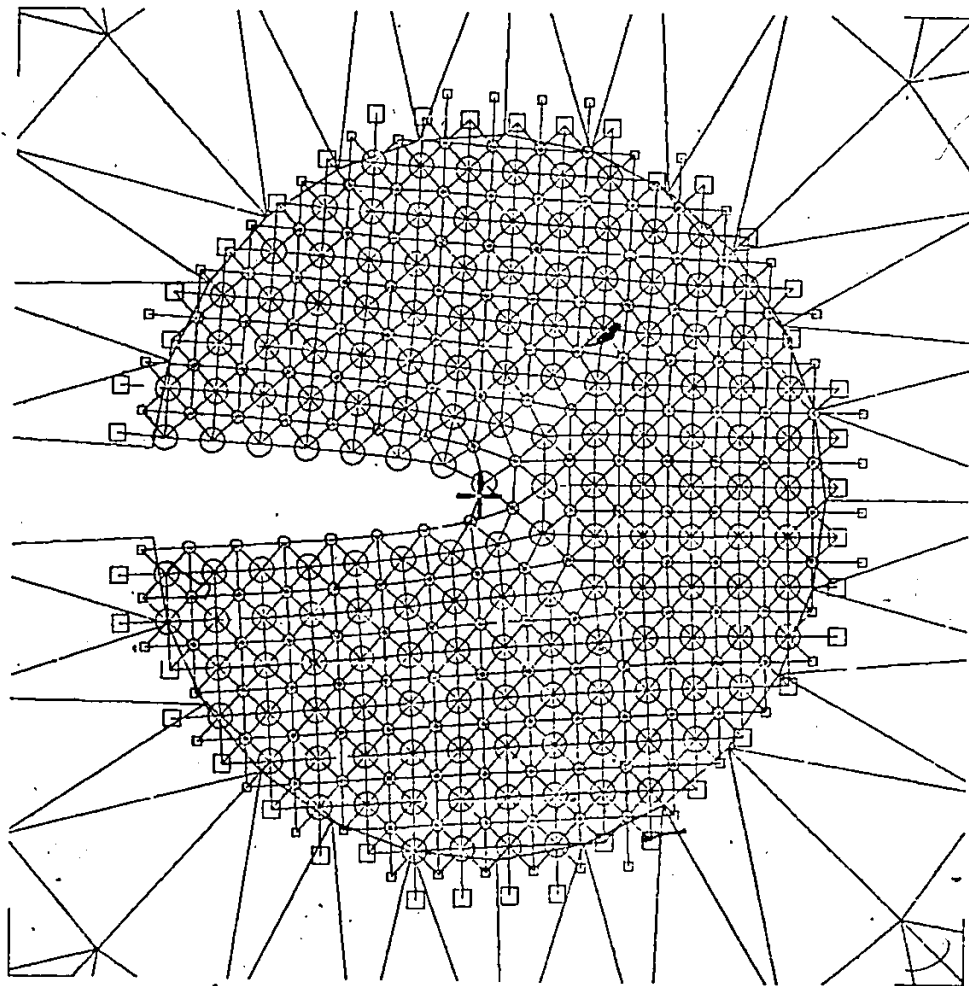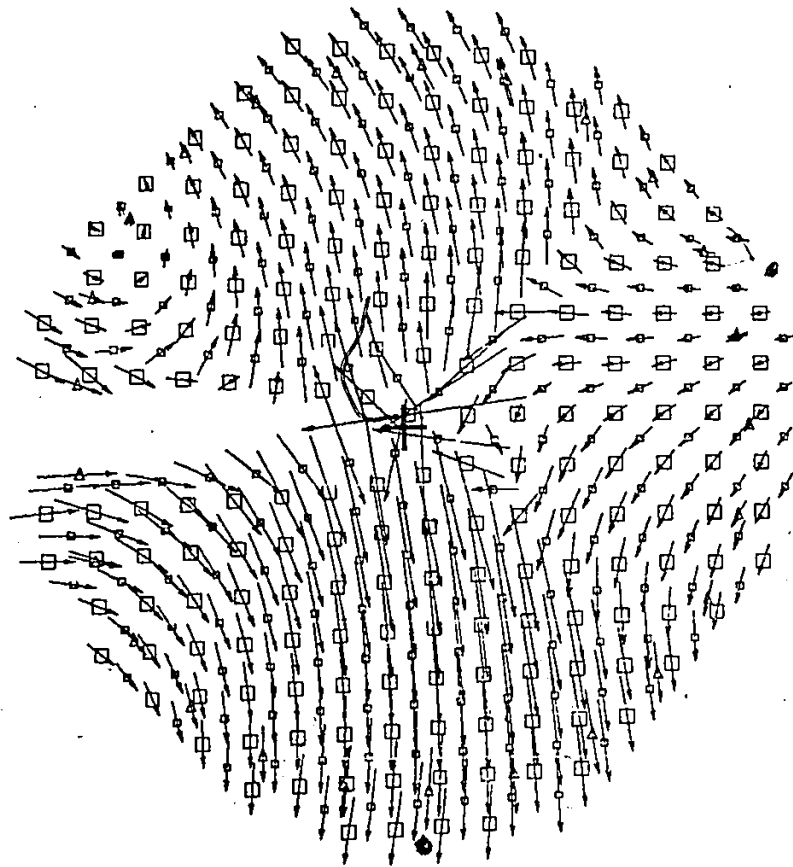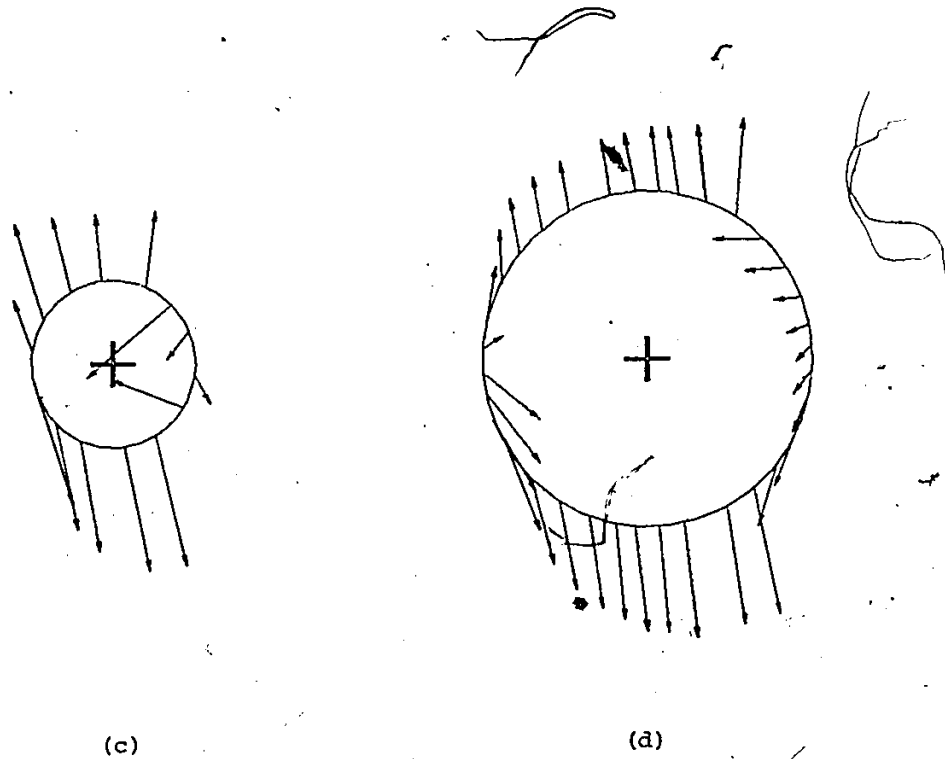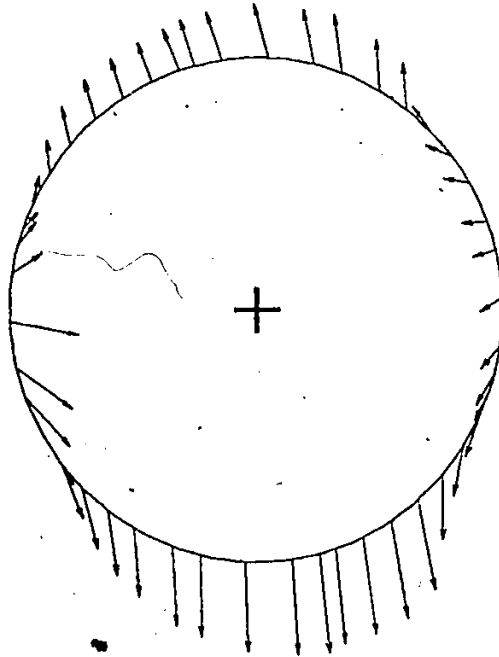   (d)   radius, r, equals 0.9 to 1.1 nm.

Figure 29(e)   Non-linear displacement magnified 20 times
for (001)[010] crack at k = 0.8 k$_c$,
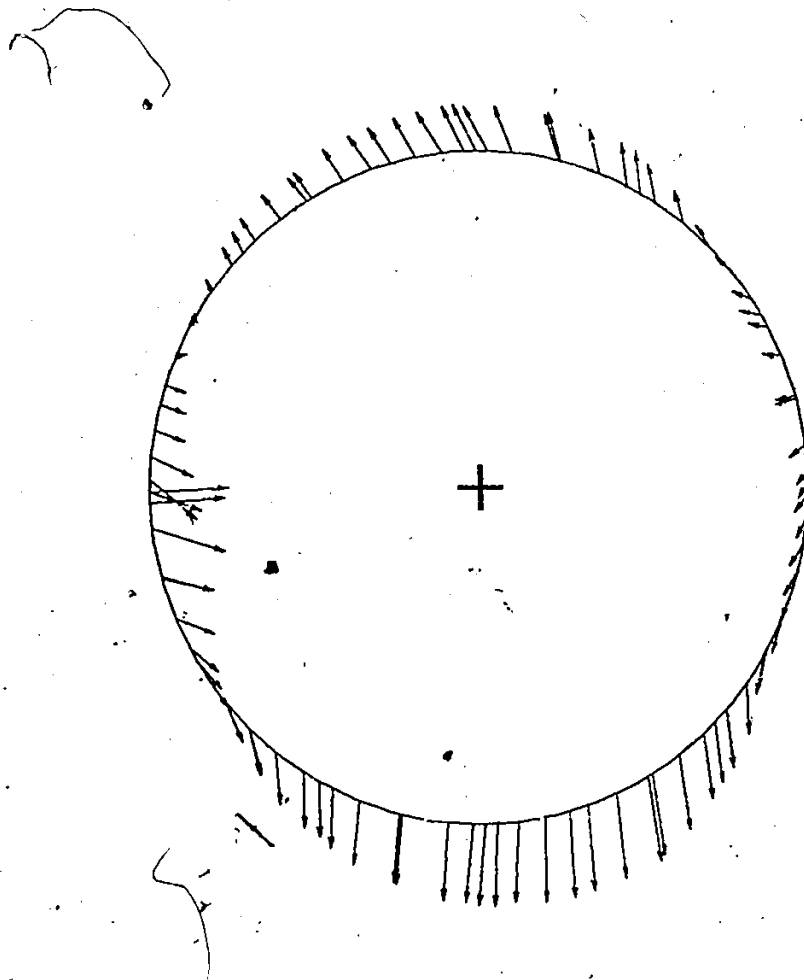for radius, r, equals 1.4 to 1.6 nm.

Figure 29(f)   Non-linear displacement magnified 20 times
                for (001)[010] crack at k = 0.8 k$_c$,
                for radius, r, equals 1.9 to 2.1 nm.

Figure 30(a)   Equilibrium position and unbroken bonds
                for (001)[010] crack at k = k.

Figure 30(b)   Non-linear displacements magnified 20 times
                for (001)[010] crack at k = k$_c$.

(c)

(d)

Figure 30 (cont.) Non-linear displacement magnified 20 times
for (001)[010] crack at k = k_c.
(c) radius, r, equals 0.4 to 0.6 nm.
(d) radius, r, equals 0.9 to 1.1 nm.

Figure 30(e)   Non-linear displacement magnified 20 times
for (001)[010] crack at $k = k_c$,
for radius, r, equals 1.4 to 1.6 nm.

Figure 30(f)   Non-linear displacement magnified 20 times
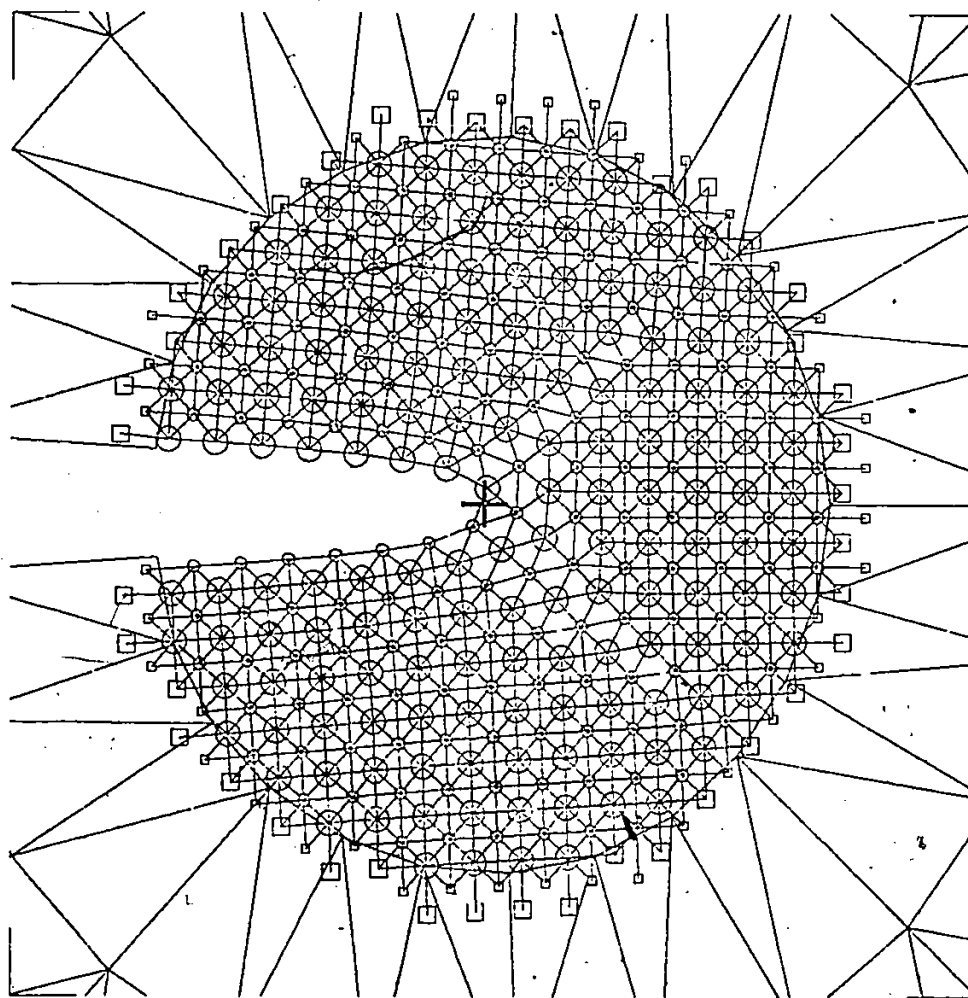for (001)[010] crack at k = k$_c$,
for radius, r, equals 1.9 to 2.1 nm.

Figure 31(a)   Equilibrium position and unbroken bonds
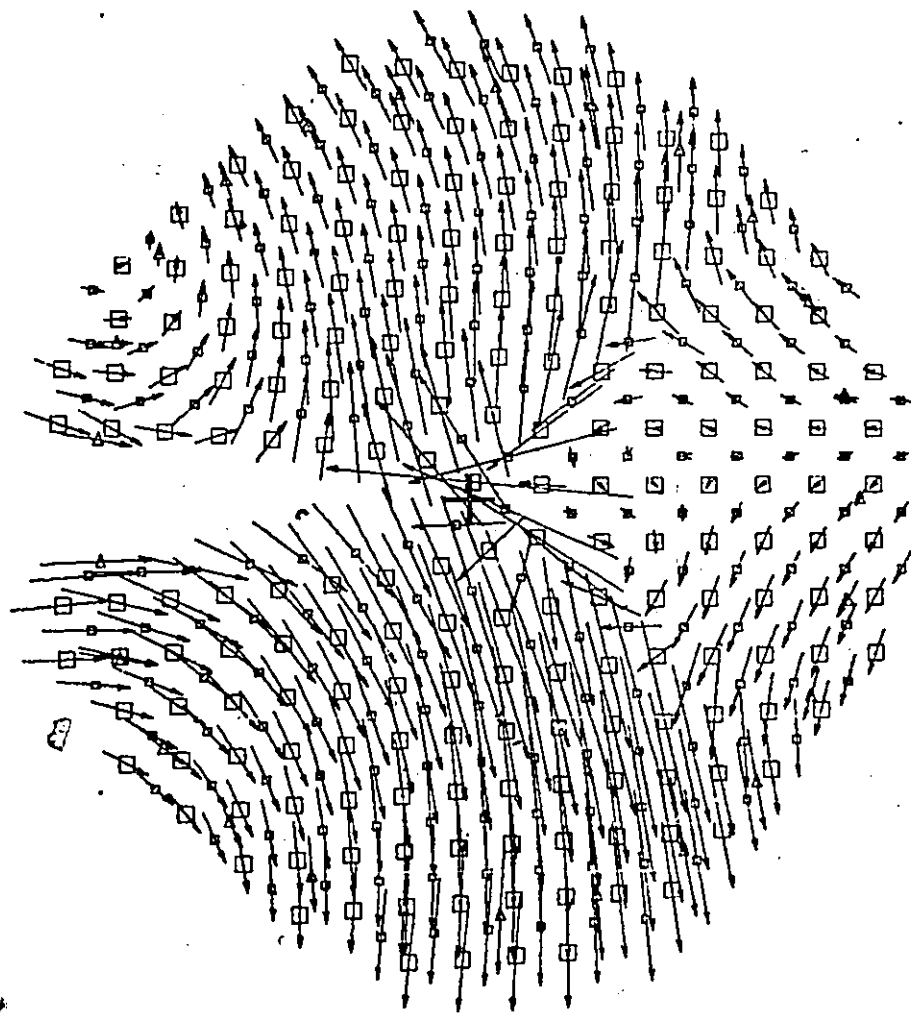for (001)[010] crack at k = 1.2 k_c.

Figure 31(b) Non-linear displacements magnified 20 times
for (001)[010] crack at k = 1.2 k_c.

(c)

(d)

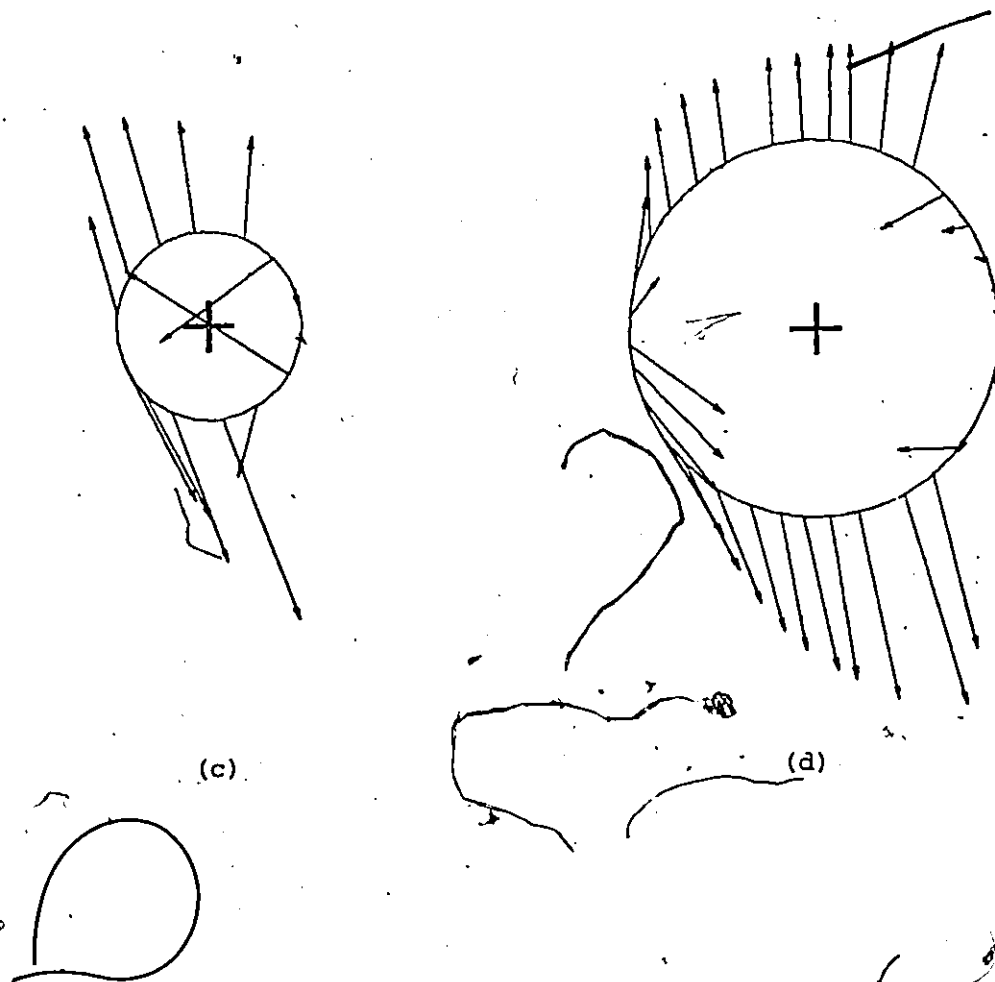Figure 31 (cont.) Non-linear displacement magnified 20 times
                   for (001)[010] crack at k = 1.2 k$_c$.
                   (c) radius, r, equals 0.4 to 0.6 nm.
                   (d) radius, r, equals 0.9 to 1.1 nm.
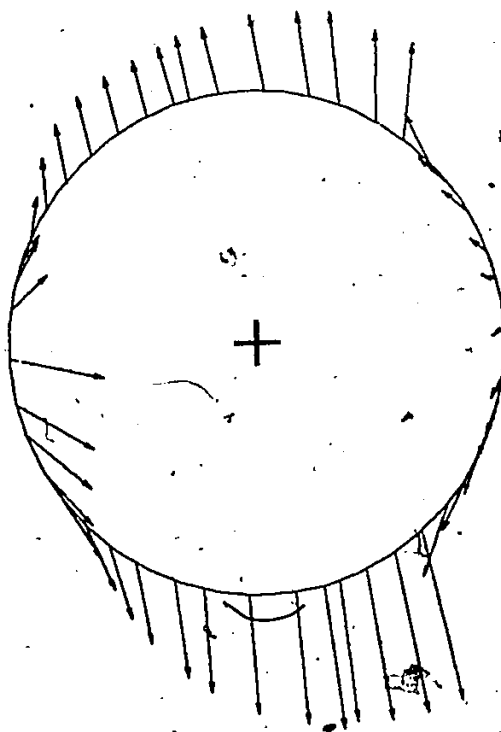
Figure 31(e)   Non-linear displacement magnified 20 times
                for (001)[010] crack at k = 1.2 k$_G$,
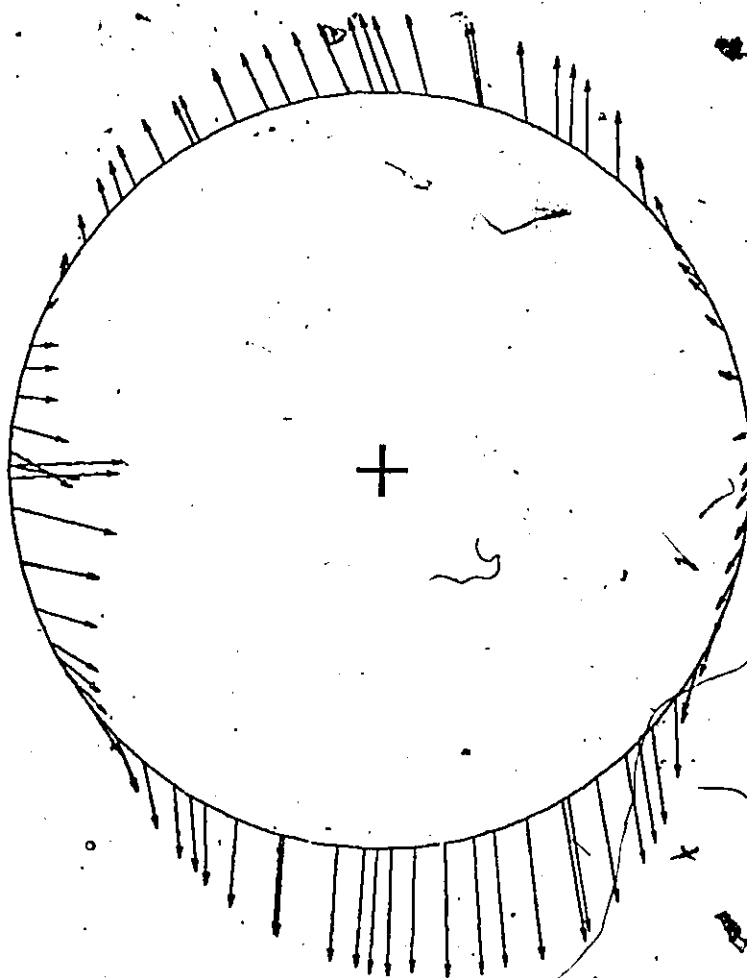   for radius, r, equals 1.4 to 1.6 nm.

Figure 3. Non-linear displacement magnified 20 times for (001)[010] crack at k = 1.2 k_c, for radius, r, equals 1.9 to 2.1 nm.
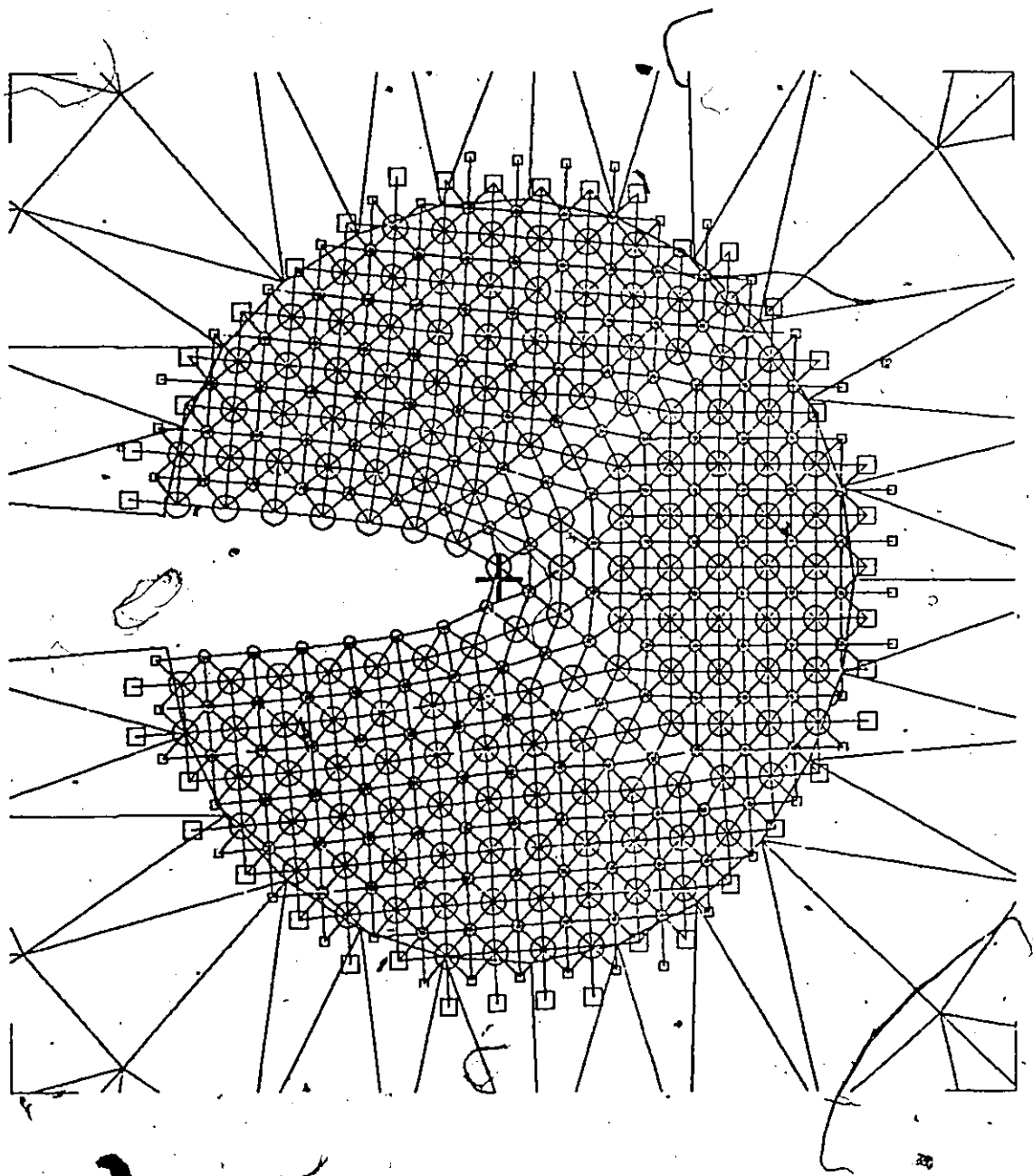
Figure 32(a)   Equilibrium position and unbroken bonds
for (001)[010] crack at k = 1.4 k.
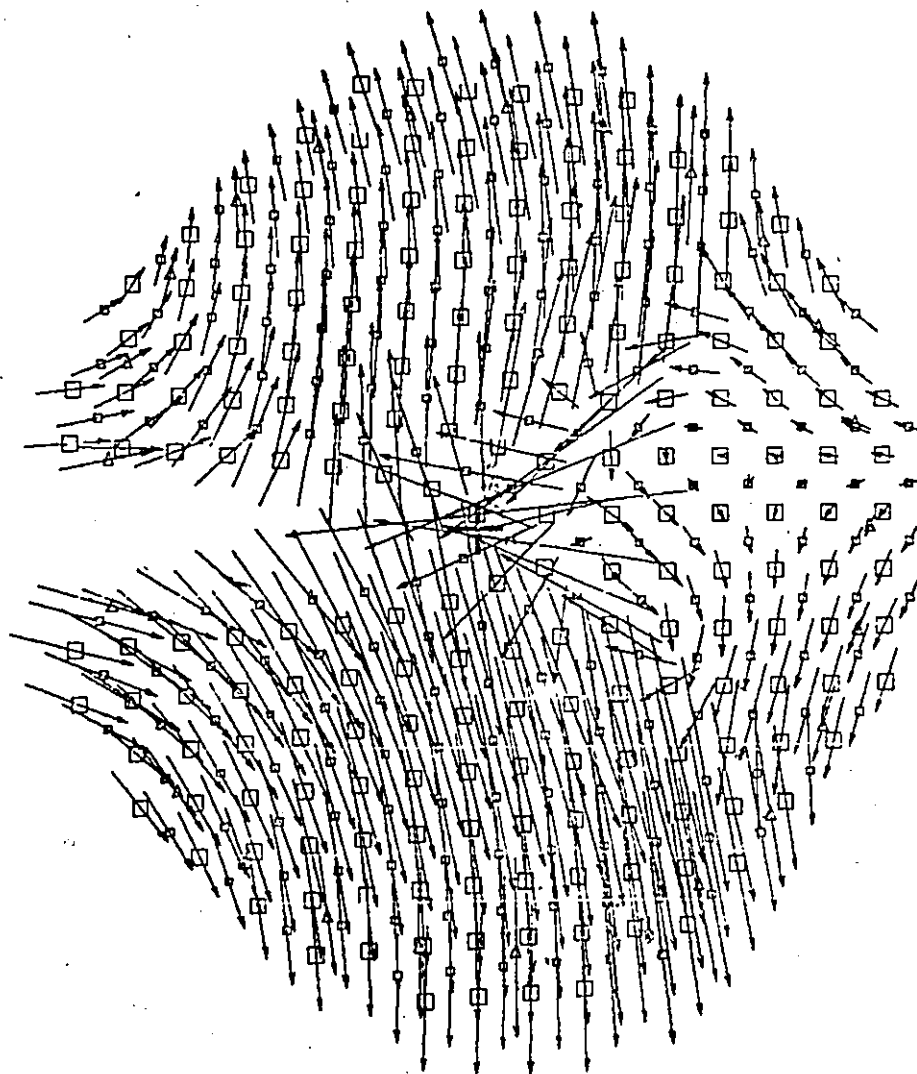
Figure 32(b)   Non-linear displacements magnified 20 times
for (001)[010] crack at k = 1.4 k$_c$.

(c)   (d)

Figure 32 (cont.)   Non-linear displacement magnified 20 times
                     for (001)[010] crack at k = 1.4 k$_c$.
                     (c)   radius, r, equals 0.4 to 0.6 nm.
                     (d)   radius, r, equals 0.9 to 1.1 nm.

Figure 32(e)   Non-linear displacement magnified 20 times
for (001)[010] crack at k = 1.4 kc,
for radius, r, equals 1.4 to 1.6 nm.

Figure 32(f) Non-linear displacement magnified 20 times
for (001)[010] crack at k = 1.4 k$_G$,
for radius, r, equals 1.9 to 2.1 nm.

Figure 33(a)   Equilibrium position and unbroken bonds
for (001)[110] crack at k = 0.9 k_c.

Figure 33(b)   Non-linear displacements magnified 20 times
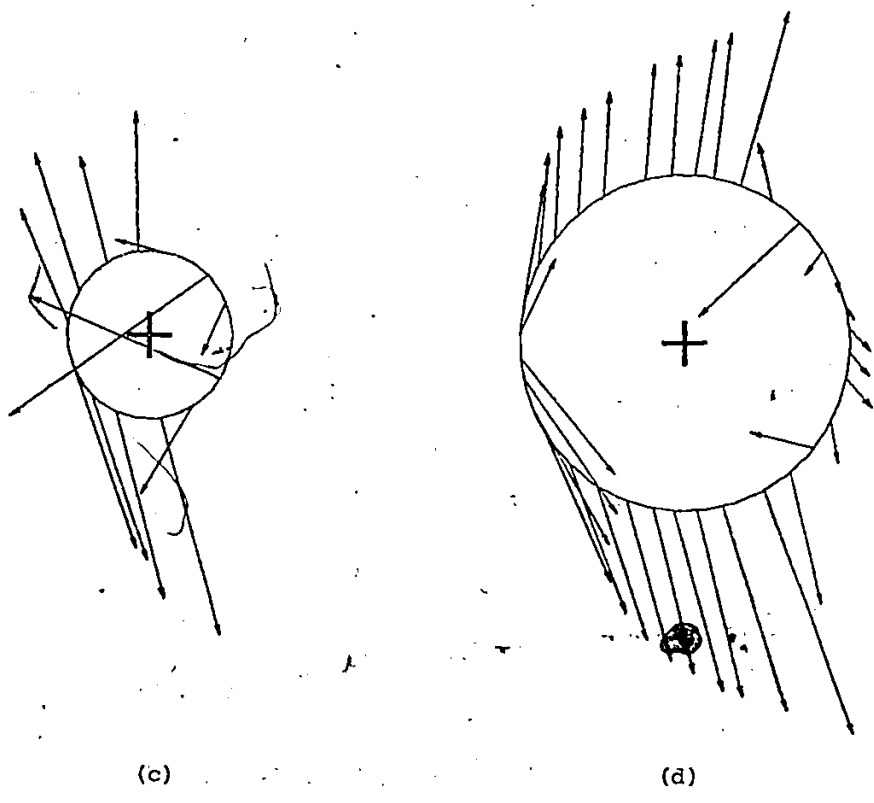   for (001)[110] crack at k = 0.9 k$_c$.

162

(c)

(d)

Figure 33 (cont.) Non-linear displacement magnified 20 times
for (001)[110] crack at k = 0.9 k$_c$.
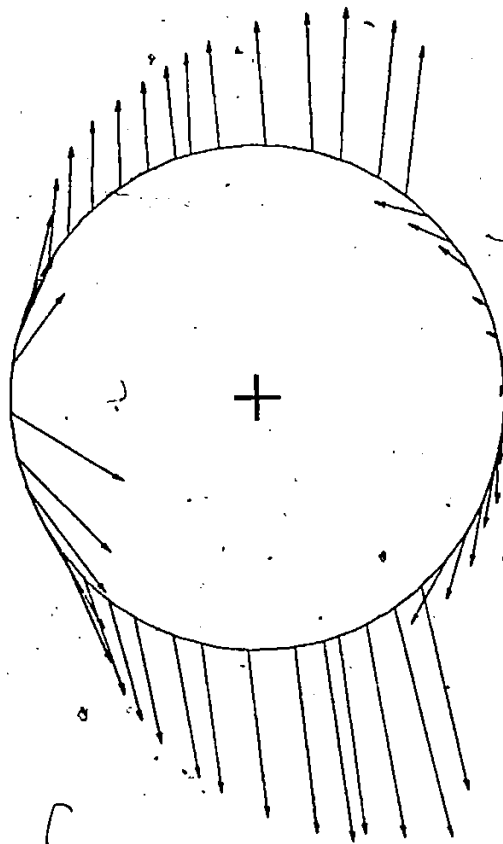(c)   radius, r, equals 0.4 to 0.6 nm.
(d)   radius, r, equals 0.9 to 1.1 nm.

-Figure 48(e)   Non-linear displacement magnified 20 times
                 for (001)[110] crack at k = 0.9 k_c,
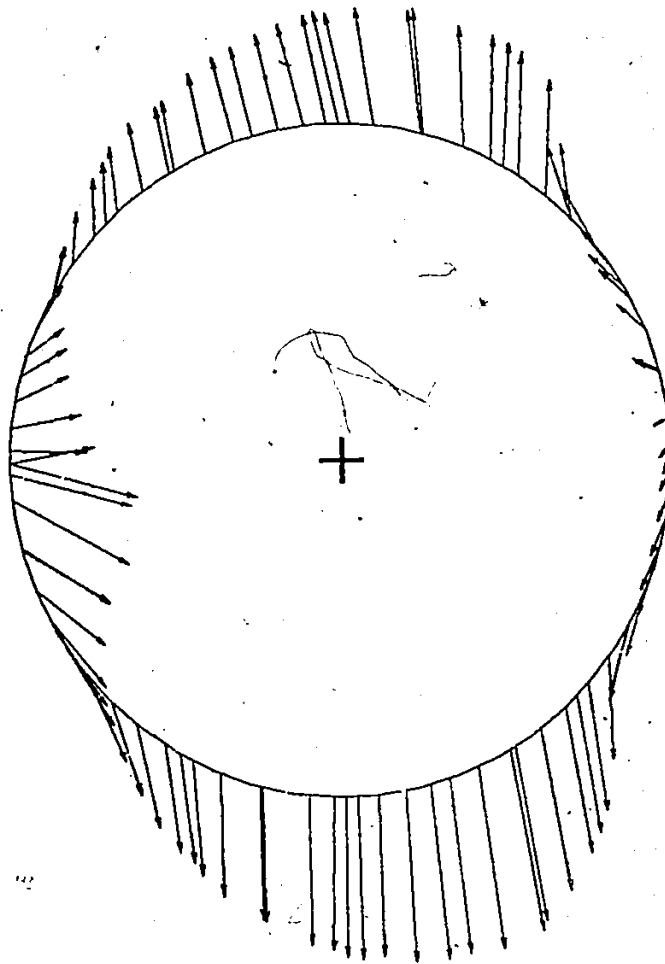   for radius, r, equals 1.4 to 1.6 nm.
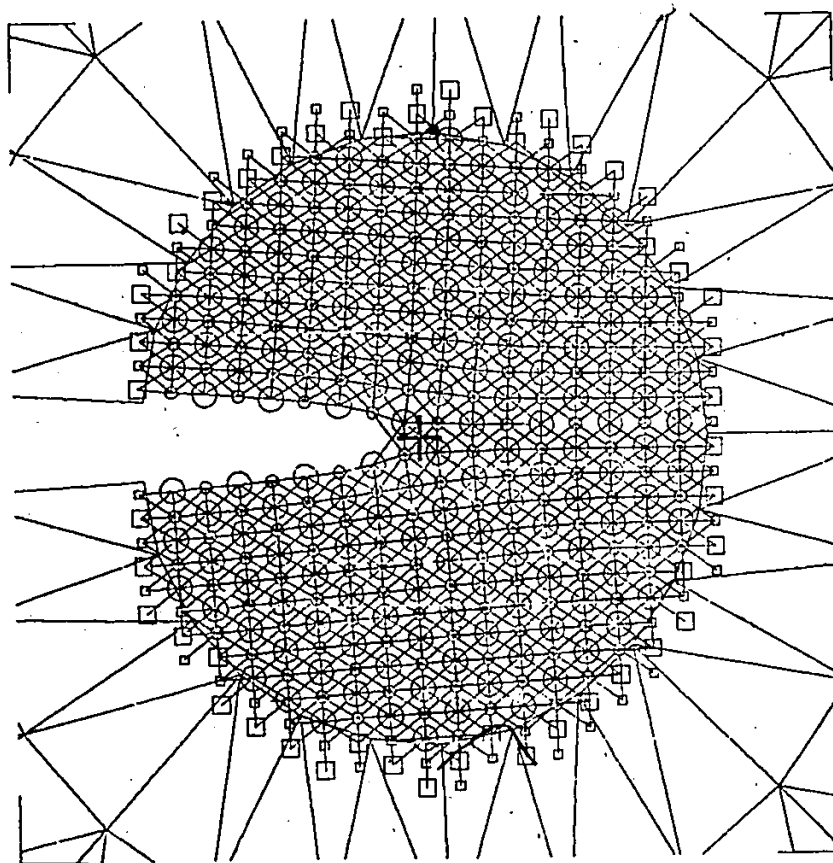
Figure 34(a)   Equilibrium position and unbroken bonds
                for (001)[110] crack at k = k.
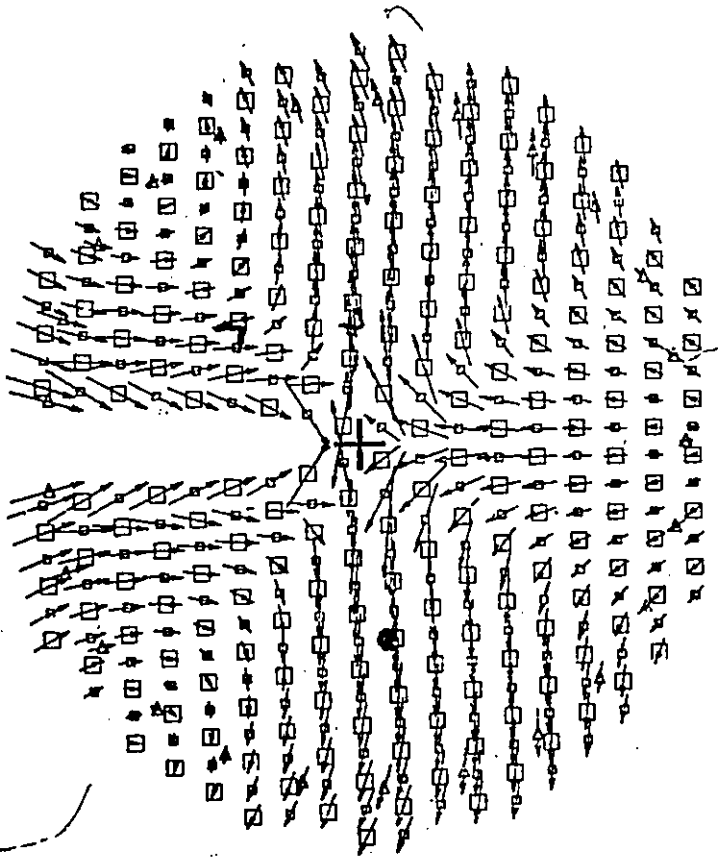
Figure 34(b)　Non-linear displacements magnified 20 times
for (001)[110] crack at k = k$_c$.

(c)   (d)

Figure 34 (cont.)   Non-linear displacement magnified 20 times
                     for (001)[110] crack at k = k_c,
                     (c)   radius, r, equals 0.4 to 0.6 nm.
                     (d)   radius, r, equals 0.9 to 1.1 nm.

Figure 34(e)   Non-linear displacement magnified 20 times
for (001)[110] crack at $k = k_c$,
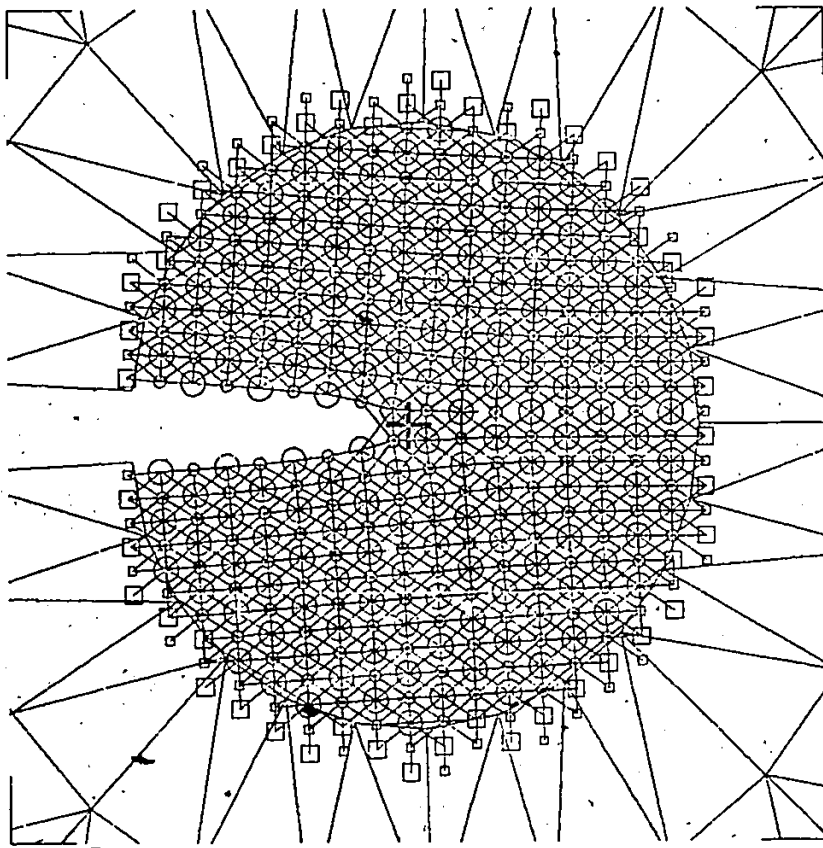for radius, r, equals 1.4 to 1.6 nm.

Figure 35(a)   Equilibrium position and unbroken bonds
            for (001)[110] crack at k = 1.1 k_c.
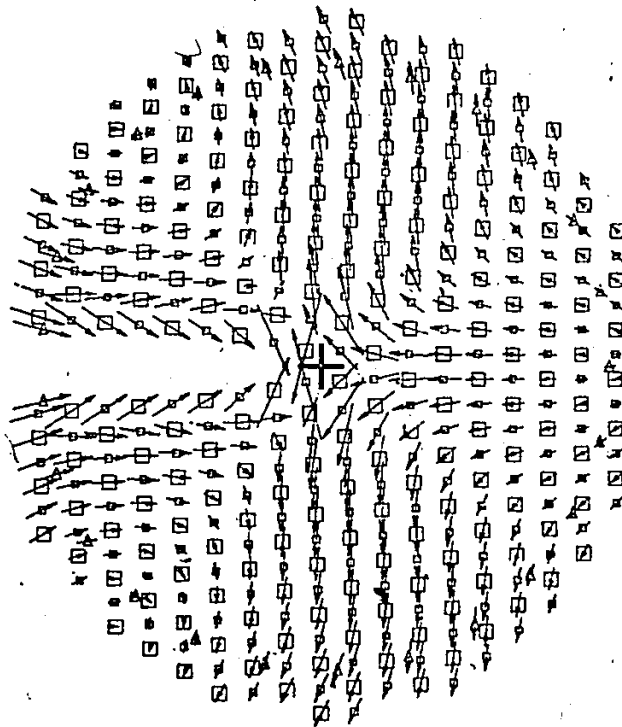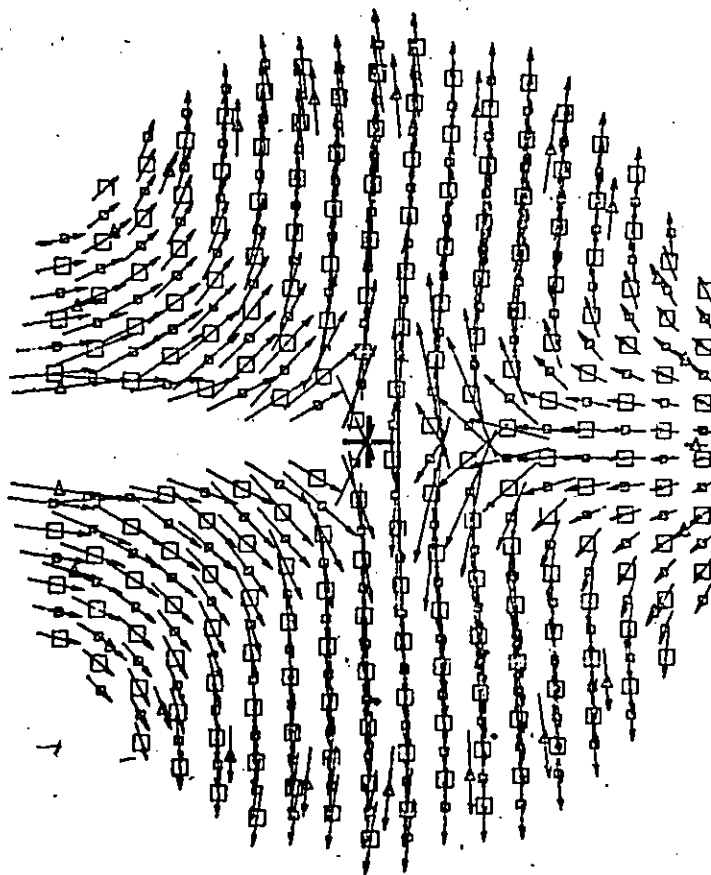
Figure 35(b)   Non-linear displacements magnified 20 times
for (001)[110] crack at k = 1.1 k_c.

(c)   (d)
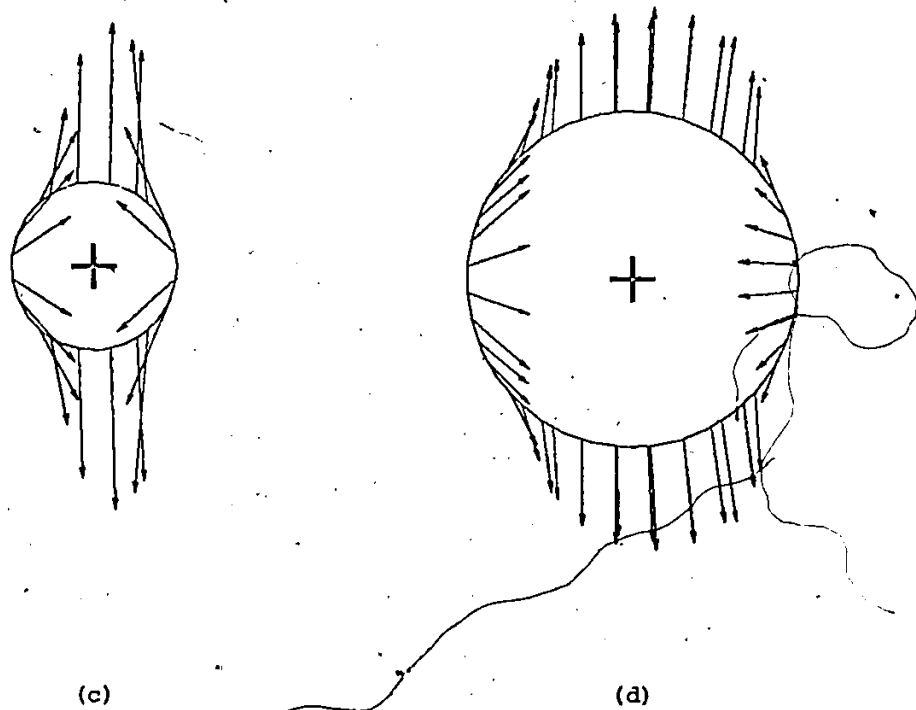
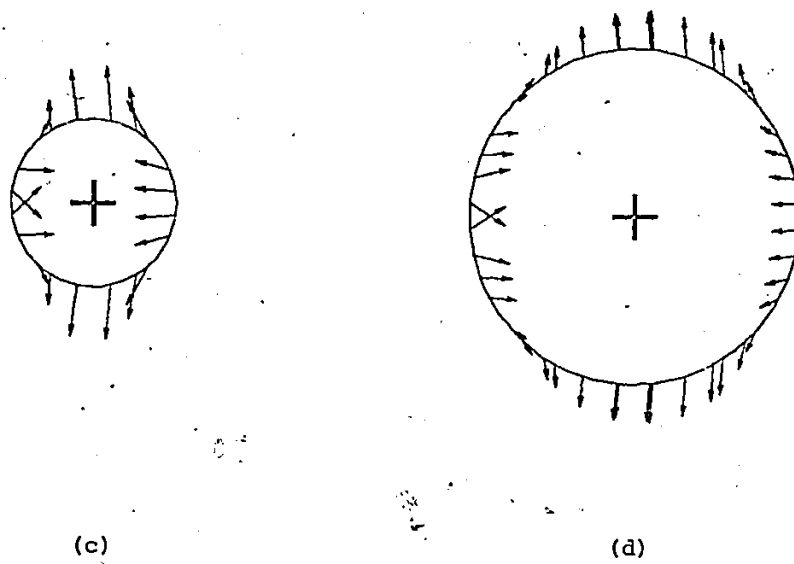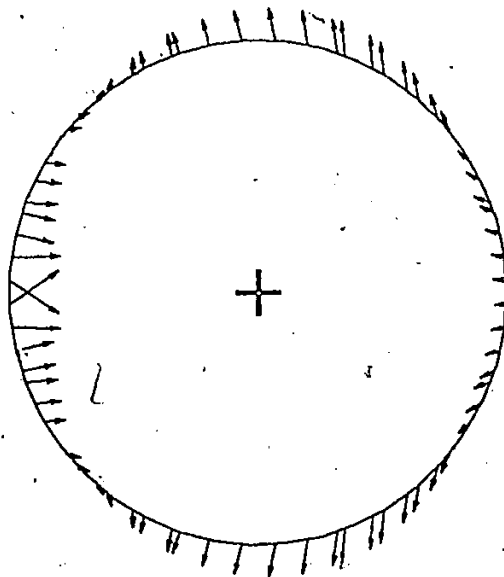Figure 35 (cont.)   Non-linear displacement magnified 20 times
                     for (001)[110] crack at k = 1.1 k$_c$,
                     (c)   radius, r, equals 0.4 to 0.6 nm.
                     (d)   radius, r, equals 0.9 to 1.1 nm.
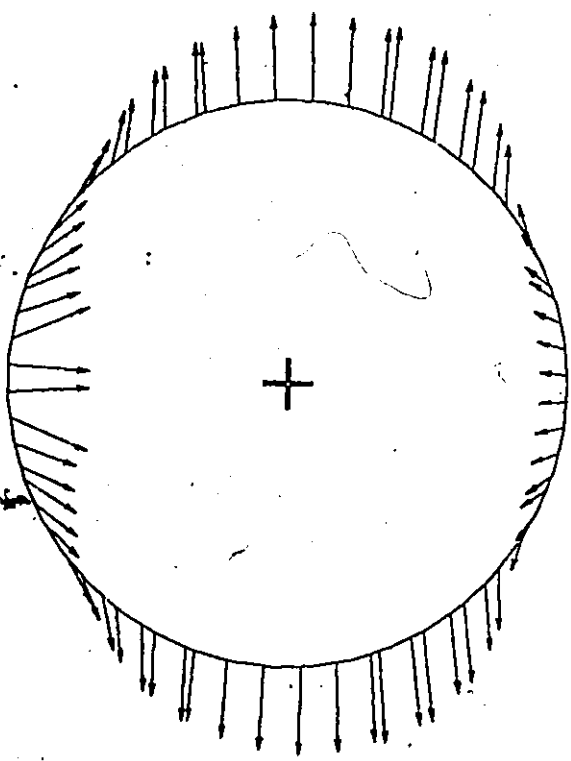
Figure 35(e)   Non-linear displacement magnified 20 times
                for (001)[110] crack at k = 1.1 k_c,
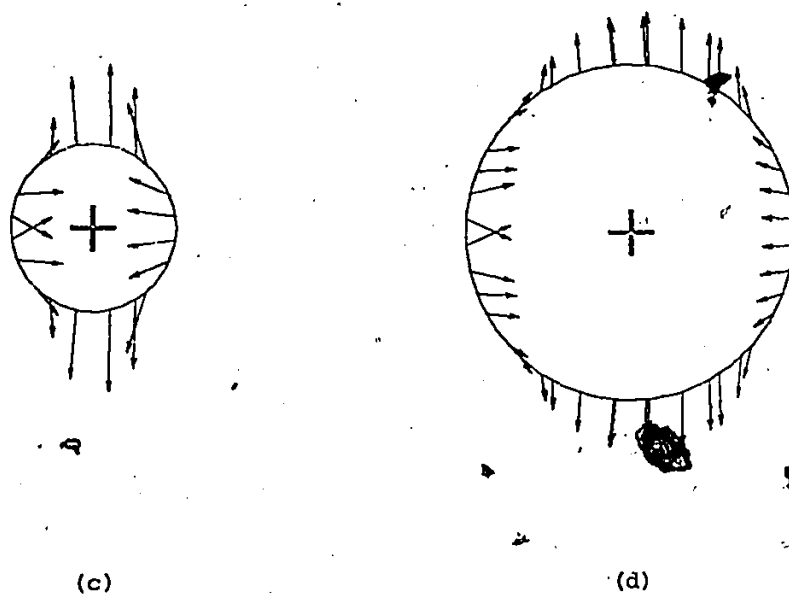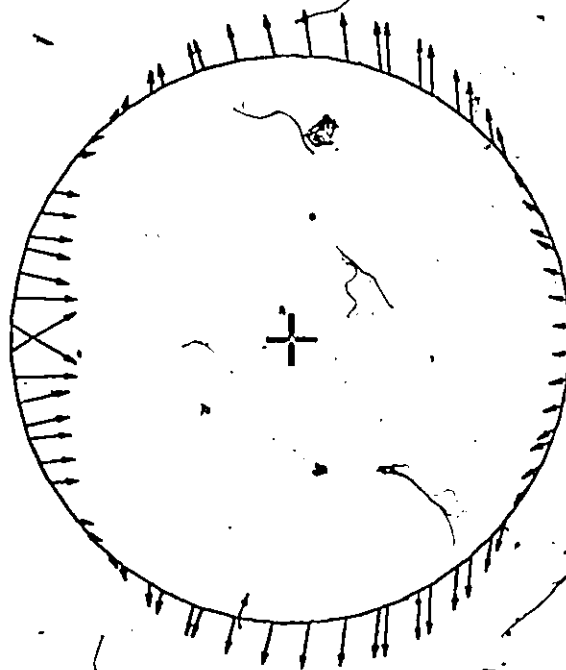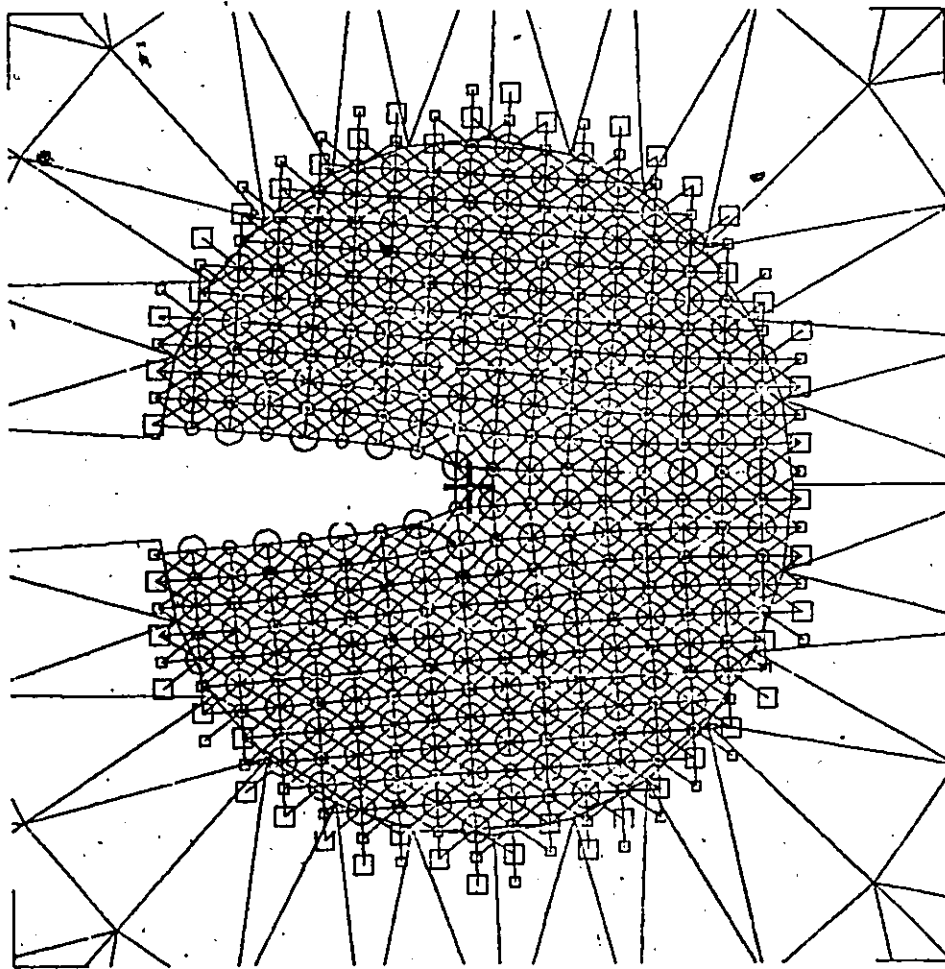   for radius, r, equals 1.4 to 1.6 nm.

6.4 Non-Linear Displacement Field - Magnitude

This section gives some information on the magnitude of the non-linear displacements as a function of radius from the crack tip, r, and angle from the x_1-axis, θ. In order to obtain this, the model was divided into various regions. Within each of these regions the RMS magnitude of the linear elastic crack tip displacements and the RMS magnitude of the non-linear displacements (total displacements minus linear elastic crack tip values) was calculated. The ratio of these two quantities is referred to as d, and is used as a measure of the magnitude of the non-linear displacements. At large radii, r, the value of d should approach zero.

The ratio, d, was evaluated for rings of atoms centered on the nominal crack tip. A series of rings was chosen so that the magnitude of d as a function of r averaged over all angles, θ, around the crack tip could be determined. The boundaries between rings were set every 0.2 nm radius. Figure 36 shows these results for stress intensity factors just inside the lattice trapping limits for the two crack directions. It can be seen that the non-linear displacements are comparable in magnitude to the linear elastic ones near the crack tip and less than 10% of them at 3 nm radius. They are less than 5% at 5 nm in all cases. Thus, the non-linear displacement field is of significant magnitude within 20 lattice parameters of the crack tip. An interesting difference between the two cracks is obvious from Fig. 36. The value of d is more dependent on k for the [110] crack than for the [010]. This is in accord with the greater ease and decisiveness of crack propagation

Figure 36.(a)   Non-linear displacement, d, vs radius from
the crack tip, r, for (001)[010] crack model.

Figure 36(b)   Non-linear displacement, d, vs radius from
                the crack tip, r, for (001)[110] crack model.

for the [110] case. Figure 37 is a log-log plot of d versus r. This is
close to a straight line with slope -1 over most of the range of r
values for almost all cases considered which indicates that d is roughly
proportional to 1/r. This may be used to estimate the radius at which
the non-linear displacements may be neglected to within a given level of
accuracy. The only exception is the [110] crack at k = 1.1 k_G which
differs considerably from this at small r. Examination of Figs. 34(a)
and 35(a) indicates that the bond distribution near the crack tip is
slightly different for the k = 1.1 k_G case compared to k = k_G for the
[110] crack. This difference may account for the different
displacements in this area.

Figure 38 shows the θ dependence of the non-linear displacements
for the two cracks at the Griffith stress intensity factor. The angle θ
is measured counterclockwise from the positive x_1-axis. The region of
the model from r = 0 to r = 2 nm (corresponding approximately to the
atomic area shown in Figs. 25 and 26) was divided into a series of 15°
wedges and the ratio d evaluated for all atoms in each wedge. This is
plotted against θ in Fig. 38. The non-symmetry of the [010] crack is
obvious. The non-linear displacements are maximum in the ±45°
directions and minimum at ±180° and +15° for the [010] case. For the
[110] crack, they are maximum at ±180° and ±45° and minumum at ±135°.
There is an additional minumum at 0° for the k = 1.1 k_G case which is
absent at k = 0.9 k_G.
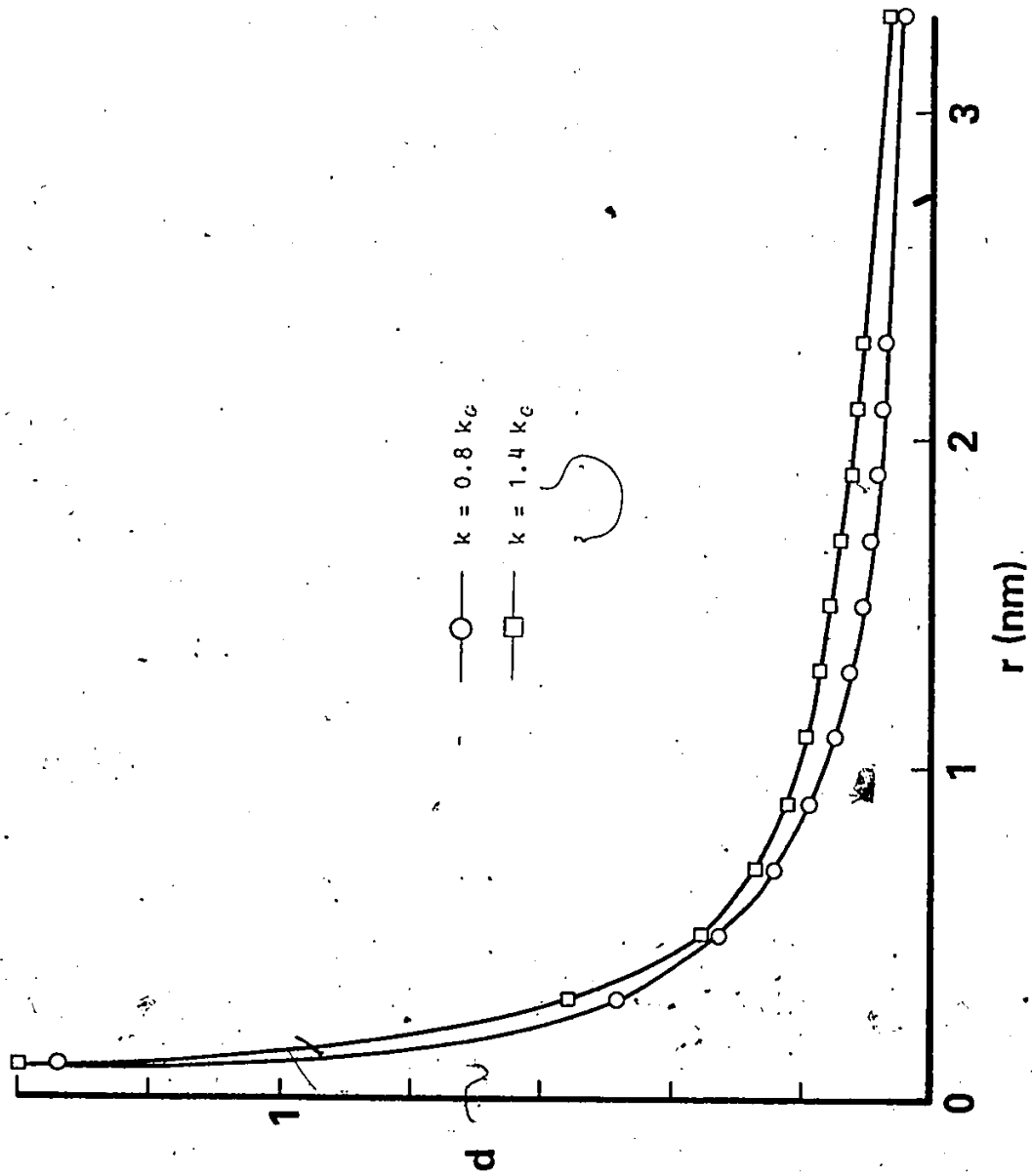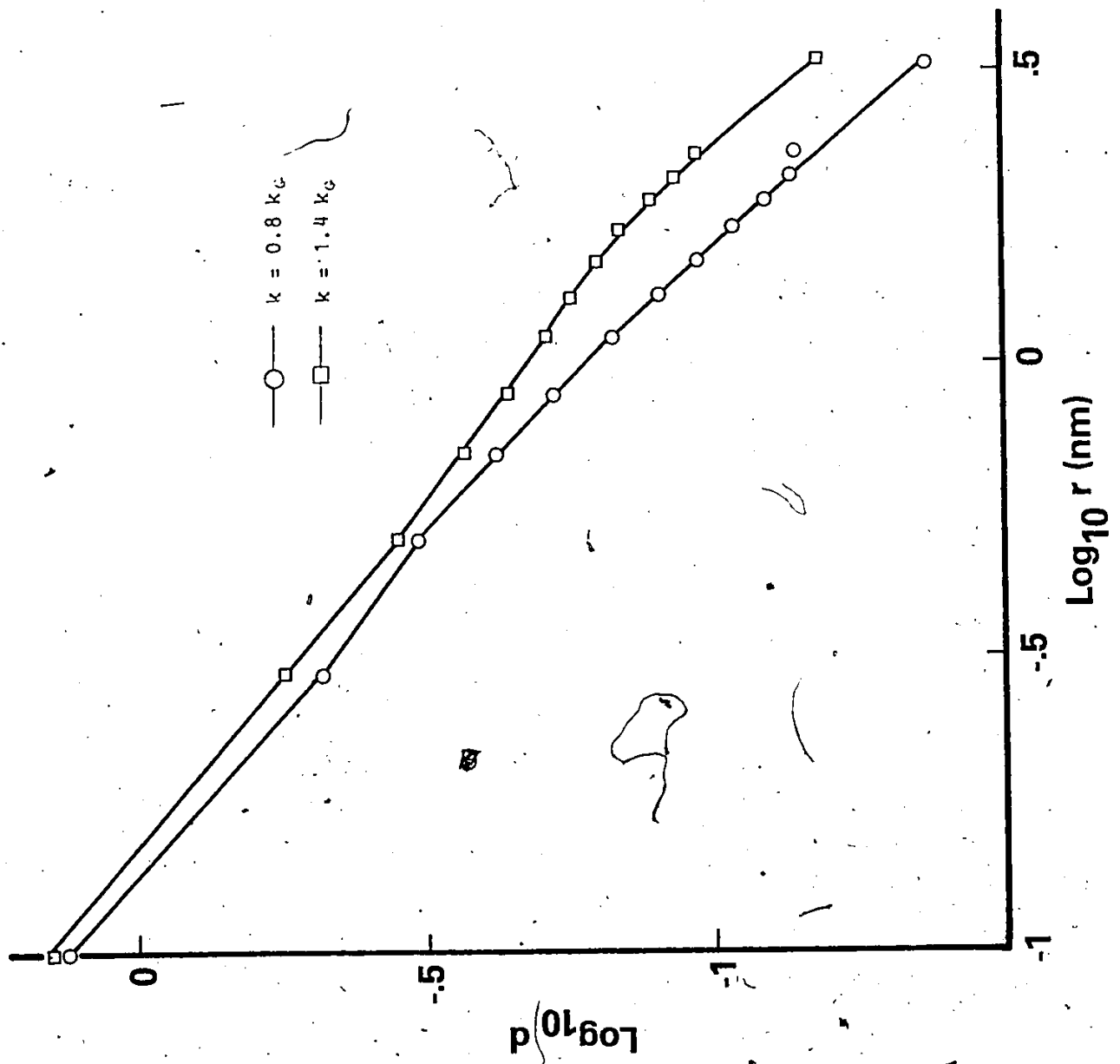
Figure 37(a)   Non-linear displacement, d, vs radius from
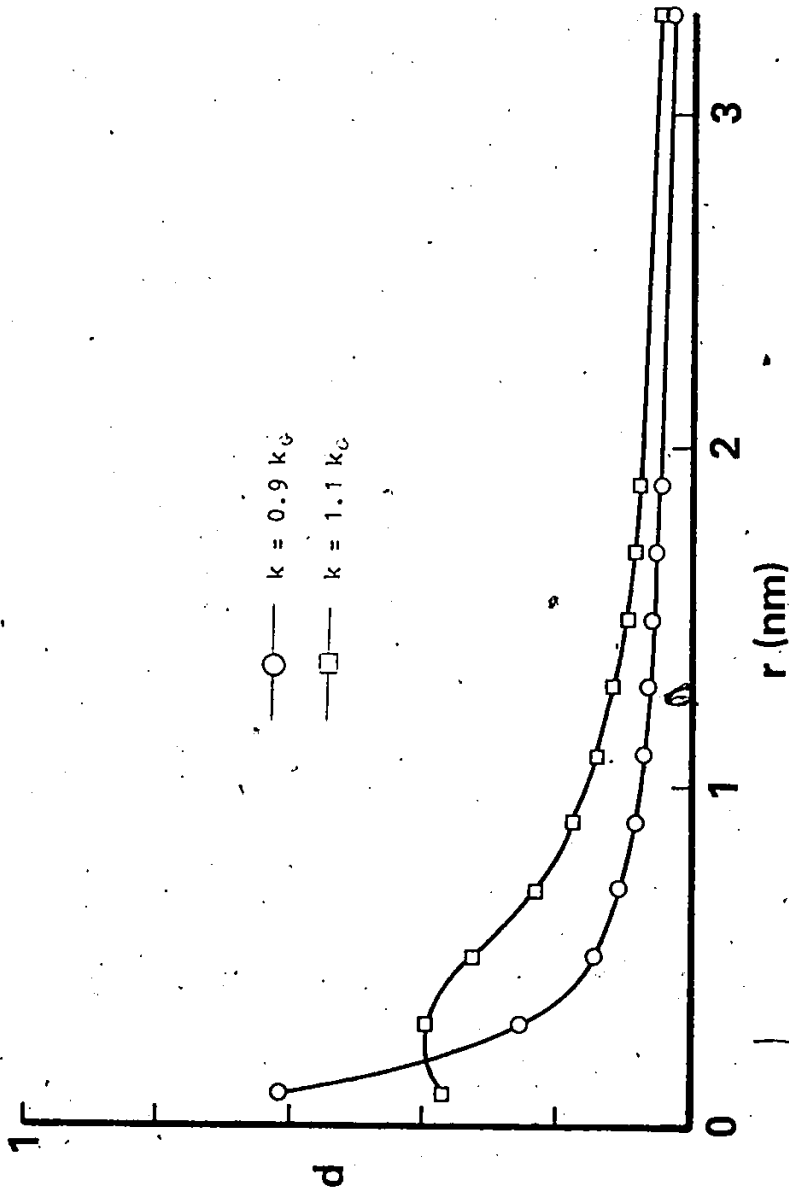   the crack tip, r, for (001)[010] crack model.
                Log-log plot.
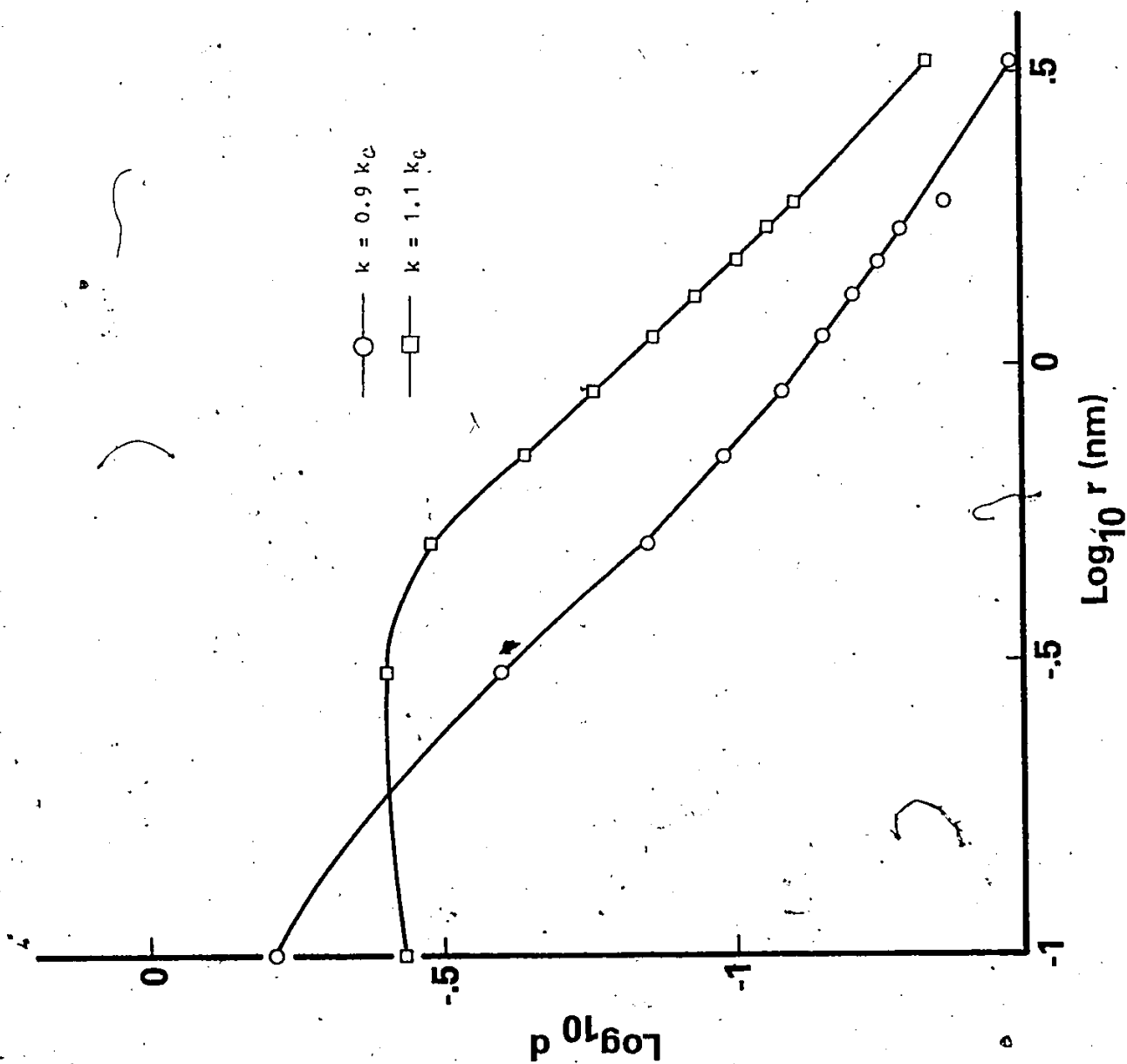
Figure 37(b)   Non-linear displacement, d, vs radius from
the crack tip, r, for (001)[110] crack model.
Log-log plot.
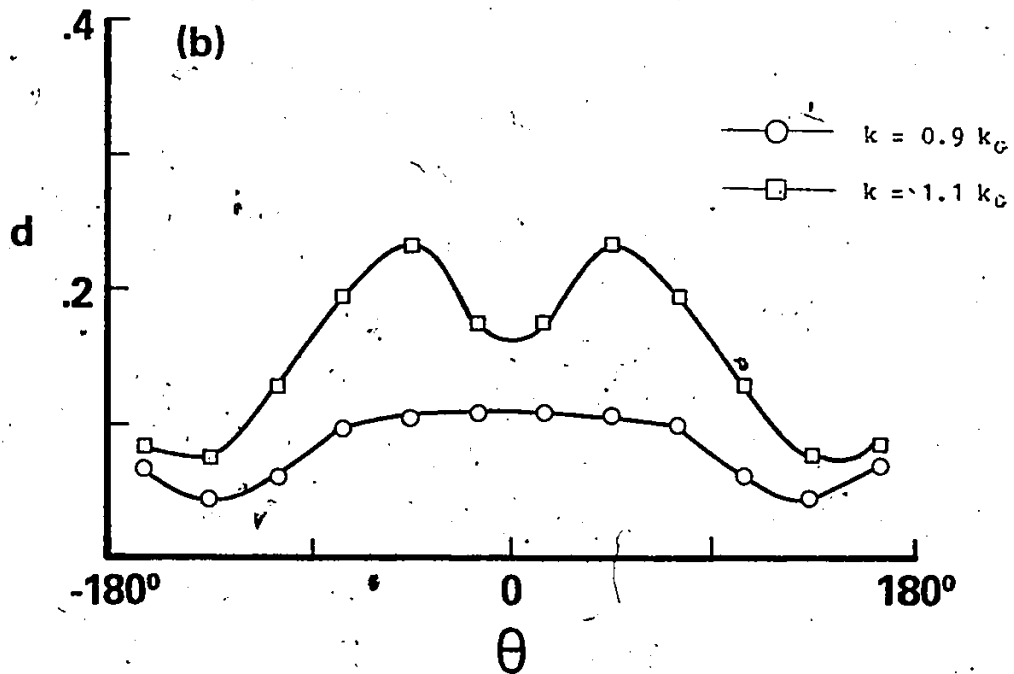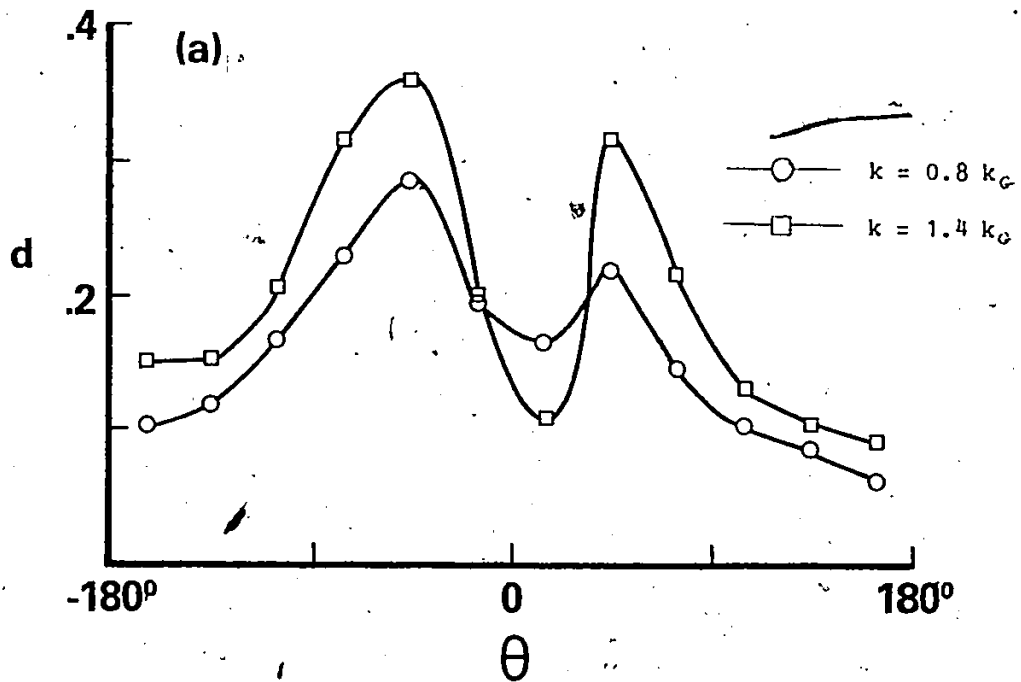
Figure 38.   Non-linear displacement, d, vs angle from the
              x_1 axis, θ.
              (a)   (001)[010] crack
              (b)   (001)[110] crack

6.5 Non-Linear Displacement Field - Shape

An attempt was made to obtain a more detailed description of the non-linear displacement field by least squares curve fitting to various well known functions. The results are described in this section.

A set of displacement functions which have been used, [75], to describe the displacements around the crack tip in atomic simulation models are the higher order terms in the solution of the linear elastic crack tip problem. These are defined in a similar manner to the first order solution given by equation (27), except that the functions $\phi_1(z)$ are now given by, [69],

$$\phi_1(z_1) = i^{n-1} \frac{\mu_m}{\mu_m - \mu_1} (2 z_1)^{-n/2} \tag{35}$$

for $l=1,2$, $m=2,1$ respectively, and $n = 1,2,\ldots$ refers to the order of the term (the order of any term will be called $n+1$ below). If the area of the model which behaves non-linearly were confined to a small cylinder around the crack tip, the remainder of the model would have displacements given by a linear combination of the first order solution given by equation (29) plus a set of higher order terms of various n given by equation (35). There is, thus, some physical justification for their use. The accuracy of the approximation which they provide will depend on the degree to which the non-linear behaviour of the model is concentrated near the crack tip. The results of the previous section indicate that it extends to a considerable distance from the crack tip so that it might be expected that the accuracy of this approximation

would be limited.

It was, in fact, found that this did not provide a good approximation to the behaviour of the model near the crack tip. Table 5 gives the RMS value of the displacements from the first order linear elastic crack tip solution positions after subtracting up to seven higher order terms for the [010] crack at various radii for $k' = k_G$. All other cases were qualitatively similar. It can be seen that less than half of the RMS displacements were removed even after fitting seven terms to the displacement field. Also, each additional term is contributing very little to the fit so that adding more would only very slightly improve the situation. This indicates that the use of these terms in boundary condition schemes for atomic simulation problems may cause inaccuracies.

Some information can be obtained from this curve fitting exercise, however. The most important crack tip term for reducing the residual displacements is the term for n = 1 in equation (35) which has an $r^{-1/2}$ dependence on distance from the crack tip. If s_1 is the coefficient of this term in the fit to the displacement field, Sinclair, [75], shows that its effect is equivalent to assuming that the crack tip is located at a position $x_1' = -s_1/k$ rather than at the nominal position $x_1 = 0$. Table 6 gives this apparent crack tip position for the cracks studied, obtained from fitting to the displacements of atoms and nodes in various regions of the model. The results are reasonably consistent from region to region. They indicate that the crack tip position apparent to most regions of the model moves to the right as k

Table 5. Fraction of original RMS non-linear displacement remaining after subtracting higher order crack tip terms for (001)[010] crack at $k = k_G$.

Terms subtracted n (see eqn. 35)	Radius (nm).				
	0.4-0.6	0.9-1.1	1.4-1.6	0.-2.1 all atoms	0.-60. all model
1	0.614	0.574	0.636	0.679	0.718
1,2	0.611	0.570	0.634	0.665	0.708
1,2,3	0.610	0.513	0.503	0.665	0.708
1,2,3,4	0.594	0.513	0.500	0.654	0.697
1,2,3,4,5	0.542	0.513	0.500	0.653	0.697
1,2,3,4,5,6	0.514	0.510	0.500	0.629	0.677
1,2,3,4,5,6,7	0.510	0.509	0.499	0.627	0.675

Table 6. Crack Tip Locations Derived From $r^{-1/2}$ Higher Order Crack Tip Term.

Crack Line Direction	[010]	[010]	[010]	[010]	[110]	[110]	[110]
k/k_G	0.8	1.0	1.2	1.4	0.9	1.0	1.1
Radius of Region (nm)	Apparent Crack Tip Location (x_i) for Region (nm)						
0.4 - 0.6	0.219	0.196	0.198	0.202	0.060	0.082	0.209
0.9 - 1.1	0.240	0.238	0.244	0.294	0.070	0.085	0.210
1.4 - 1.6	0.207	0.217	0.239	0.323	0.050	0.057	0.175
0. - 2.1 all atoms	0.198	0.197	0.204	0.259	0.044	0.056	0.167
0. - 60. all model	0.187	0.189	0.196	0.259	0.040	0.051	0.162

increases. The change in position as a function of k seems more dramatic for the [110] crack than for the [010], again illustrating the difference between the two cases.

Visual inspection of the form of the non-linear displacements before and after subtracting the higher order crack tip terms indicated two primary reasons for the poor fit. It can be seen in part (b) of Figs. 29 to 32 that dislocation-like shearing exists near the crack tip across the ($\bar{1}01$) and (101) planes at $\pm 45^{\circ}$ to the x_1-axis for the [010] crack. This effect is less prominent for the [110] case which shows a smoother variation of displacement in this area. This shear strain is difficult to account for with the crack tip terms. Fitting to two Volterra dislocations at the origin does not provide a good fit, however, apparently because conditions in other areas, especially near the crack faces, do not correspond well to the dislocation displacement field. The area near the crack face is the other region where the higher order crack tip terms have difficulty producing a good fit for both the [010] and [110] cracks. As discussed in section 5.1, there is some ambiguity in applying the embedded atom forces to the grid in this area. The method described there appeared reasonable and was used for the results presented here. Several other possiblilities were tried but all gave results that were even more difficult to fit than the one used here.

6.6 Dislocation-Like Displacements

The appearance of dislocation-like displacements with the [010] crack is an interesting effect. The question of when a crack will propagate in a brittle fashion and when it will blunt by emitting dislocations is potentially one of the most important points which could be illuminated by computer simulation. No complete dislocations were emitted during any of the solutions performed in the work described above. The kinetic energy of the model during the quenching solutions which were done for this work was always less than that corresponding to a temperature of 100 K. Experimentally, fracture of iron is apparently brittle at these temperatures (as described in the literature survey), in agreement with this result. The appearance of the displacement field, however, indicates that there is some tendency to form dislocations. The components of this displacement in the x_1-x_3 plane would seem to indicate that these are of type ($\bar{1}$01)/[111] but no significant out of plane movement occurred which would be expected for dislocations of this type. This may be an effect of the modelling procedure since the atoms are free to move in all three coordinate directions but the grid is restrained to move in the x_1-x_3 plane in the present model. This restriction could be inhibiting the formation of complete [111] dislocations. The finite element boundary conditions can be used to allow this movement but this has not yet been done. Alternatively, it may be that the symmetry of the problem is high enough that out of plane movements are inhibited and some non-uniformity in the x_2-direction, such as a jog in the crack front, may be necessary to

stimulate [111] dislocation emission. Such a jog was considered by Kanninen, et al, [68], using rigid boundary conditions. No dislocations were observed, but it would be interesting to examine such a model with the present boundary condition scheme.

The fact that these dislocation-like displacements are more prominent in the [010] model than in the [110] may be associated with the higher value for the upper lattice trapping limit for the [010] case. If some energy were directed into the formation of dislocations, then less would be available to produce crack propagation, and higher stress intensity levels would be required to produce fracture. This finding is similar to that of Ayres and Stein, [18], who predicted that dislocation activity should be greater for the [010] than [110] crack direction by counting the active slip planes in each case.

Rice and Thomson, [15], have also provided a method of evaluating the likelihood of dislocation emission from a crack tip based on the linear elastic solution for the displacement field around the crack tip and dislocations. Their analysis is, of course, based on a greatly simplified model of the real crack tip situation but it is interesting to compare the results of their analysis to the more detailed ones presented here. The basis of their method was presented in the literature survey. They calculate a critical distance, ξ_c, beyond which dislocations will tend to move away from the crack tip. They assume that if ξ_c is less than the core cut-off distance of the dislocation, spontaneous emission will occur. This is obviously difficult to judge in many borderline cases of which iron is one. It

may be stated, however, that the smaller the value of ξ_c, the greater is the tendency to emit dislocations by their analysis. Substituting the parameters of the Johnson-I potential into the formulas given by Rice and Thomson leads to the values shown in Table 7. It can be seen that their method predicts the [010] crack to be more likely to emit dislocations than the [110]. The appearance of dislocation-like displacements in the present [010] crack model, but not in the [110], apparently supports this conclusion. Note also that [001] dislocations have a significant chance of being emitted from the [010] crack. No sign of these was seen in the simulations described to this point which correspond to low temperature materials but one was observed in a thermally activated model which is described below.

The dislocation-like displacements observed here can be compared to the dislocation displacement field assumed by the Peierls dislocation model, [37]. In this model, all the displacement or disregistry caused by a dislocation in a simple cubic lattice is assumed to be between two adjacent planes of atoms. A simple sinusoidal interatomic force law is assumed. The disregistry, g, as a function of distance, x, along the dislocation glide plane from the dislocation center is given by

$$g = g_o \left[1 - \frac{2}{\pi} \tan^{-1}\left(\frac{x}{\zeta}\right) \right] . \tag{36}$$

where g_o is the value of g at x = 0, and

Table 7.   Rice and Thomson, [15], Results for Johnson-I Potential, [59].

Crack System	Slip System	ξ_c
(001) [010]	($\bar{1}$01) [111]	2.66
(001) [010]	(100) [001]	2.34
(001) [110]	($\bar{1}$10) [111]	3.56
(001) [110]	($\bar{1}$12) [$1\bar{1}1$]	2.97

$$\zeta = \frac{h}{2(1-\nu)} \tag{37}$$

In equation (37), h = the spacing between atom planes, and ν = the Poisson's ratio of the material.

The Voight average Poisson's ratio for the Johnson-I material is 0.25 . From part (a) of Figs. 29 to 32 it appears that most of the disregistry due to the dislocation-like displacements occurs between two (101) planes seperated by $\frac{1}{2}[\bar{1}01]$ at the lower k values, and across two of these planes seperated by $[\bar{1}01]$ for higher k. Since the dislocations are more likely to be emitted at higher k values, the corresponding $[\bar{1}01]$ seperation between adjacent planes will be used. This corresponds to a value of h of 0.405 nm. Using these values, ζ given by equation (37) is 0.270 nm. Values for the disregistry, g, as a function of distance were read off parts (c) to (f) of Figs. 29 to 32. The results are plotted in Fig. 39.

In order to compare these results to the Peierls model, the curve defined by equation (36) is also plotted. The value taken for g was chosen as follows. In the Peierls model of a dislocation in the center of a crystal, g_0 is one half of the Burgers vector. For the case considered here, in which the dislocation is forming at the free surface of the crack face, g_0 was taken to be the total Burgers vector. Considering only the x_1-x_3 plane component of the Burgers vector for a $\frac{1}{2}[111]$ dislocation (since this is all that is observed as described above) gives $g_0 = 0.202$ nm.

Figure 39(a). Disregistry, g, vs $\tan^{-1}(x/\zeta)$ for dislocations along $(\bar{1}01)$ planes for $(001)[010]$ crack. The dashed line is equation (36).
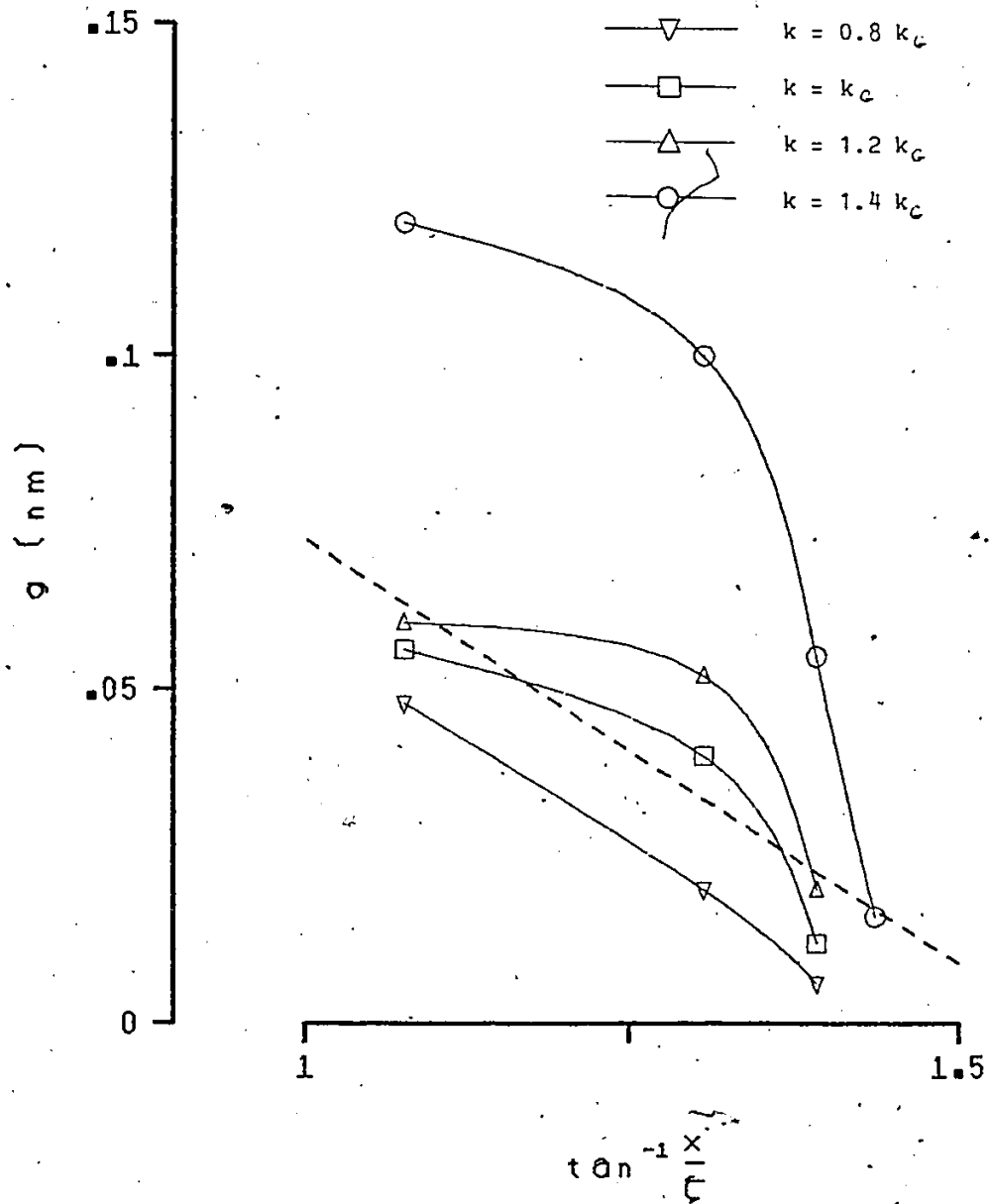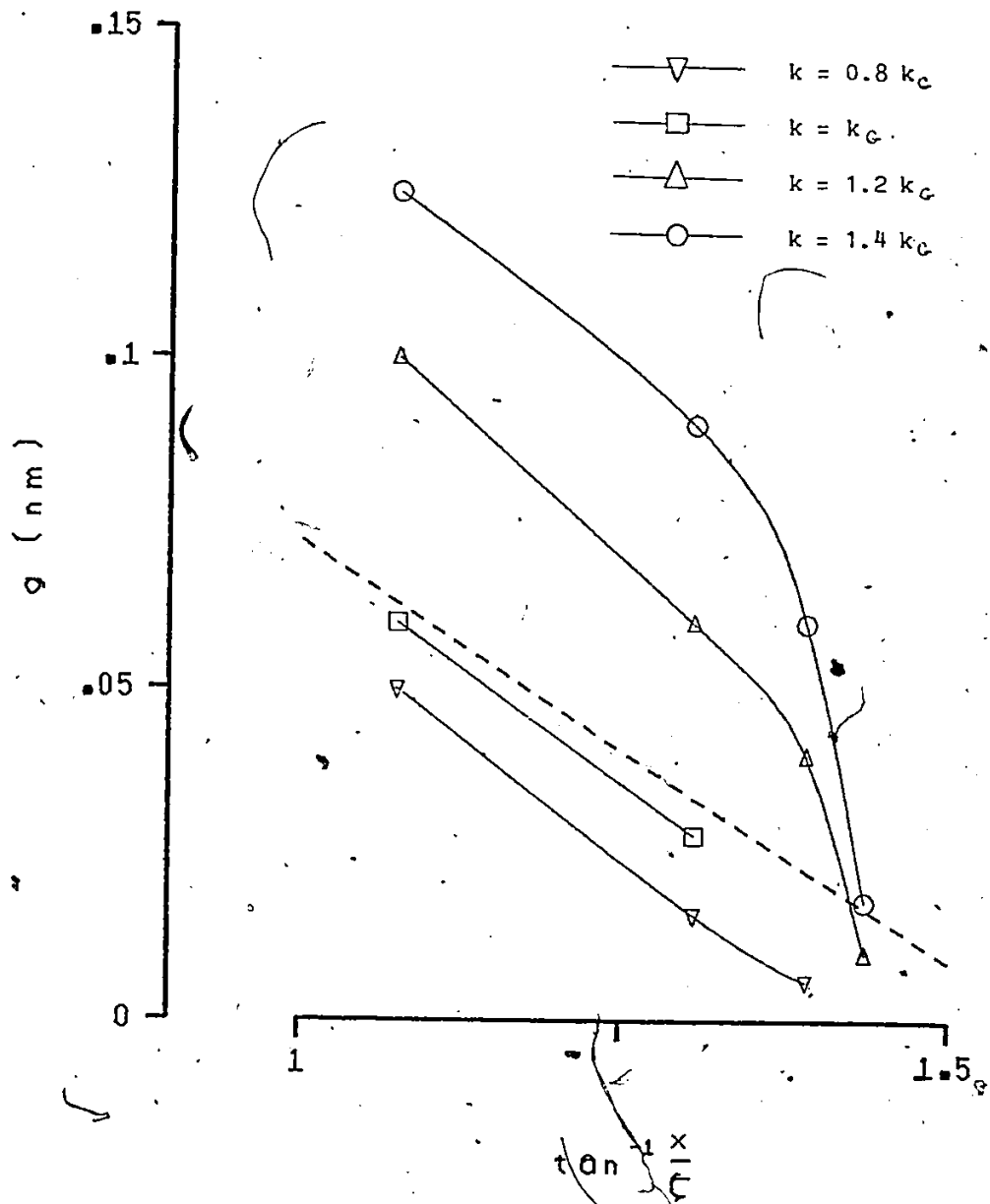
Figure 39(b)   Disregistry, g, vs $\tan^{-1}(x/\zeta)$ for dislocations along (101) planes for (001)[010] crack. The dashed line is equation (36).

This description of the information plotted in Fig. 39 indicates that there are a great many assumptions involved in comparing the results of the model used in the present work with the Peierls model. The Peierls model itself contains many simplifying assumptions. Thus, the comparison must be considered to have only very limited accuracy. Nevertheless, the results show that the general trend of the disregistries for $k = 0.8 k_G$ and of one of the dislocations for $k = k_G$ are straight lines as required by equation (36). The curves for $k = 1.2 k_G$ and $1.4 k_G$ are steep enough at large radii that, if extrapolated to $x = 0$ with these large slopes, they would indicate that the disregistry there is larger than that required to cause a dislocation of the type considered. It can be seen, however, that these curves are not straight lines, deviating close to the crack tip. Thus, the dislocation-like displacements at the crack tip never become large enough to cause a complete dislocation there, even though it would appear that this would be possible if only the low k solutions are considered. This may be due to the non-linearity in this model, which becomes especially severe at the high strain levels encountered near the crack tip at high k, and causes significant deviation from the Peierls model and the non-linearity in the force law assumed for it.

6.7 Elliptic Expansion Center

The appearance of the non-linear displacement field for the [110] crack indicated that an elliptic expansion center at the apparent crack tip might provide a good fit. Such an expansion center was used

Table 8.   Elliptic Expansion Center Strengths for [110] Crack.
b = Lattice Parameter = 0.286 nm for α-Iron.

k/k_G	M_1 (nN)	M_3 (nN)	δA (nm^2)	$\delta A/b^2$
0.9	-1.64	4.68	0.00659	0.081
1.0	-1.95	6.29	0.00941	0.115
1.1	-0.61	14.72	0.03058	0.374

by Gehlen, et al, [44], to describe the non-linear displacement field around a [100] edge dislocation in α-iron. For the [110] crack in the present study, it was found that subtracting an elliptic expansion center at the crack tip could reduce the RMS value of the non-linear displacement field by 20 to 30%. This is more than the effect of any higher order crack tip term indicating that it is an important component of the crack tip displacement field although it still leaves much of this field undescribed. The parameters of the best fit expansion centers are given in Table 8. The expansion center is defined by two dipole forces at right angles to each other. M_1 is the dipole strength in the x_1-direction, M_3 the strength in the x_3-direction. The volume expansion, δA, associated with this term of the displacement field is also given. A complete description of this type of displacement field was given by Gehlen, et al, [44].

6.8 Thermal Activation of the Model

To examine the possiblity of thermally activated dislocation emission at high temperatures, the [010] crack was loaded to $k = 2\ k_G$. The atoms were initially given randomly distributed kinetic energies and the model was occasionally partially quenched so that the total kinetic energy in the system remained close to that corresponding to a temperature of approximately 400 K for 1000 fs. The appearance after this time is shown in Fig. 40. It can be seen that a [001] dislocation appears to have been emitted from the crack tip, blunting it before crack propagation could occur. The finite element area is not flexible
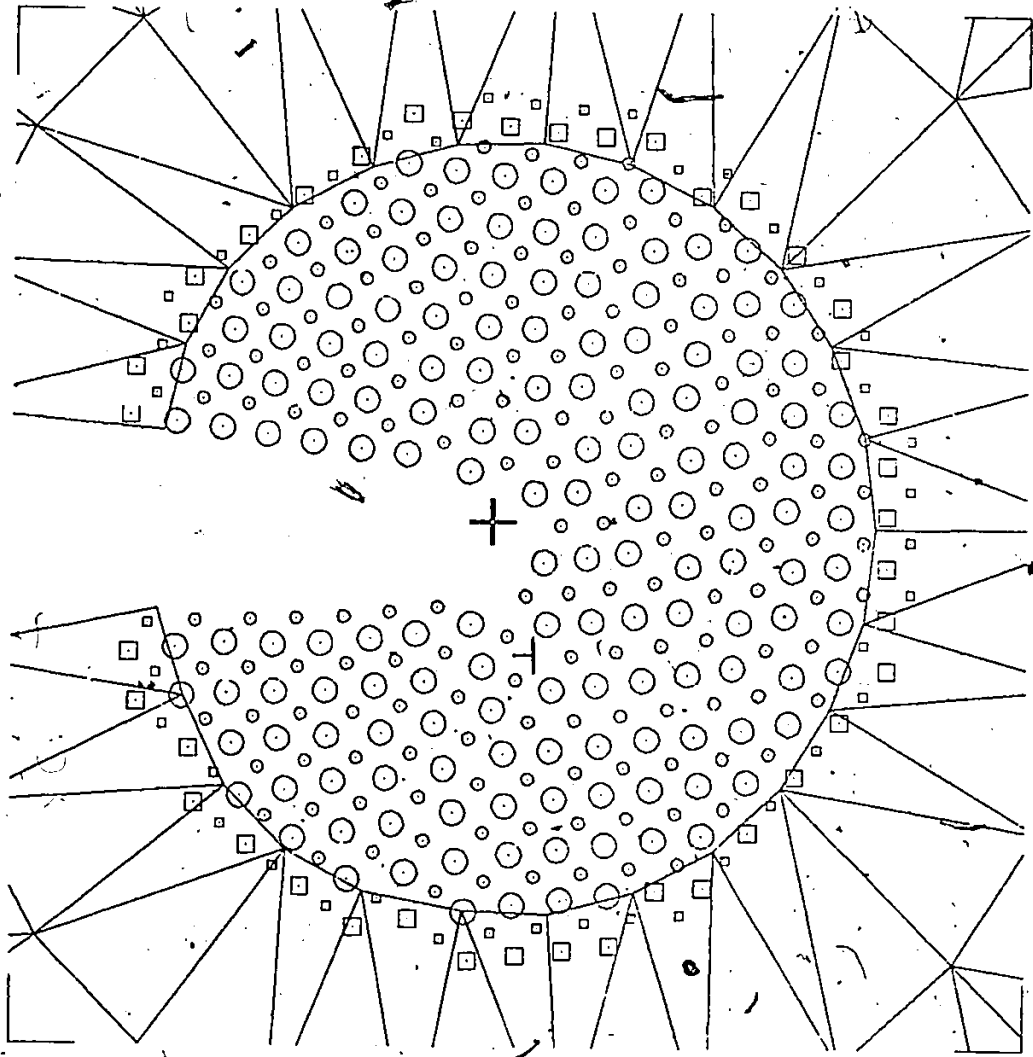
Figure 40.   (001)[010] crack at $k = 2 k_c$ after 1500 fs showing the dislocation emitted from the crack tip.

enough with the current grid to allow the dislocation to move farther. The dislocation is not complete since the material has not closed above it after it moved past. This may be a result of the relatively short cut-off of the Johnson potential compared to that probable in real materials. It does, however, appear that thermally activated dislocation emission is likely in this material and the fact that an [001] dislocation was emitted corresponds to the prediction of the model of Rice and Thomson given in Table 7. As discussed above, the reason that no [111] dislocations were emitted may be the restriction imposed by the grid, the high symmetry of the model in the x_2-direction, or it may indicate a real effect. This result may be compared to that of Gehlen, et al, [66], who used a model with rigid boundary conditions for thermal activation tests. No rupture or dislocation emission could be obtained with that model.

6.9 Stresses

The stress field around a crack tip is important in determining, for example, vacancy formation and migration energies in its vicinity, [9]. Stress can be defined only on a continuum basis, but a "pseudo-stress" was calculated for the discrete area of the models studied in this work. Each atom was considered to be centered within a cube with axes parallel to the coordinate axes. The force in each bond to this atom which passes through each face was resolved to give normal and shear stresses on each of these faces. Averaging the values on opposite faces gave an approximation to the stress state at this point.

Figures 41 and 42 show σ_3 along the positive x_1-axis for each case. This is the largest stress component. The streses given by the Griffith model are also shown and it can be seen that they give a reasonable approximation to these values at large radii but that there is significant deviation at smaller radii where the Griffith stress approaches infinity. There is a maximum in the value of σ_3 in the present model ahead of the crack tip. Very close to the crack tip the stress is lower than the Griffith stress. At larger distances, the stress is slightly higher than the Griffith value, balancing the lower stress near the tip. This is reminiscent of the results for the continuum theory of cracks when material and geometrical non-linearity is included, [7,8]. In the continuum theory this result has led to the proposal (supported by experimental evidence, [11]) that in ductile materials at high temperature, crack propagation proceeds by repeated void nucleation at the point of maximum σ_3 (and corresponding maximum hydrostatic tension) followed by necking failure of the material between this void and the old crack tip. An analogous type of behaviour could be responsible for the propagation of the atomically sharp, brittle cracks studied in the present work. A vacancy is most likely to form at, or migrate to, the point of maximum hydrostatic tension and the crack may then move through the (weakened) material between the vacancy and the old crack tip. This would be a source of temperature dependence for the propagation of brittle cracks, since the vacancy formation rate is temperature dependent, and may be of interest to theories of slow crack growth by vacancy diffusion, [9]. Although the pseudo-stress distribution indicates that this may occur, discrete lattice

Figure 41. σ_3 vs x for (001)[0ī0] crack. The curve shows the stresses predicted by the Griffith crack model.
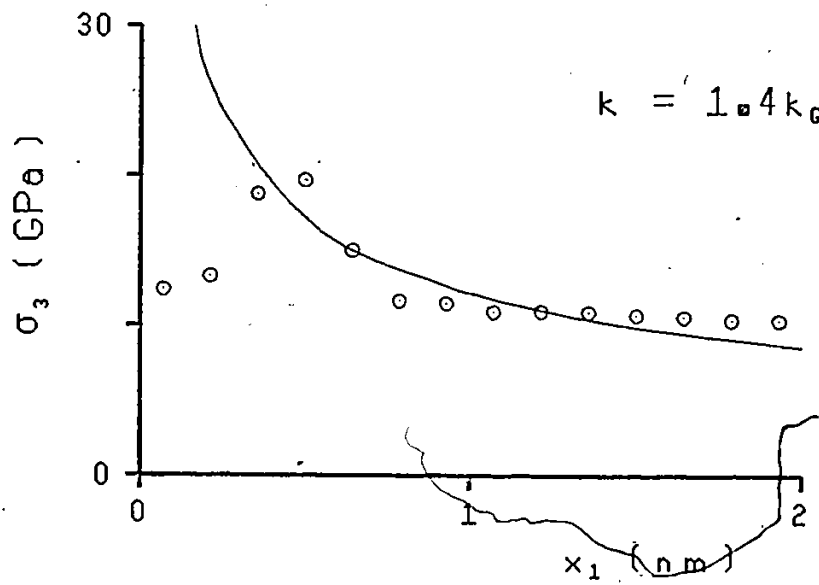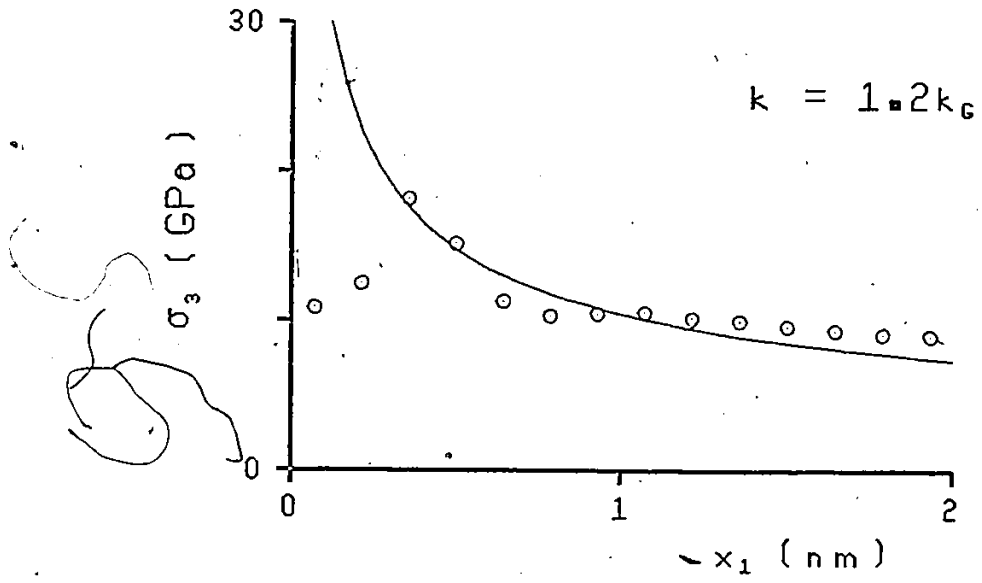
Figure 41 (cont.) σ_1 vs x_1 for (001)[010] crack.

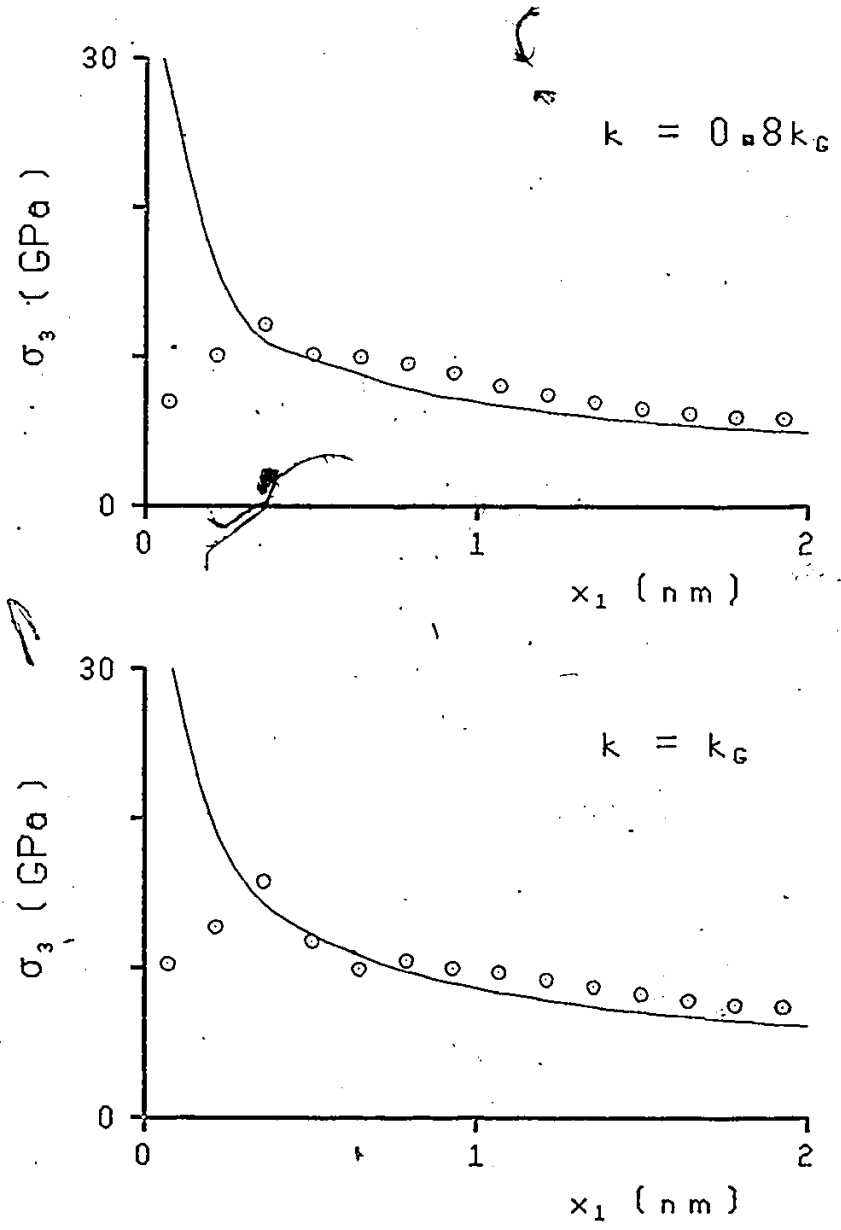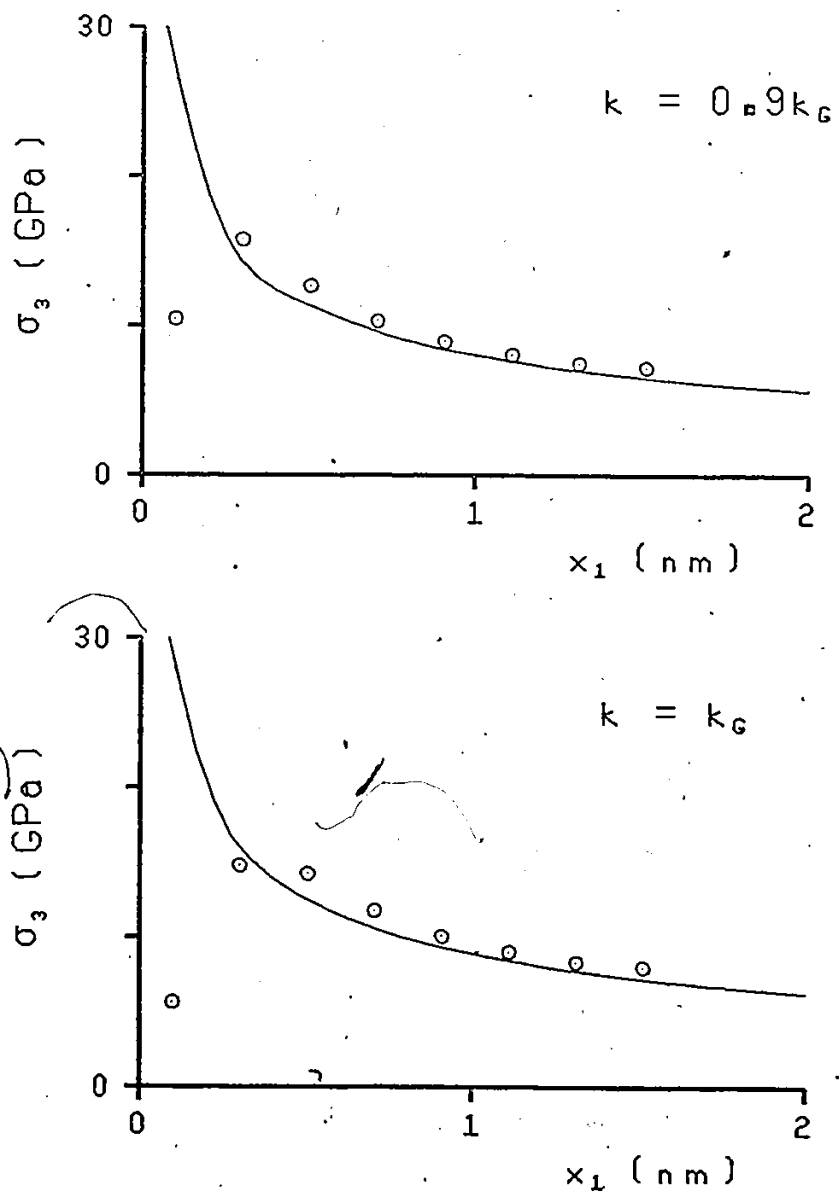Figure 42. σ_3 vs x for (001)[110] crack. The curve shows the stresses predicted by the Griffith crack model.
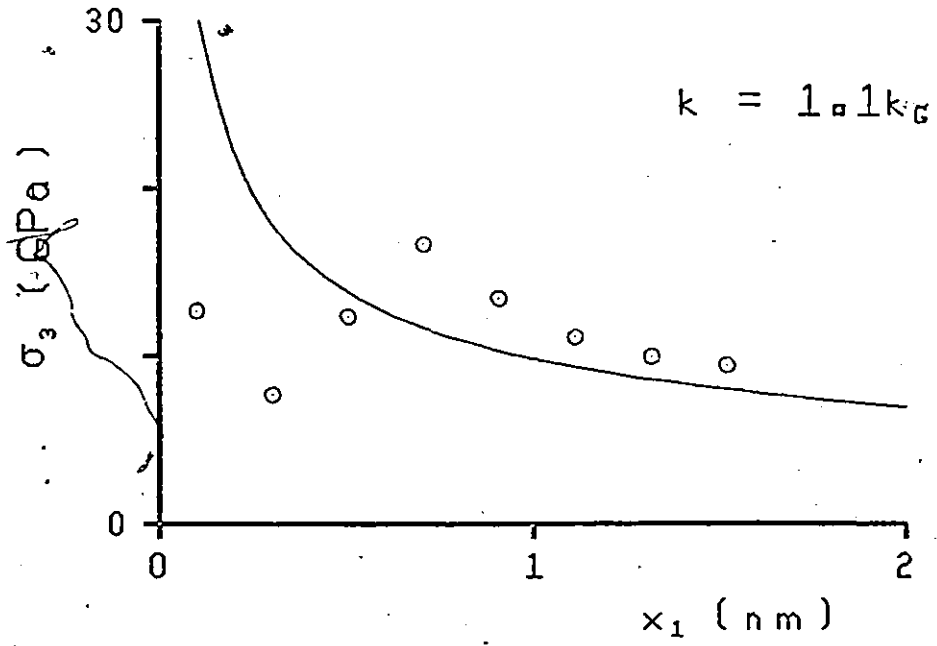
Figure 42 (cont.) σ_1 vs x_1 for (001)[110] crack.

calculations would be necessary to obtain accurate values of energies for crack tip-vacancy interactions.

The [110] crack at k = 1.1 k_G has a more complicated stress distribution with two peaks. This is probably related to the different bond distribution in this case compared to that at lower stress intensity factors as discussed in section 6.4 .

6.10 Conclusions

The major conclusions of this chapter may be summarized as

1)   When the finite element boundary scheme was applied to the (001) plane crack in α-iron, crack propagation on the (001) plane could be obtained for two dimensional cracks with directions of [010] and [110].

2)   Significant differences were observed in the lattice trapping limits and crack propagation speeds for these two directions. Some published experimental results seem to support these conclusions but more experimental work will need to be done before they can be confirmed.

3)   The non-linear component of the displacement field (defined as the difference between the total model displacements and those given by linear elastic fracture mechanics) is of significant magnitude out to 20 lattice parameters from the crack tip. The shape of this non-linear displacement field is complex and it is not well

represented by the higher order linear elastic crack tip terms, by Volterra dislocations at the crack tip, or by an elliptic expansion center, although it shows components of all these.

4) The dislocation-like displacements, apparent around the [010] crack tip, are especially interesting. They indicate the possiblility of dislocation emission from the crack tip, although this did not occur in low temperature simulations. A simulation at 400 K, however, did apparently result in the emission of a dislocation from the crack tip.

5) The "pseudo-stress" distribution shows a maximum in σ_3 just ahead of the crack tip in these models. This may be interesting for theories of slow crack growth by vacancy diffusion.

7 CONCLUSIONS AND DISCUSSION

The work which has been presented in this thesis has been concerned with some aspects of atomic level computer simulation models, with regard to both improving the efficiency and accuracy of these models in general, and in applying them to the study of (001) plane fracture in α-iron. The major conclusions and achievements of this work may be stated as follows:

1.a) Selection of the optimum method for solution of an atomic simulation problem can result in a decrease of computer time used by factors of two or three over that required by other, often used, methods.

b) The best method of those tested for integration of the equations of motion of a model depends on the accuracy level required for dynamic models, and on the stability limits of the integrator for static models. They may be chosen as described in Chapter 4.

c) The conjugate gradient method appeared significantly better than the quenching solution methods for the attainment of equilibrium positions (when the slight modification noted in Chapter 4 is included in the conjugate gradient scheme).

d) Alternate equilibria appear to be more easily obtained than had been previously considered.

203

e) The sum square atomic force provides a reasonable estimate of the energy error in a static solution simulation model.

2. A new boundary scheme which utilizes the finite element method has been proposed which offers several advantages over previous methods. These are outlined in section 5.5.

3. a) The new boundary scheme has been applied to the (001) plane crack in α-iron. Two dimensional models with crack line directions of [010] and [110] were studied.

b) (001) plane fracture was obtained for both cracks with no dislocations emitted from either crack model at low temperatures.

c) Significant differences were observed between the two crack directions which are supported by some published experimental work, although this support must be considered tentative at present.

d) The non-linear component of the displacement field is complex and not well represented by any of the displacement fields considered in Chapter 6 .

e) Although no dislocations were emitted at low temperatures, dislocation-like displacements were observed around the [010] crack tip. A dislocation was, apparently, emitted from this crack during a dynamic simulation at 400 K.

A great deal of future work in this area is possible, and desirable. With regard to improving the accuracy and efficiency of the

computer models used, tests such as that presented in Chapter 4 should be carried out on larger models with a variety of boundary conditions. Some analysis of the effect of alternate equilibria in these models and solution methods which can obtain all or, at least, most of these is needed. Improvements possible in the finite element boundary scheme over the particular implementation used in this thesis were indicated in section 5.5.. Regarding the (001) plane α-iron crack, further studies such as that presented in section 6.8 would be desirable in order to determine under what conditions dislocations can be emitted from the crack tip, since this is fundamental to the fracture behaviour of this, and many other materials. Three dimensional models should be considered for this, as discussed in section 6.6, but they are expensive at present. In addition, no studies appear to have been made on cracks under k_{II} or k_{III} type loadings. This is still an open area.

Areas in which studies such as these can be expected to find the most immediate everyday engineering application are in non-destructive testing methods such as acoustic emission in which the sound produced by moving crack tips or dislocations is measured and correlated with failure probabilities; nuclear radiation damage to materials, important for energy research and, inherently, an atomic level effect; and in the production of very pure crystals used in, for example, electronic components, so that it may be possible to determine the conditions under which such materials can be produced with a minimum of atomic scale defects. It is hoped that the work presented in this thesis may contribute in some way to these studies.

8 REFERENCES

1. A.G. Guy, Introduction to Materials Science (McGraw-Hill, New York, 1972).

2. S.T. Rolfe, J.M. Barsom, Fracture and Fatigue Control in Structures (Prentice-Hall, Englewood Cliffs, N.J., 1977).

3. H. Liebowitz, ed., Fracture, vols. 1-6 (Academic Press, New York, 1968-1972).

4. P.D. Hilton, G.C. Sih, "Applications of the Finite Element Method to the Calculations of Stress Intensity Factors" in Methods of Analysis and Solutions of Crack Problems, edited by G.C. Sih (Noordhoff International, Leyden, 1973) pp.426-483.

5. A.A. Griffith, "The Phenomena of Rupture and Flow in Solids", Phil. Trans. Roy. Soc. (London), A-221 (1920) pp.163-198.

6. R.G. Hoagland, Vanderbilt University, personal communication.

7. J.R. Rice, M.A. Johnson, "The Role of Large Crack Tip Geometry Changes in Plane Strain Fracture" in Inelastic Behaviour of Solids, edited by M.F. Kanninen, W.F. Adler, A.R. Rosenfield, R.I. Jaffee (McGraw-Hill, New York, 1970) pp.641-672.

8. J.E. Sinclair, "Dislocation-Based, Geometrically Consistent, Model of Plasticity in Fracture" in Proceedings of the International Conference on Computer Simulation for Materials Application , pt.1, Gaithersburg, Md., 19-21 Apr., 1976, pp.388-404.

9. R.N. Stevens, R. Dutton, "The Propogation of Griffith Cracks at High Temperatures by Mass Transport Processes", Mat. Sci. Eng., 8 (1971) pp.220-234.

10. R. Raj, M.F. Ashby, "Intergranular Fracture at Elevated Temperatures", Acta. Met., 23 (1975) pp.653-666.

11. C. Crussard, R. Borione, J. Plateau, Y. Mouillon, F. Maratray, "A Study of Impact Tests and the Mechanics of Brittle Fracture", J. Iron and Steel Inst. (London), 183 (1956) pp.146-177.

12. G.T. Hahn, M.F. Kanninen, A.R. Rosenfield, "Fracture Toughness of Materials", Ann. Rev. of Mat. Sci., 2 (1972) pp.381-404.

13. A.W. Thompson, P.F. Wiebrauch, "Ductile Fracture. Nucleation at Inclusions", Scr. Met., 10 (1976) pp.205-210.

14. A. Kelly, W.R. Tyson, A.H. Cottrell, "Ductile and Brittle Crystals", Phil. Mag., 15 (1967) pp.567-586.

15. J.R. Rice, R. Thomson, "Ductile versus Brittle Behaviour of Crystals", Phil. Mag., 29 (1974) pp.73-97.

16. R. Thomson, "Some Microscopic and Atomic Aspects of Fracture" in The Mechanics of Fracture, AMD-Vol.19, edited by F. Erdogan (ASME, New York, 1976) pp.1-21.

17. D. Hull, Introduction to Dislocations (Pergamon Press, Oxford, 1975).

18. R. Ayres, D.F. Stein, "A Dislocation Dynamics Approach to Prediction of Cleavage Planes in B.C.C. Metals", Acta. Met., 19 (1971) pp.789-794.

19. G.M. Pharr, D.M. Barnett, W.D. Nix, "A Critique of the Ayres-Stein Method of Predicting Cleavage Planes in Metals", Scr. Met., 12 (1978) pp.973-978.

20. W.R. Tyson, "Estimation of Surface Energies from Phonon Frequencies for BCC and FCC Metals", J. Appl. Phys., 47 (1976) pp.459-465.

21. M.C. Inman, H.R. Tipler, "Interfacial Energy and Composition in Metals and Alloys", Metall. Rev., 8 (1963) pp.105-166.

22. J.J. Gilman, "Direct Measurements of the Surface Energies of Crystals", J. Appl. Phys., 31 (1960) pp.2208-2218.

23. A.T. Price, H.A. Holl, A.P. Greenough, "The Surface Energy and Self-Diffusion Coefficient of Solid Iron Above 1350 C", Acta. Met., 12 (1964) pp.49-58.

24. A.S. Tetelman, W.D. Robertson, "Direct Observation and Analysis of Crack Propogation in Iron-3% Silicon Single Crystals", Acta. Met., 11 (1963) pp.415-426.

25. J.M. Berry, "Cleavage Step Formation in Brittle Fracture Propogation", Trans. Amer. Soc. Metals, 51 (1959) pp.556-588.

26. D. Hull, P. Beardmore, "Velocity of Propogation of Cleavage Cracks in Tungsten", Int. J. Frac. Mech., 2 (1966) pp.468-487.

27. J. Liu, J.C. Bilello, "Effects of Plastic Relaxation on the Semi-Brittle Fracture of <100> Oriented Tungsten Single Crystals", Phil. Mag., 35 (1977) pp.1453-1472.

28. J.E. Cordwell, D. Hull, "The Brittle Fracture of [100] Axis Tungsten Single Crytals", Phil. Mag., 19 (1969) pp.951-966.

29. O. Vingsbo, "Application of the Morse Function to Cleavage", Mater. Sci. Eng., 8 (1971) pp.32-40.

30. J.R. Beeler, "The Role of Computer Experiments in Materials Research", Adv. in Mat. Res., 4 (1970) pp.295-476.

31. P.C. Gehlen, J.R. Beeler, R.I. Jaffee, eds., Interatomic Potentials and Simulation of Lattice Defects (Plenum Press, New York, 1972).

32. A. Rahman, "Correlations in the Motion of Atoms in Liquid Argon", Phys. Rev., 136 (1964) pp.A405-A411.

33. A. Rahman, F.H. Stillinger, "Molecular Dynamics Study of Liquid Water", J. Chem. Phys., 55 (1971) pp.3336-3359.

34. J.M. Dickey, A. Paskin, "Computer Simulation of the Lattice Dynamics of Solids", Phys. Rev., 188 (1969) pp.1407-1418.

35. R.A. Johnson, P.J. White, "Calculations for Surface Energies and Displacements Using Empirical Interatomic Forces", Phys. Rev. B, 13 (1976) pp.5293-5302.

36. R.A. Johnson, "Interstitials and Vacancies in α Iron", Phys. Rev., 134 (1964) pp.A1329-A1336.

37. J.P. Hirth, J. Lothe, Theory of Dislocations (McGraw-Hill, New York, 1968).

38. M. Doyama, R.M.J. Cotterill, "The Energy and Atomic Configuration of an Edge Dislocation in an F.C.C. Metal", Phys. Letters, 13 (1964) pp.110-111.

39. R.M.J. Cotterill, M. Doyama, "The Energy and Atomic Configuration of a Screw Dislocation in an F.C.C. Metal",, *Phys. Letters*, 14 (1965) pp.79-80.

40. R. Chang, L.J. Graham, "Edge Dislocation Core Structure and the Peierls Barrier in Body-Centered Cubic Iron", *Physica Status Solidi*, 18 (1966) pp.99-103.

41. R. Chang, "Screw Dislocation Core Structure in Body-Centered Cubic Iron", *Phil. Mag.*, 16 (1967) pp.1021-1029. .

42. R. Bullough, R.C. Perrin, "Atomic Configuration and Nonlinear Aspects of the Core of Dislocations in Iron" in *Dislocation Dynamics*, edited by A.R. Rosenfield, G.T. Hahn, A.L. Bement, R.I. Jaffee (McGraw-Hill, New York, 1968) pp.175-190.

43. P.C. Gehlen, A.R. Rosenfield, G.T. Hahn, "Structure of the <100> Edge Dislocation in Iron", *J. Appl. Phys.*, 39 (1968) pp.5246-5254.

44. P.C. Gehlen, J.P. Hirth, R.G. Hoagland, M.F. Kanninen, "A New Representation of the Strain Field Associated with the Cube-Edge Dislocation in a Model of α-Iron", *J. Appl. Phys.*, 43 (1972) pp.3921-3933.

45. R.G. Hoagland, J.P. Hirth, P.C. Gehlen, "Atomic Simulation of the Dislocation Core Structure and Peierls Stress in Alkali Halide", *Phil. Mag.*, 34 (1976) pp.413-439.

46. G.C. Hasson, C. Goux, "Interfacial Energies of Tilt Boundaries in Aluminum. Experimental and Theoretical Determination.", *Scr. Met.*, 5 (1971) pp.889-894.

47. T. Johannesson, A. Tholen, "On the Influence of Grain Boundaries on Mechanical Properties", *Phil. Mag.*, 21 (1970) pp.1223-1228.

48. R.J. Harrison, G.A. Bruggeman, G.H. Bishop, "Computer Simulation Methods Applied to Grain Boundaries" in *Grain Boundary Structure and Properties*, edited by G.A. Chadwick, D.A. Smith (Academic Press, London, 1976) pp.45-91.

49. J.B. Gibson, A.N. Goland, M. Milgram, G.H. Vineyard, "Dynamics of Radiation Damage", *Phys. Rev.*, 120 (1960) pp.1229-1253.

50. A. Paskin, G.J. Dienes, "Molecular Dynamic Simulations of Shock Waves in a Three-Dimensional Solid", _J. Appl. Phys._, 43 (1972) pp.1605-1610.

51. W.A. Porter, D.L. Parker, "Gravitational Effects on Process-Induced Defects in Single Crystal Silicon", _AIAA J._, 13 (1975) pp.1518-1520.

52. G. Cortellazzi, S. Boffi, C. Caglioti, F. Rossitto, "A Lattice Dynamics Approach to the Acoustic Signal by a Uniformly Moving Dislocation", _J. Appl. Phys._, 44 (1973) pp.1518-1523.

53. R.M. Fisher, J.S. Lally, "Microplasticity Detected by an Acoustic Technique", _Can. J. Phys._, 45 (1967) pp.1147-1159.

54. K. Fuchs, "A Quantum Mechanical Calculation of the Elastic Constants of Monovalent Metals", _Proc. Roy. Soc. A_, 153 (1936) pp.622-639.

55. R.A. Johnson, "Relationship Between Two-Body Interatomic Potentials in a Lattice Model and Elastic Constants", _Phys. Rev. B_, 6 (1972) pp.2094-2100.

56. R.A. Johnson, "Relationship Between Two-Body Interatomic Potentials in a Lattice Model and Elastic Constants. II", _Phys. Rev. B_, 9 (1974) pp.1304-1308.

57. C.M. Zener, _Elasticity and Anelasticity of Metals_ (University of Chicago Press, Chicago, 1948).

58. L.A. Girifalco, V.G. Weizer, "Application of the Morse Potential Function to Cubic Metals", _Phys. Rev._; 114 (1959) pp.687-690.

59. R.A. Johnson, "Point-Defect Calculations for an FCC Lattice", _Phys. Rev._, 145 (1966) pp.423-433.

60. R.A. Johnson, W.D. Wilson, "Defect Calculations for FCC and BCC Metals" in _Interatomic Potentials and Simulation of Lattice Defects_, edited by P.C. Gehlen, J.R. Beeler, R.I. Jaffee (Plenum Press, New York, 1972) pp.301-319.

61. W.A. Harrison, _Pseudopotentials in the Theory of Metals_ (W.A. Benjamin Inc., New York, 1966).

62. G.C. Sih, H. Liebowitz, "Mathematical Theories of Brittle Fracture" in _Fracture_, v.2, edited by H. Liebowitz (Academic Press, New York, 1968) pp.67-190.

63. J.E. Sinclair, "Improved Atomistic Model of a BCC Dislocation Core", _J. Appl. Phys_., 42 (1971) pp.5321-5329.

64. R. Chang, "An Atomistic Study of Fracture", _Int. J. Frac. Mech._, 6 (1970) pp.111-125.

65. P.C. Gehlen, M.F. Kanninen, "An Atomic Model for Cleavage Crack Propogation in α Iron" in _Inelastic Behaviour of Solids_, edited by M.F. Kanninen, W.F. Adler, A.R. Rosenfield, R.I. Jaffee (McGraw-Hill, New York, 1970) pp.587-605.

66. P.C. Gehlen, M.F. Kanninen, "The Effect of Temperature on the Extension of a [001] Crack in a Model of BCC Iron", Proceedings of the Third Inter-American Conference on Materials Technology, Rio de Janeiro, 14-17 Aug., 1972, pp.415-419.

67. M.F. Kanninen, P.C. Gehlen, "Atomic Simulation of Crack Extension in BCC Iron", _Int. J. Frac. Mech._, 7 (1971) pp.471-473.

68. M.F. Kanninen, P.C. Gehlen, "A Study of Crack Propogation in Alpha-Iron" in _Interatomic Potentials and Simulation of Lattice Defects_, edited by P.C. Gehlen, J.R. Beeler, R.I. Jaffee (Plenum Press, New York, 1972) pp.713-724.

69. J.E. Sinclair, B.R. Lawn, "An Atomistic Study of Cracks in Diamond-Structure Crystals", _Proc. Roy. Soc._ (London) A, 329 (1972) pp.83-103.

70. C. Hsieh, R. Thomson, "Lattice Theory of Fracture and Crack Creep", _J. Appl. Phys._, 44 (1973) pp.2051-2063.

71. W.T. Ashurst, W.G. Hoover, "Microscopic Fracture Studies in the Two-Dimensional Triangular Lattice", _Phys. Rev. B_, 14 (1976) pp.1465-1473.

72. B.R. Lawn, "An Atomistic Model of Kinetic Crack Growth in Brittle Solids", _J. Mat. Sci._, 10 (1975) pp.469-480.

73. B.J.S. Wilkins, R. Dutton, "Static Fatigue Limit With Particular Reference to Glass", _J. Am. Ceram. Soc._, 59 (1976) pp.108-112.

74. D.M. Esterling, "Lattice Theory of Three-Dimensional Cracks", _J. Appl. Phys._, 47 (1976) pp.486-493.

75. J.E. Sinclair, "The Influence of the Interatomic Force Law and of Kinks on the Propogation of Brittle Cracks", _Phil. Mag._, 31 (1975) pp.647-671.

76.   P.C. Gehlen, G.T. Hahn, M.F. Kanninen, "Crack Extension by Bond
       Rupture in a Model of BCC Iron", _Scr. Met._, 6 (1972)
       pp.1087-1090.

77.   P.C. Gehlen, "Crack Extension in a Model of α-Iron", _Scr. Met._,
       7 (1973) pp.1115-1117.

78.   J.E. Sinclair, R. Fletcher, "A New Method of Saddle-Point
       Location for the Calculation of Defect Migration Energies",
       J. Phys. C: Solid State Phys., 7 (1974) pp.864-870.

79.   M.J. Box, "A Comparison of Several Current Optimization Methods,
       and the Use of Transformations in Constrained Problems",
       Comp. J., 9 (1966) pp.67-77.

80.   J.M. Smith, _Mathematical Modelling and Digital Simulation for
       Engineers and Scientists_ (Wiley Interscience, New York, 1977).

81.   L. Lapidus, J.H. Seinfeld, _Numerical Solution of Ordinary
       Differential Equations_ (Academic Press, New York, 1971).

82.   T.E. Hull, A.L. Creemer, "Efficiency of Predictor-Corrector
       Procedures", _J. Assoc. Comp. Mach._, 10 (1963) pp.291-301.

83.   J.R. Beeler, G.L. Kulcinski, "Agenda Discussion: Computer
       Techniques" in _Interatomic Potentials and Simulation of Lattice
       Defects_, edited by P.C. Gehlen, J.R. Beeler, R.I. Jaffee (Plenum
       Press, New York, 1972).

84.   C.W. Gear, _Numerical Initial Value Problems in Ordinary
       Differential Equations_ (Prentice-Hall, Englewood Cliffs, N.J.,
       1971).

85.   A. Nordsieck, "On Numerical Integration of Ordinary Differential
       Equations", _Math. of Comp._, 16 (1962) pp.22-49.

86.   J. Dyer, "Generalized Multistep Methods in Satellite Orbit
       Computation", _J. Assoc. Comp. Mach._, 15 (1968) pp.712-719.

87.   L.A. Girifalco, _Statistical Properties of Materials_ (John Wiley
       and Sons, New York, 1973).

88.   R.C. Weast, ed., _Handbook of Chemistry and Physics_ (The Chemical
       Rubber Co., Cleveland, 1979) p.D-183.

89.   Y.S. Touloukian, ed., _Thermophysical Properties of High
       Temperature Materials_, v.1 (The MacMillan Co., New York, 1967)
       p.583.

90. O.C. Zienkiewicz, The Finite Element Method (McGraw-Hill, London, 1977).

91. L. Kahn, Battelle Columbus Laboratories, personal communication.

APPENDIX A

The numerical integrators tested in Chapter 4 are described in this appendix. In what follows, each degree of freedom of each atom is treated identically and its value at time t is represented by $x(t)$. Its derivatives with respect to time are $\dot{x}$, $\ddot{x}$, $\dddot{x}$, x^{iv}, and x^{v}. The force on this atom in the direction of the degree of freedom, x, is F. This is calculated for all atoms when all degrees of freedom, x, ie. the positions of all atoms in each coordinate direction, are given. Since it is a function of the atomic coordinates, it is specified as F[x]. It must be emphasized that this is a vector relation. All forces, F, may be calculated when, and only when, all degrees of freedom, x, have been specified. The integration time step used is h. The atomic mass is m.

2-Step Difference [49]

The form used here is equivalent to that given in reference [49], but it is written in a different notation for easier comparison to the other methods:

$$x(t+h) = 2\,x(t) - x(t-h) + h^2 \ddot{x}(t) \tag{A1}$$

5-Step Difference   [81], p.27

$$x(t+h) = 2 \, x(t) - x(t-h) + h^2/240 \, [\, 299 \, \ddot{x}(t)$$
$$- 176 \, \ddot{x}(t-h) + 194 \, \ddot{x}(t-2h) \tag{A2}$$
$$- 96 \, \ddot{x}(t-3h) + 19 \, \ddot{x}(t-4h) \,]$$

Runge-Kutta   [84], p.49

This is a 3rd order Runge-Kutta scheme for 2nd order differential equations:

$$k_1 = h^2 F[\, x(t) \,] \, / \, 2m$$
$$k_2 = h^2 F[\, x(t) + 2 \, h \, \dot{x}(t)/3 + 4k_1/9 \,] \, / \, 2m \tag{A3}$$
$$x(t+h) = x(t) + h \, x(t) + (k_1 + k_2)/2$$
$$\dot{x}(t+h) = \dot{x}(t) + (k_1 + 3k_2)/2h$$

It can be seen that two force evaluations are required per time step for this method.

Nordsieck Methods   [85] and [84], p.148

These are equivalent to Adams methods but are written in a slightly different form mainly to facilitate changing the step size. They are predictor-corrector methods. If the predictor operation is specified by P, the corrector by C, and the evaluation of the forces by E, then a single application of each may be expressed PEC. This is a q=1 scheme. If the corrector is applied twice, q=2 and we have PECEC or $P(EC)^2$. In general, changes in q are described by $P(EC)^q$. The

number of force evaluations per step equals q. The P and C operations for the p=4 and p=6 methods used are described below where

$$y_0 = x \qquad\qquad y_3 = \dddot{x}\, h^3/6$$

$$y_1 = \dot{x}\, h \qquad\qquad y_4 = x^{iv}\, h^4/24 \qquad\qquad (A4)$$

$$y_2 = \ddot{x}\, h^2/2 \qquad\qquad y_5 = x^v\, h^5/120$$

and superscript p refers to predicted values, c to corrected values.

p=4 Predictor

$$y_0^p(t+h) = y_0(t) + y_1(t) + y_2(t) + y_3(t)$$

$$y_1^p(t+h) = y_1(t) + 2\, y_2(t) + 3\, y_3(t) \qquad\qquad (A5)$$

$$y_2^p(t+h) = y_2(t) + 3\, y_3(t)$$

$$y_3^p(t+h) = y_3(t)$$

p=4 Corrector

From $y_0^p(t+h) = x^p(t+h)$, get the predicted force, $F^p[\, x^p(t+h)\,]$, at t+h. Calculate $W = F^p h^2/2m - y_2^p(t+h)$. Correct all y's by setting

$$y_i^c(t+h) = y_i^p(t+h) + c_i W \qquad\qquad (A6)$$

where

$$c_0 = 1/6 \qquad\qquad c_2 = 1$$

$$c_1 = 5/6 \qquad\qquad c_3 = 1/3$$

p=6 Predictor

$$y_0^p(t+h) = y_0(t) + y_1(t) + y_2(t) + y_3(t) + y_4(t) + y_5(t)$$

$$y_1^p(t+h) = y_1(t) + 2 y_2(t) + 3 y_3(t) + 4 y_4(t) + 5 y_5(t)$$

$$y_2^p(t+h) = y_2(t) + 3 y_3(t) + 6 y_4(t) + 10 y_5(t) \tag{A7}$$

$$y_3^p(t+h) = y_3(t) + 4 y_4(t) + 10 y_5(t)$$

$$y_4^p(t+h) = y_4(t) + 5 y_5(t)$$

$$y_5^p(t+h) = y_5(t)$$

p=6 Corrector

The procedure is similar to that for the q=4 corrector with

$$c_0 = 3/16 \qquad\qquad c_3 = 11/18$$

$$c_1 = 251/360 \qquad\qquad c_4 = 1/6$$

$$c_2 = 1 \qquad\qquad c_5 = 1/60$$

Hybrid [86]

Note that there are some errors in the formulas given in reference [86]. The second derivatives below are calculated by $\ddot{x} = F[x]/m$.

First, the non-step point

$$x(t+.7h) = \bar{\alpha}_1 x(t) + \bar{\alpha}_2 x(t-h) + \bar{\alpha}_3 x(t-2h) + \bar{\alpha}_4 x(t-3h)$$
$$+ h^2[\ \bar{\gamma}_1 \ddot{x}(t) + \bar{\gamma}_2 \ddot{x}(t-h) + \bar{\gamma}_3 \ddot{x}(t-2h) \qquad (A8)$$
$$+ \bar{\gamma}_4 \ddot{x}(t-3h)\ ]$$

where

$$\bar{\alpha}_1 = -1.9320993 \qquad \bar{\gamma}_1 = 0.8625005$$

$$\bar{\alpha}_2 = 6.4719549 \qquad \bar{\gamma}_2 = 3.0303805$$

$$\bar{\alpha}_3 = -3.4476119 \qquad \bar{\gamma}_3 = 0.4336798$$

$$\bar{\alpha}_4 = -0.0922437 \qquad \bar{\gamma}_4 = -0.0072178$$

Then, the full step

$$x(t+h) = \alpha_1 x(t) + \alpha_2 x(t-h) + \alpha_3 x(t-2h) + \alpha_4 x(t-3h)$$
$$+ h^2[\ \gamma_1 \ddot{x}(t) + \gamma_2 \ddot{x}(t-h) + \gamma_3 \ddot{x}(t-2h) \qquad (A9)$$
$$+ \gamma_4 \ddot{x}(t-3h)\ ] + h^2 \gamma \ddot{x}(t+.7h)/m$$

where

$$\alpha_1 = 2.0580497 \qquad \gamma_1 = 0.7044318$$

$$\alpha_2 = -0.9634579 \qquad \gamma_2 = 0.0872588$$

$$\alpha_3 = -0.2472333 \qquad \gamma_3 = -0.1544589$$

$$\alpha_4 = 0.1526415 \qquad \gamma_4 = -0.0095188$$

$$\gamma = 0.1615960$$

Two force evaluations per time step are required by this method.